POLITECNICO
MILANO 1863

SCUOLA DI INGEGNERIA INDUSTRIALE
E DELL'INFORMAZIONE

Preliminary design and part load analysis of supercritical carbon dioxide power cycles for gas turbine bottoming applications

TESI DI LAUREA MAGISTRALE IN
ENERGY ENGINEERING

Author: **Francesco Colombo**

Student ID: 10581667
Advisor: Dario Alfani
Academic Year: 2022-23

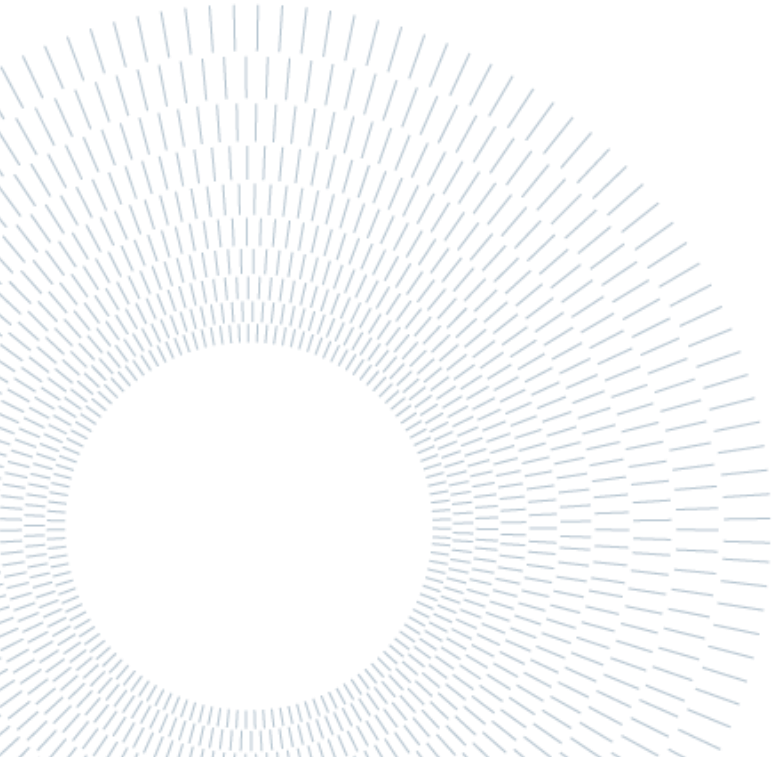

Abstract

Renewables are increasingly growing in the energy mix, causing regulation and control problems for the grid due to their intermittent and unpredictable nature. in the Thus, in the next future conventional fossil fuels power plants will have to shift towards peaker operation and, in this context, combined cycles power plants adopting supercritical CO2 bottoming cycles could be more flexible than steam based ones.
This thesis work is developed around one of the replication sites of the CO2OLHEAT project, an EU-funded H2020 project, which aims to enhance waste heat recovery in the industrial and power generation sector by developing a sCO2 power cycle in an operational environment. The replication site is located in the Paris region, where EDF is proposing to convert a power plant consisting of two gas turbines into a combined cycle with a sCO2-based-bottoming configuration. Thus, the objectives of this thesis are to study possible configurations that can be applied to the system and to study their techno-economical performance under nominal and off-design operation.
The thesis work mainly focused on two consequent analyses: firstly, the nominal design of the bottoming cycle and secondly its part-load and off design operation, also considering a brief economic evaluation and a preliminary yearly simulation.
This Simple Recuperated Configuration (SRC) was selected as it represents the optimal solution for the studied application (i.e., a peaker plant) thanks to its compact dimensions, also leading to lower investment cost.
By setting the boundaries (i.e. ambient temperature and gas turbine load) of the analysis, several operative and performances maps have been generated for both the cooling solutions considered in the work, ambient air and water. These maps provide insights on how to operate the power cycle under optimal terms, knowing the optimized variables and inventory and obtaining the maximum power output under those conditions.
Finally, the maps of the cycle optimal off-design operation have been employed for a preliminary yearly simulation and techno-economic analysis, obtaining the not discounted payback time of the bottoming system.
Even if it resulted evident that considering today's peaker plant load schedule and 2019 electricity prices the plant may not seem feasible from an economic point of view, considering the conservative assumptions the technology still results interesting for the considered application.

Key-words: climate change; supercritical CO_2; bottoming cycle; gas turbine; off design.

Abstract in italiano

Le rinnovabili sono sempre più in crescita nel mix energetico, causando problemi di regolazione e controllo della rete elettrica a causa della loro natura intermittente e imprevedibile. Per questo motivo nel futuro imminente le centrali elettriche convenzionali a combustibili fossili dovranno gradualmente operare sempre più come impianti "peaker" e, in questo contesto, una soluzione tecnologica basata su cicli combinati che adottano in bottoming cicli supercritici a CO2 potrebbero essere più flessibili di quelle tradizionali che usano cicli Rankine a vapore.
Questo lavoro di tesi è stato quindi sviluppato attorno a uno dei casi studio del progetto H2020 CO2OLHEAT, il quale mira a migliorare il recupero del calore di scarto del settore industriale e della generazione di energia dimostrando il potenziale dei cicli a sCO2 in ambiente operativo. Il caso studio considerato è localizzato vicino Parigi, dove EDF propone di convertire una centrale costituita da due turbine a gas in un ciclo combinato con un ciclo di bottoming a sCO2. Gli obiettivi di questa tesi sono pertanto lo studio delle possibili configurazioni di impianto e delle loro prestazioni tecnico-economiche in condizioni di funzionamento nominale e fuori progetto.
Il lavoro di tesi si è concentrato principalmente su queste due analisi conseguenti: in primo luogo è stato svolto il progetto nominale del ciclo di bottoming e successivamente è stato studiato il suo funzionamento a carico parziale e fuori progetto al variare del carico della turbina a gas e della temperatura ambiente. In conclusione è stata svolta anche una breve valutazione economica e una simulazione annuale preliminare.
La configurazione simple recuperative cycle (SRC) è stata selezionata in quanto rappresenta la soluzione ottimale per l'applicazione studiata (peaker plant) grazie alle sue dimensioni compatte, che comportano anche un costo di investimento inferiore.
Dopo aver fissato le condizioni al contorno dell'analisi in termini di temperatura ambiente e carico turbina a gas, diverse mappe operative e prestazionali sono state generate per entrambe le soluzioni di raffreddamento considerate nel lavoro, cioè aria ambiente e acqua. Queste mappe forniscono informazioni sul funzionamento ottimale del ciclo di potenza, e riportano i valori delle le variabili di controllo e della quantità di fluido di lavoro all'interno del sistema, ottimizzati in modo da ottenere la massima potenza per ogni condizione operativa.
Infine, le mappe dell'operazione ottimale del ciclo sono state utilizzate per una simulazione annuale preliminare e un'analisi tecnico-economica, ottenendo il tempo di ritorno dell'investimento del sistema bottoming a sCO2. Seppur con le assunzioni

fatte, essendo molto conservative, la tecnologia risulta ancora interessante per l'applicazione considerate.

Parole chiave: cambiamento climatico, CO_2 supercritica, ciclo bottoming, turbina a gas, off design

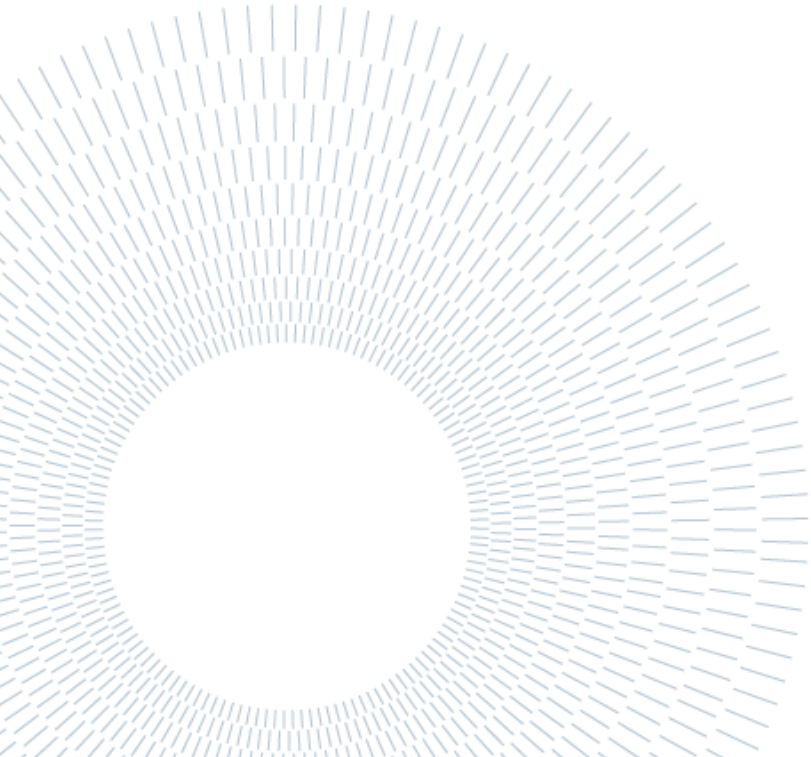

Contents

Abstract ..... **i**

Abstract in italiano ..... **iii**

Contents ..... **vii**

1 Introduction **1**

1.1. Climate change 1

1.2. Waste heat recovery 3

1.3. State-of-the-Art thermodynamic cycles for WHR 5

1.4. sCO_2 cycles for WHR 6

1.4.1. sCO_2 thermodynamic properties 6

1.4.2. Background 9

1.5. CO_2OLHEAT project 11

1.6. Case study and thesis objectives 13

1.6.1. Technical objectives 13

1.6.2. Economic objectives 13

1.6.3. Flexibility objectives 14

2 Nominal plant design **15**

2.1. Simulation tools 15

2.2. Topping cycle 15

2.3. Heat source modelling 16

2.4. sCO_2 cycle components 17

2.4.1. Materials 17

2.4.2. Turbomachinery 18

2.4.3. Primary heat exchanger (PHE) 20

2.4.4. Recuperators 21

2.4.5. Heat rejection unit (HRU) 23

2.5. Design assumptions 26

* this assumption is used only in the part load analysis 26

2.6. Cycle configurations 27

2.6.1. Simple recuperative cycle (SRC) 27

2.6.2. Recompressed recuperative cycle (RRC) 28

2.6.3. Simple recuperative cycle with recuperator bypass (SRCB) 30
2.6.4. Recompressed recuperative cycle with high temperature recuperator bypass (RRCB) 30
2.6.5. Turbine split flow cycle (TSF) 31
2.6.6. Single heated cascade cycle (SHC) 32
2.6.7. Dual heated cascade cycle (BHC) 33
2.7. Energy analysis 34
2.8. Thermodynamic optimization 35
2.8.1. Methodology 35
2.8.2. Optimization variable analysis 36
2.8.3. Results 38
2.9. Techno economic analysis 39
2.9.1. Cost correlations 39
2.9.2. Results 40
2.10. Simple recuperative cycle (SRC) results 41
3 Part load analysis 44
3.1. Boundary conditions 44
3.2. Methodology 47
3.2.1. Water cooled 48
3.2.2. Air cooled 50
3.3. Part load operations of the components 51
3.3.1. Recuperator off-design modelling 51
3.3.2. Compressor off-design modelling 51
3.3.3. Turbine off-design modelling 52
3.3.4. HRU off-design modelling 52
3.4. Cycle operational limits 53
3.4.1. Compressor 53
3.4.2. HRU 53
3.5. Operating strategies 54
3.6. Results 56
3.6.1. Boundary conditions 56
3.6.2. HRU with water as cooling medium 58
3.6.3. HRU with air as cooling medium 65
3.6.4. Compressor operations 72
3.6.5. Comparison between the cooling mediums 74
3.6.6. Preliminary annual economic analysis 79
4 Conclusion 83

4.1. Future developments 83
Bibliography **87**
A Appendix A **93**
B Appendix B **95**
List of Figures **97**
List of Tables **101**
List of symbols **103**
Ringraziamenti ..... Error! Bookmark not defined.

1 Introduction

1.1. Climate change

One of the greatest challenges facing humanity in the near future is the battle against climate change.
Data show how the average temperature of earth is increasing year by year, and the majority of scientific studies agree that the cause of the phenomenon is the rising emissions of greenhouse gases produced mostly by combustion of fossil fuels.
In Figure 1.1 is possible to notice the progression of this effect and it is visible how we have almost reached a 1°C increase over the pre-industrial level [1].

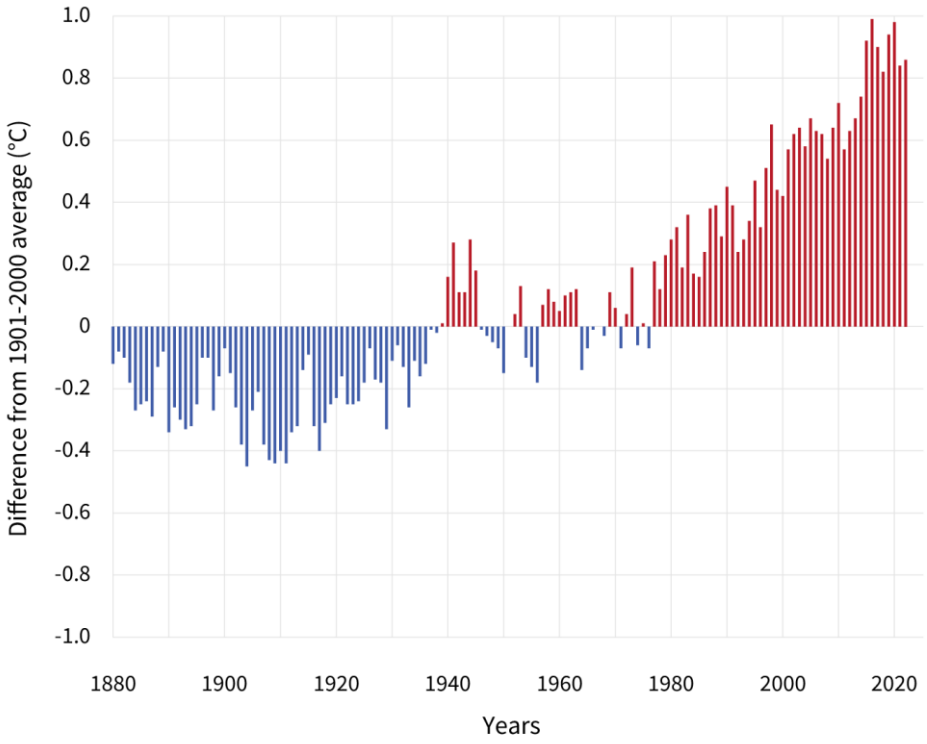

Figure 1.1: Global average temperature increase difference year by year during the last century [1]

Global warming has a direct impact on our planet. Extreme weather conditions will be increasingly likely, moving from violent thunderstorms and floods to droughts and water shortages. Many areas on earth will become inhospitable to human life leading to a huge number of migrations and wars for the possession of the still livable territories [2].

Swiss Re Institute's stress-test analysis reveals that World economy is set to lose up to 18% GDP from climate change if no action is taken [3].
In recent years, through iconic public figures such as Greta Thunberg, humanity has begun to become aware of its responsibilities toward topics such as global warming and sustainable socio-economic growth.
Fridays-for-future events also prompted policy makers and international community to take up these issues, and in 2015 in Paris 197 member states of the United Nations Framework Convention on Climate Change (UNFCCC) adopt what is known as the first universal and legally binding understanding on climate change. The agreement aims to contain the global average temperature increase well below the threshold of 2°C above pre-industrial levels, limiting that increase to 1.5°C [4].
In this framework, the energy sector plays a crucial role since every year 75% of global green-house gases emissions derive from electricity and heat production alone [5].
Hence, the decarbonization of this sector is the key to reach the policies goals and it is based on three main pillars:

- **Increasing share of renewable energy in total gross final consumption**
- **Saving of energy consumption by rising energy efficiency**
- **End users switching to electric sources**

The European Union has been pushing these goals in recent years; the increase of renewables in the European energy mix is already visible and is expected to gradually rise for the foreseeable future [4]. However, some renewables such as wind and solar possess the inherent characteristic of having unpredictable production profiles, making these technologies not able to guarantee dispatchability at low cost due to the need of an expensive and inefficient large-scale electrochemical storage [6].
Conventional fossil fuel power plants will have to gradually shift their role from base-load operation to cover peak demand and to provide energy services to the electrical grid. However, current power plants, mainly based on steam cycles, are not suitable for following the trend of rapid load changes (see Table 1.1), which is the main feature to compensate for unpredictable nature of renewable energies.

Table 1.1: Comparison of the main flexibility parameters (averages) for conventional types of power plants [7]

Type of plant	Hot/cold start-up time	Start-up cost (instant start)	Minimum load	Efficiency at 100% load	Efficiency at 50% load
Hard coal	2 - 10 h	>100 $/MW	25 - 40%	43%	40%
Lignite	4 - 10 h	>100 $/MW	50 - 60%	40%	35%
CCGT	1 - 4 h	55 $/MW	40 - 50%	52 - 57%	47 - 51%

In this context, supercritical CO_2 power cycles are gaining increasing attention and interest from industry, institutions and academia as shown in the growing number of articles and publications on the topic.

The second pillar of the decarbonization process mentioned earlier is based on increasing energy efficiency. One of the areas where there is still considerable potential for improvement is in the reutilization of waste heat from power plants and industrial processes, which is commonly referred to as waste heat recovery (WHR).

1.2. Waste heat recovery

Repurposing usable waste heat power will become increasingly crucial in the near future addressing global energy stability and security.
It is forecast that global energy consumption will continue to increase until 2035, and then will begin to decline slightly from there on [8]. In Figure 1.2 is displayed the distribution every 5 years divided by world regions.

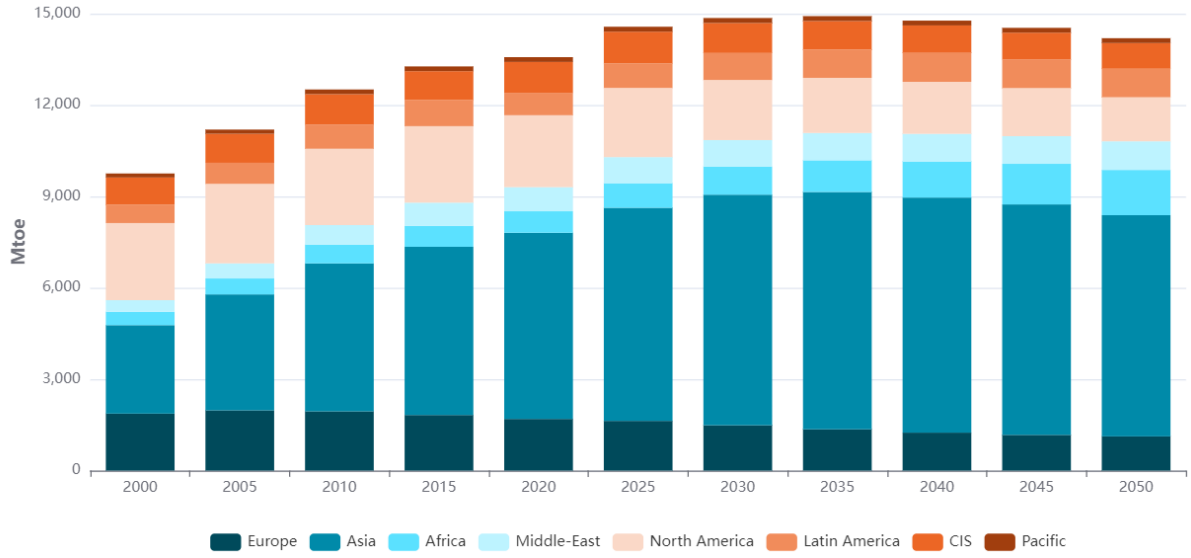

Figure 1.2: Total Primary Energy Consumption by Region from 2000 to 2050 [8]

It has been estimated that the 63% of the overall global energy consumption is lost after combustion and heat transfer processes [9]. For this reason, it is of extreme importance to recover at least some of this energy.
There are many kinds of forms of waste heat resources. According to the investigation by Galanis et al. [10], waste heat energy is released from industrial processed to the environment via four main states of matter:

- Liquid streams at temperatures between 50°C and 300°C.
- Exhaust at temperatures range between 150°C to 800°C.
- Steam at temperatures ranging from 100°C to 250°C.
- Process gases and vapors within a temperature range of 80°C and 500°C.

Furthermore, low temperature (< 350°C) waste heat accounts for the majority in the end-use energy sectors [11].
Figure 1.3 shows that 63% of the waste heat streams are available at a temperature lower than 100°C and the largest proportion of it comes from the electricity sector [11].

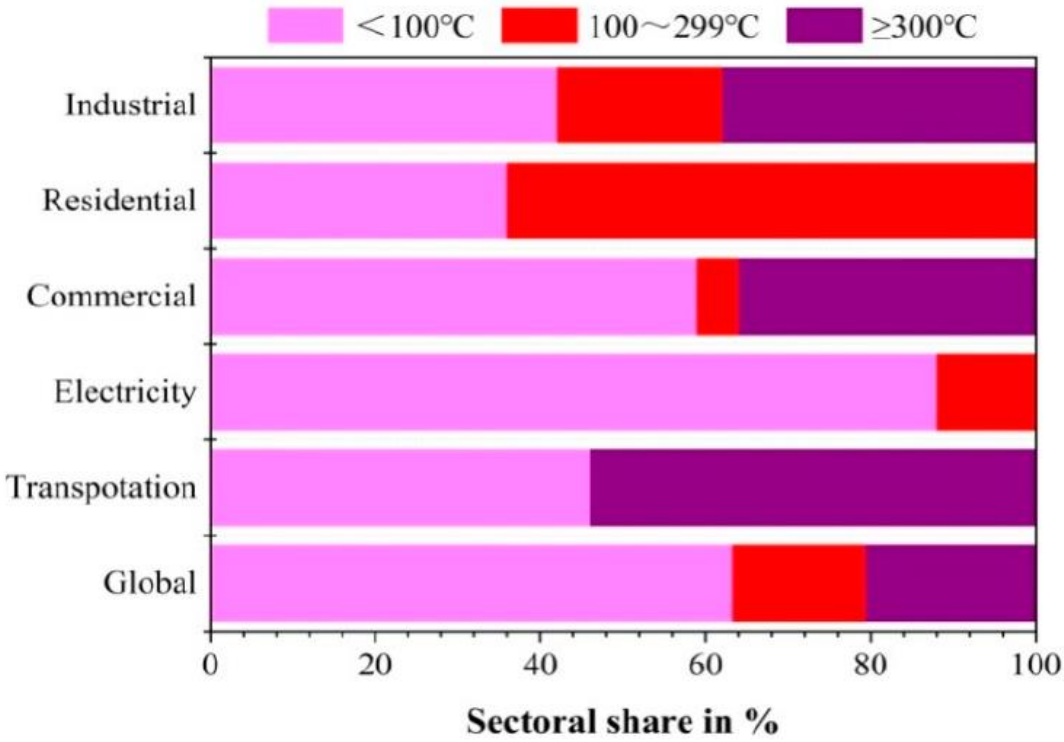

Figure 1.3: Sectoral shares of worldwide waste heat distribution [11]

From a thermodynamic point of view, this energy can be reused in various ways.
In particular, two main approaches can be pursued. The direct re-use of the waste heat recovered or its conversion in electrical power. In the first case, the thermal energy demand must be within the industrial site or in its vicinity. While the electrical energy recovery is much more favorable in terms of energy management since the surplus of energy can be injected in the electrical grid [12]. In addition, electricity is considered more valuable from an economic perspective [13].
The majority of the technologies for converting waste heat into electricity are based on thermodynamic cycles. However, various solutions can be employed depending on the heat source conditions and the power plant size.

1.3. State-of-the-Art thermodynamic cycles for WHR

Different cycle configurations can be used in waste heat recovery applications. The choice is made based on two main parameters: heat source temperature and bottoming cycle scale.
Figure 1.4 depicts the possible thermodynamic cycles and the range of their relevant operation temperatures.

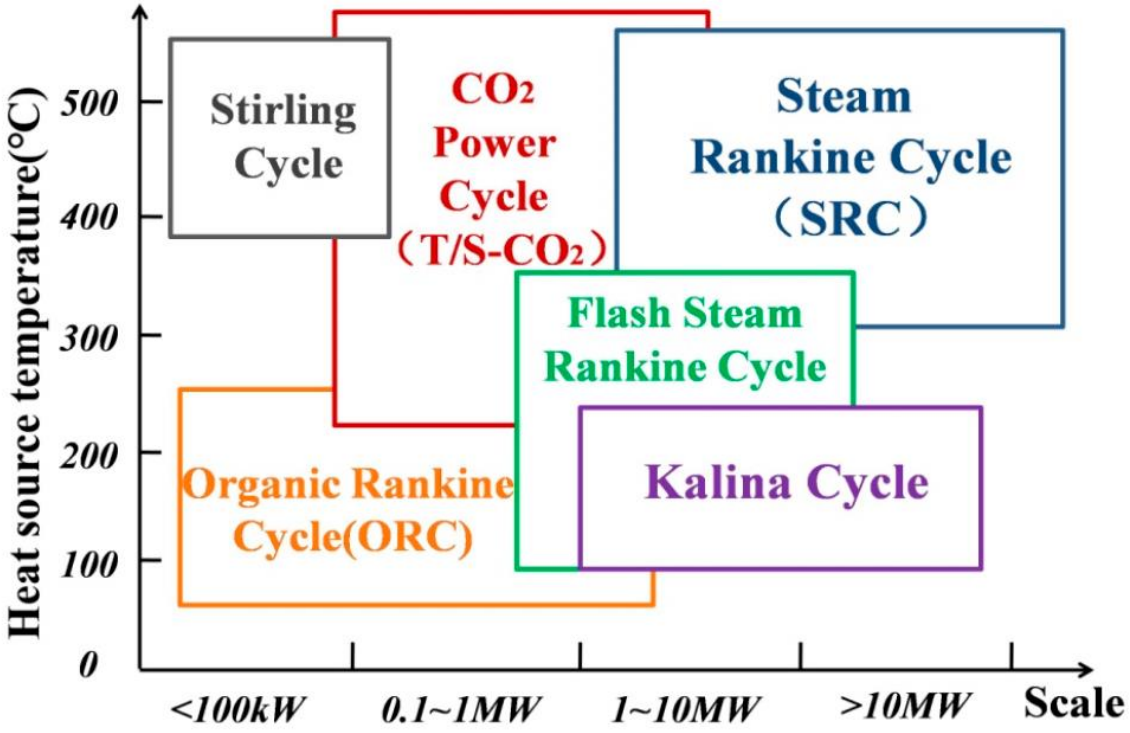

Figure 1.4: Thermodynamic cycles for waste heat recovery at various temperature levels and scales [11]

Steam Rankine cycle is suitable for medium-high temperatures, between 300°C and 600°C. The lower limit is given by the low vapor pressure of the water, while the upper one by material and technological constraints. They are designed for medium to high power cycles, more than 1 MW [11]. Below this threshold the turbine blade heights become critically low causing severe losses in the high pressure stages. More advanced cycles, like the ultra-supercritical steam power systems, can also exploit heat sources beyond 620°C, but they require significant investment costs in addition [12].

Therefore, Organic Rankine Cycles (ORC) which use lower boiling point organic fluids, have been largely studied in the last few decades for low power applications [11]. An appropriate temperature range to obtain competitive efficiency is from 90°C to 250°C. The upper limit is imposed by the flammability and the low chemical stability of the organic fluids at high temperatures, while the lower one depends on the reduction of efficiency and output of ORC units at extremely low temperatures [12].

Additionally, a possibility for higher scales is the Kalina cycle, which uses a mixture of ammonia and water as working fluid to meet the temperature profile of the waste heat sources during the phase change heat transfer process, between 100°C and 450°C [11].

Finally, using the CO_2 in a WHR cycle was investigated only in recent years, but it is gaining more and more attention. Such layouts use CO_2 in transcritical or supercritical conditions, due to the relatively low critical point. These cycles can not only replace the steam Rankine ones, but they can also cover a wide range of operating conditions. Furthermore, they can offer potentially higher efficiencies with a much smaller environmental footprint. The number of publications on this cycle has risen exponentially in the last decade, however the great potential of this technology needs to be further explored [11].

1.4. sCO_2 cycles for WHR

In this paragraph the thermodynamic characteristics of CO_2 under supercritical conditions and a review of some studies concerning sCO_2 bottoming cycle applications are addressed.

1.4.1. sCO_2 thermodynamic properties

Carbon dioxide (CO_2) is an ideal working fluid for closed-loop power generation applications. It is a low-cost resource, its cost is only 1/10 of helium and 1/70 of an organic working fluid like R-134a [14]. In addition, it is non-toxic, non-flammable, non-corrosive and readily available [15].
The main advantages of this technology are linked to CO_2 critical temperature and pressure. The critical temperature, which is equal to 31.1°C, is a simple value to obtain since it is close to the ambient temperature of most locations. Secondly, the critical pressure, being equal to 73.8 bar, can be easily handled from a technical point of view [16].
In supercritical conditions, CO_2 can be defined neither as a liquid nor as a gas, but it has physical properties in between gas and liquid phases. In particular, the trend is to possess viscosities more similar to gases while keeping densities closer to liquids. In the supercritical state, when CO_2 is close to the critical point, it has a high density (600-800 kg/m^3) and low compressibility factor (0.2-0.4), which enables to downsize the equipment with respect to more conventional technologies such as gas turbines or steam power plants (the size of a sCO_2 turbine can be up to 1/10 of a steam turbine with the same power output [17]). The reduced dimension of the components allows to decrease investment and maintenance costs as well as the footprint of the whole system. In contrast, this aspect also introduces serious challenges in designing high power turbomachinery components with such small rotor diameters and excessive rotational speed [18].

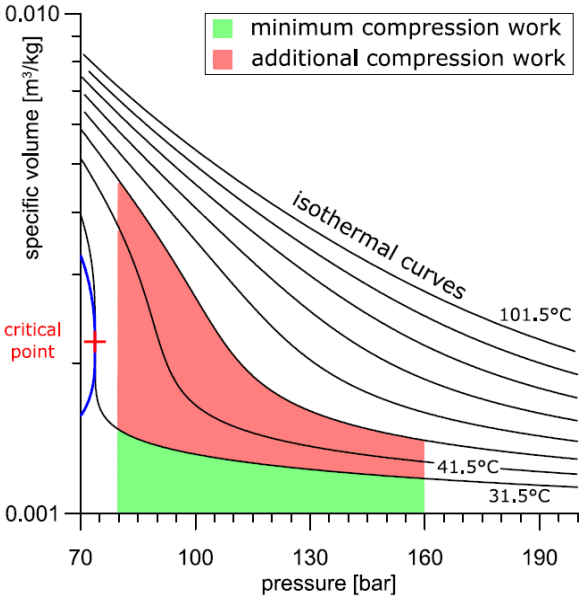

Figure 1.5: v-p diagram of CO_2 compression at different temperature levels [12]

Another advantage of working above but close to the critical point is the high values of specific heat capacity at constant pressure and isothermal compressibility. These properties, combined with the high densities of the fluid, ensure a reduction of the mechanical work for fluid compression [12].
The beneficial effect of the compression near the critical point is clearly displayed in Figure 1.5. The green area is the work needed at a temperature of 31.5°C, just over the critical one. While the red area is the compression energy when the temperature is over 41.5°C. The compression considered is from 80 to 160 bar and it is clear how the closer the temperature is to the critical one, the more the compression work is reduced.

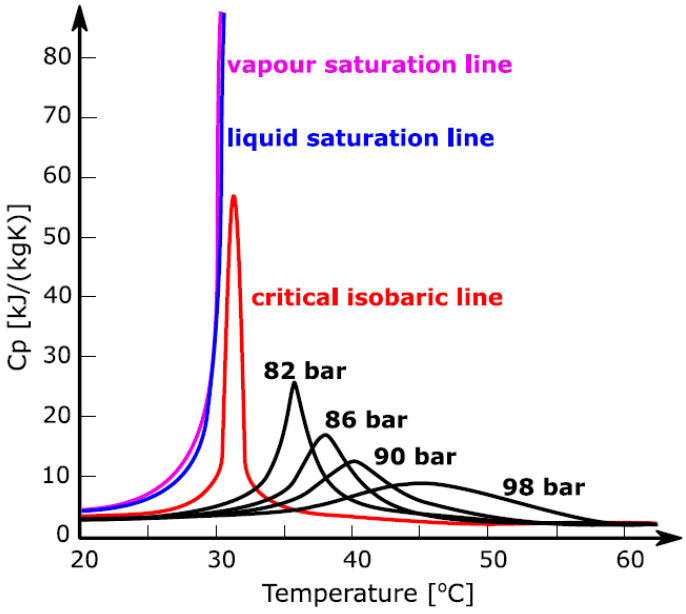

Figure 1.6: Specific heat of CO_2 as a function of temperature and pressure [12]

Nevertheless, starting the compression process close to the critical point introduces significant precautions in compressor design because small variations of temperature and pressure lead to significant and sharp variations of the working fluid thermodynamic and transport properties. The closer the fluid approaches the critical point the more its thermodynamic properties change (Figure 1.6). This poses a challenge in terms of control and regulation since accurate instrumentation is required [12].

The minimum pressure of the sCO_2 cycle is fixed by critical transition and the maximum pressure by technological constraints (typically around 250-300 bar) [12].

So, the typical maximum pressure ratio achievable in the cycle is around 4, which is extremely low compared to the one of 200 in Rankine technologies.

The low ratio achieved leads to an increase in the temperatures at the end of the expansion and then a high level of recuperation is needed to obtain reasonable performance. However, at these temperatures CO_2 may assume a strong corrosive behavior, requiring the development of materials that can withstand such harsh operating conditions [12].

The last advantage considered is referred to the so-called pinch point (i.e. the minimum temperature difference between two streams in a heat exchanger) in the PHE.

In a subcritical Rankine cycle this point is always at the inlet of the evaporator, then, during the evaporation process, temperature and pressure of the water do not change and this causes larger temperature differences between the steam and the exhaust gases, increasing irreversibility.

In contrast, when the working fluid is CO_2, due to its single-phase characteristics above the critical point, the average temperature differences are much lower, and a higher fluid temperature can be achieved for the same heat source [15].

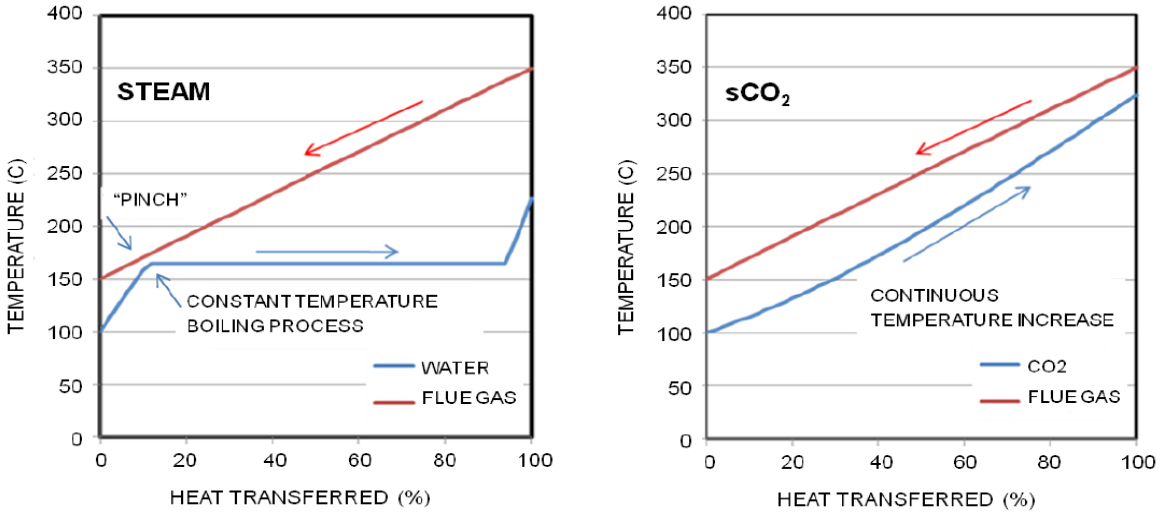

Figure 1.7: T-Q diagrams of a HRSG (on the left) and a flue gases and sCO_2 PHE (on the right) [15]

1.4.2. Background

The first documented consideration for sCO_2 cycles as gas turbine bottoming layouts dates from the 1970's, where it was studied the potential for heat recovery in a compact physical device for its use in shipboard applications [19]. Following, other studies on sCO_2 power cycles for waste and exhaust heat recovery [20] and oxyfuel combustion cycles for primary power [21] have come to light. Many of these early studies were focused on theoretical cycle development, although significant advances have been made in laboratory-scale experimental systems.

The first sCO_2-based WHR equipment in combined heat and power solution (CHP) was commercialized in 2014 by Echogen Power Systems, a US private company founded in 2007 leading producer of large-scale heat to power systems. The company has studied several variants of sCO_2 cycles that are optimized for bottoming and heat recovery applications. Over the full range of configurations investigated, the sCO_2 cycles generate higher power output at a lower cost than the comparable steam cycles, leading to a significant LCOE advantage [22].

Echogen analyzed different sCO_2 power cycle layouts. Starting from the simplest configuration, known as "simple recuperative cycle", which has the minimum number of components, thus reducing the system complexity and investment costs. However, more complex cycles architectures, such as the so called recompression cycles enable higher thermodynamic efficiencies and they are mainly suitable for nuclear and CSP applications.

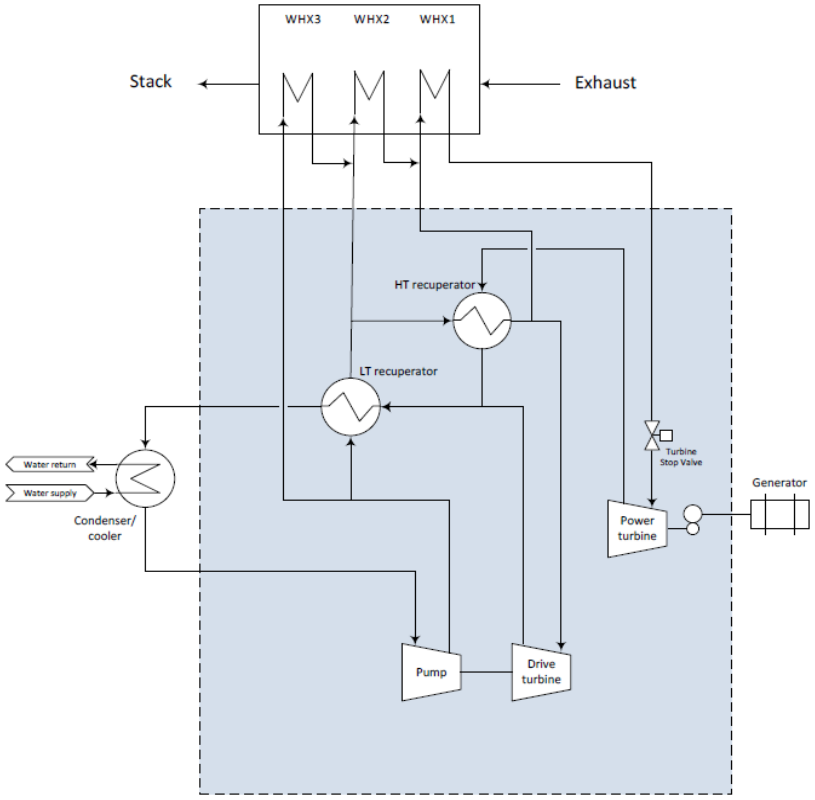

Figure 1.8: Dual Rail's layout [22]

Another interesting architecture is the Dual Rail configuration. As represented in Figure 1.8 the sCO_2 stream, after being compressed in the main compressor, is then split into more fractions that are directed to the recuperation processes or to the primary heater. After being heated up, they go towards the two turbines, one driving the compressor. The residual heat at the outlet of the turbines is used in the recuperative heat exchangers.
This configuration represents a balance between the contribution of heat from the outside and the one recovered internally, because thanks to flow split valves the sCO_2 stream can be directed either to the external heat exchanger or to the internal recuperators. The ability to tailor the flow rate sequentially through these two paths allows to minimize temperature differences in both heat exchangers maximizing cycle performance. Since 2012, several works have been published confirming the feasibility and competitiveness of the Echogen solution [22]. However, the main issue is related to the significant number of components and the complexity in operation.
Currently, the most widely used technology as bottoming of a gas topping cycle is the steam Rankine cycle. Huck et al. [23] have tried to compare it with sCO_2 power cycles, studying the layout shown in Figure 1.9.

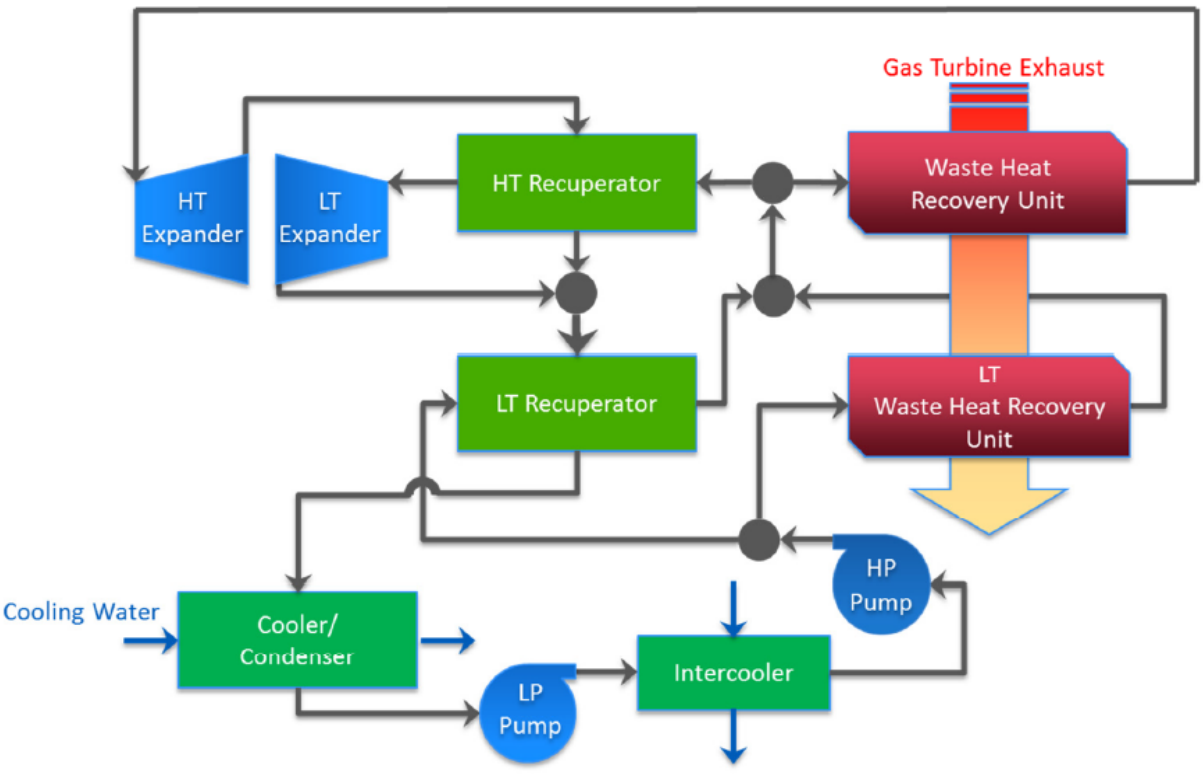

Figure 1.9: sCO2 power cycle schematic [23]

They divided the analysis into two parts, depending on the type of topping cycle considered.

1. For large heavy-duty gas turbines as topping, such as the GE H-Class, the baseline as bottoming is a three-pressure reheat (3PRH) steam cycle. The comparison is performed considering a maximum fluid temperature of 600°C and 700°C.
   In this scenario, only assuming turbine and compressor with high isentropic efficiencies of 95%, the sCO_2 can outperform the 3PRH steam, but with a maximum pressure that needs to exceed 300 bar (a difficult value to achieve considering the type of materials that needs to be employed). While if those isentropic efficiencies are reduced to more feasible levels obtained with steam-based turbomachinery, the sCO_2 performance is always lower than 3PRH steam in combined cycle net efficiency.
2. For small aeroderivative gas turbines as topping, such as the GE LM2500, the baseline as bottoming is a two pressure not-reheat (2PNR) steam cycle. The comparison is performed considering a maximum fluid temperature of 500°C.
   In this case, even if realistic values of isentropic efficiencies are assumed, the sCO_2 can outperform the 2PNR steam with only a pressure above 200 bar.

This study provides insight into the potential of the sCO_2 as bottoming cycle, which could allow for better performance than the more proven steam cycle considering medium to small scale power plants.

Finally, in recent years several European projects have been dealing with the topic. One of them is the so called CO_2OLHEAT project, which is also the case study of this thesis project.

1.5. CO_2OLHEAT project

CO_2OLHEAT is an EU-funded H2020 project to address energy efficiency and decarbonization challenges of European REIIs (Resource and Energy Intensive Industries). The project, which also includes the contribution of Politecnico di Milano, is thought to focus on unused waste heat and its efficient and cost-effective conversion into electrical energy.

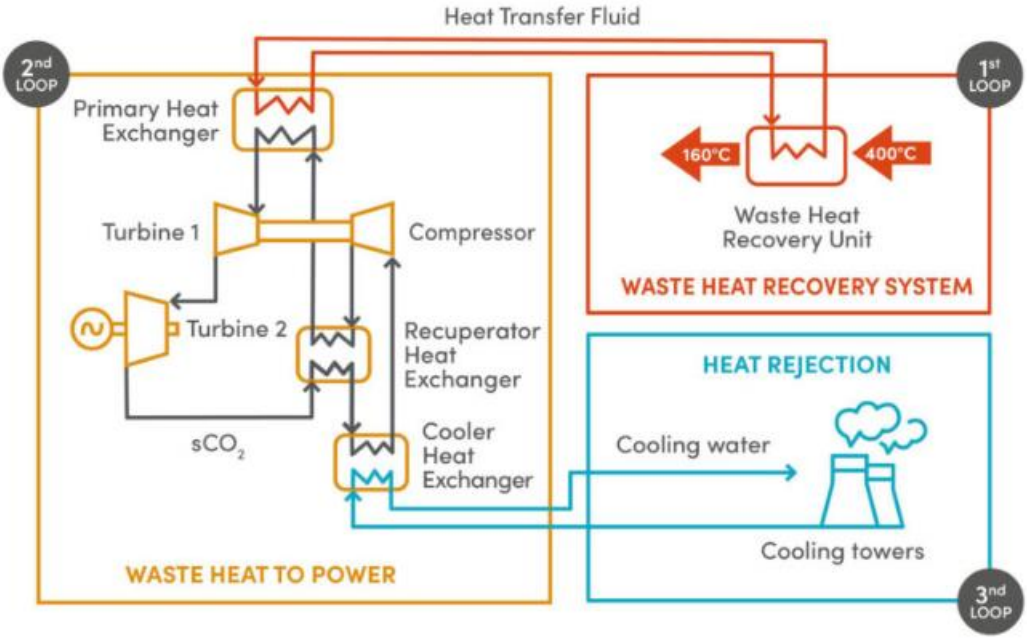

Figure 1.10: Schematic design of the sCO_2 power plant [24]

Three main key goals can be identified:

- **Untapping Industrial Waste Heat Potential**
  Design of a novel WH2P plant layout for waste heat valorization in an efficient and cost effective way.
- **Innovations, economic viability, and easy replicability**
  The innovative and state-of-the-art technology will be used to design and develop the sCO_2 power block, with outstanding economic and replicability features in other REIIs as well as power generation sectors
- **Increase of energy efficiency**
  Improvement of REII's energy efficiency by their waste heat valorization, its conversion into electricity and re-injection into the industrial process.

State-of-the-art sCO_2 technologies are used to design and demonstrate the first sCO_2 plant of its kind in the EU in a real industrial environment.

The chosen demonstration site is the CEMEX cement plant in Prachovice (Czech Republic). The plant has substantial unexploited waste heat potential, which is currently unused and is being discarded using water cooling towers. The CO_2OLHEAT 2 MW power plant will be able to meet approximately 10% of the plant's electricity needs, saving € 750000 per year with a short payback period (estimated at 4 to 8 years) [17].

Other replication sites are considered, among them there is a gas turbine-based power plant located in the Paris region (Montereau Fault Yonne). EDF, the largest energy producer and distributor in France, is proposing to convert this plant consisting of two gas turbines into a combined cycle with a gas topping cycle and a sCO_2 bottoming cycle.

The exhaust gas from one of them, GT13E2 type combustion turbine with a capacity of 210 MW, will be considered for upgrading the CO_2OLHEAT cycle.
This conversion aims to increase the total power by 50 MW and the plant's efficiency from 38% to 55% and it will also provide a new type of ultra-flexible cycle to compensate for the variability of renewable sources [17].

1.6. Case study and thesis objectives

This thesis work will be developed starting from the premises of the replication site within the CO_2OLHEAT project and will try to investigate, through numerical simulation tools, the potential of sCO_2 cycles as bottoming of gas turbines.

1.6.1. Technical objectives

First of all, it is essential to study the system from a thermodynamic and technical point of view. The various objectives of this analysis are:

- Literature review regarding the most mentioned and studied configurations for sCO_2 bottoming applications with a focus towards the ones with complexity reduction.
- Comprehension of the configurations already developed in the code within the s-CO_2 flex project.
- Implementation of a new pair of configurations, not existing in the code, that from studies show good performance.
- Implementation of a new design criterium to vary the flue gases specific heat so that it is no longer constant but a function of temperature and composition of exhaust gases.
- Resolution of the gas topping cycle, to derive the input conditions of the sCO_2 bottoming system.
- Thermodynamic optimization with a numerical software analysis of all configurations, deriving net power and efficiency values for each.
- Performance comparison based on the results obtained and selection of the best performing configuration(s) from a technical and economic point of view.

1.6.2. Economic objectives

The technical analysis alone is not enough to justify the investment. It is undoubtedly important to develop a working sCO_2 that is feasible within the energy market. Thus, a look will also be given at the plant costs depending on the configuration employed. An initial analysis will be performed, based only on investment costs of each individual component in order to obtain total investment cost of the power plant and specific cost in relation to the total net power produced.
Future developments should also include a deeper study including operability and maintenance costs over the lifetime of the plant.

1.6.3. Flexibility objectives

Finally, the analysis will also be conducted at partial loads, thus by varying the ambient conditions and the gas turbine load the bottoming cycle's boundaries will change and a new optimum operational cycle point will have to be found.
Dynamic analysis is not covered, as a specific tool would be necessary and it is beyond the scope of the thesis.
The goals of this analysis are:

- Selection of a configuration with proficient results among those studied in the previous analyses.
- Performance comparison of this configuration in on-design considering two different cooling method, with water and air.
- Study of the selected cycle's performance in off-design in the two different cooling methods.
- Analysis of the off-design points found in the previous step discarding those that are not feasible.
- Final discussion of the results obtained by analyzing the differences between the two cooling methods used.
- Identification of the optimal control strategy to be applied to the sCO_2 bottoming cycles.

2 Nominal plant design

In this section the sCO_2 cycle under nominal conditions is studied. Initially, the topping cycle is analysed to derive the heat source entering the bottoming system. Thereby, different layouts are proposed and optimized to figure out the one(s) that are most promising from a thermodynamic point of view. Finally, a brief economic analysis on the investment costs for each configuration is provided.

2.1. Simulation tools

A numerical tool developed in MATLAB [25] is used to study the performance of the cycle configurations chosen. The tool consists of several subroutines for the definition of the cycle thermodynamic streams, the modeling and the simulation of the system components and the solution of the thermodynamic cycles.
This code was designed within the s-CO_2 flex project by Politecnico di Milano and it allows to perform single- or multi-objective optimizations [26].
Carbon dioxide thermodynamic properties are computed through the NIST REFPROP 9.1 database [27] or by using interpolating methods, which results to be particularly useful to decrease the numerical code computational time [18].
Eventually the numerical tool is able to compute and to display the most significant diagrams, such as the Ts (temperature – specific entropy) or the TQ (temperature – thermal power) diagrams.
The mass flow rate, temperature and composition of the exhaust gases of the topping cycle are found using the commercial software THERMOFLEX [28], which integrates a large components library including many different commercial models.
The NASA polynomials [29] are used for ideal mixtures of ideal gases such as air and flue gas.

2.2. Topping cycle

The topping cycle gas turbine model is a General Electric GT13E2 with a power output of 210 MW [17]. The main characteristics are summed up in the table below.

Table 2.1: Datasheet of a GT13E2 gas turbine [30]

Net power output [MW]	210
Net heat rate [kJ/kWh, LHV]	9474
Net efficiency [LHV]	38%
Ramp rate [MW/minute]	14-36
Startup Time [RR Hot, Minutes]	25

Furthermore, with a potential of more than 14 million operating hours, this gas turbine can fit nearly every possible power plant application since its ambient temperature's range of operation is from -50°C to 55°C and it can achieve combined cycle efficiencies greater than 55% [30].

2.3. Heat source modelling

By using Thermoflex software and considering ambient conditions (T = 25°C and p = 1 atm), the thermodynamic properties at the exhaust of the gas turbine are derived, thus temperature, pressure, and composition of the flue gases.

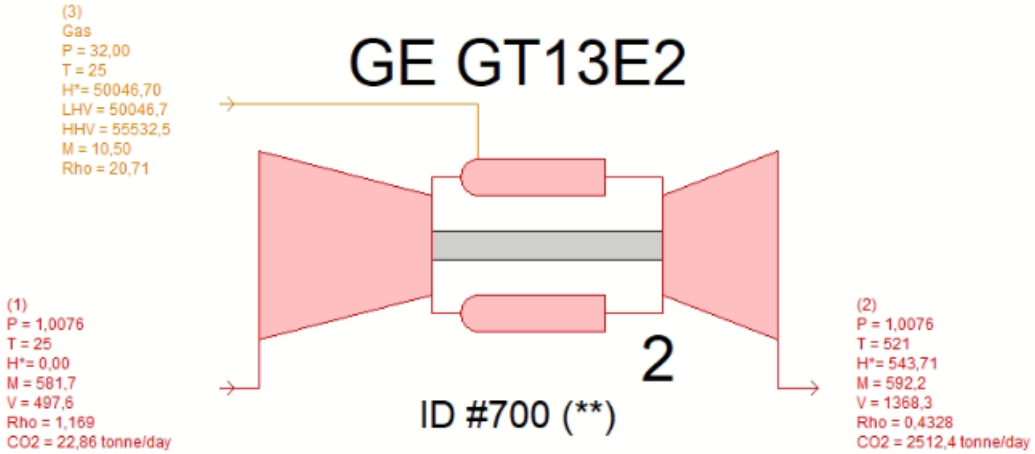

Figure 2.1: GT13E2 gas turbine's layout [28]

All the following on-design calculations will be based on these data. In nominal conditions the exhaust gases have a mass flow rate m_{hs} of 592.2 kg/s and a maximum temperature $T_{hs,max}$ of 521°C. The nominal molar composition of the flue gases is shown in the table below.

Table 2.2: Exhaust gases composition at the outlet of the turbine

xO_2	xCO_2	xH_2O	xN_2	xAr
0.136	0.032	0.081	0.742	0.009

The total net electrical power output in ambient conditions is 198.22 MW, while the heat power inlet is 525 MW, considering a natural gas with LHV of 50 MJ/kg and a flow rate of 10.5 kg/s. Hence, the total efficiency is roughly 37.8%.
The minimum temperature of the heat source $T_{hs,min}$ is set to 90°C, in order to avoid any formation of acid condenses and fouling on heat transfer surfaces.
The flue gases specific heat $c_{p,hs}$ is computed as a function of the temperature and the composition of the gases, with $T_{hs,min}$ equal to 90°C.

2.4. sCO_2 cycle components

sCO_2 power cycles are composed of a limited number of components. Their simple layout represents an important advantage with respect to steam Rankine cycle.
Turbomachines, primary heaters, recuperators, and heat rejection units are well known and proven for steam cycle applications, whereas for sCO_2 cycles they are still under development and study because of the fluid properties and working conditions that pose several challenges in terms of design and operation [24].
In this section, the principal technological solutions that could be adopted for each component are described as well as their technological readiness, and the main assumptions related to each component and employed in the simulation is reported.
First of all, a brief review is provided about the most studied materials for sCO_2 power cycle applications.

2.4.1. Materials

Material selection for sCO_2 energy system components is not a trivial issue, as the selected materials must withstand significant mechanical and thermal stress when exposed to high temperature (500–800°C) and high pressure (20–30 MPa) environments. The key components concerning material's selection are the primary heater, the recuperators, especially the high temperature one, and the turbine.
Since the CO_2 temperature is much lower, compressors will not experience thermal corrosion. However, they may be subject to electrolytic corrosion if the CO_2 purity is not high enough and water contamination is present [34].
Turbines and primary heaters are susceptible to high temperature corrosion phenomena, mainly oxidation and carburization. The design of the main heater must carefully consider the trade-off between the manufacturing cost of the component and its performance. While the adoptions of expensive high performance nickel-based superalloys is allowed for sCO_2 turbines due to their compact structure.

Several different classes of metal are generally employed for the power system's components depending on their operating temperature and pressure.
In Figure 2.2 four possible material solutions are depicted considering the allowable stress for each of them as a function of the metal temperature

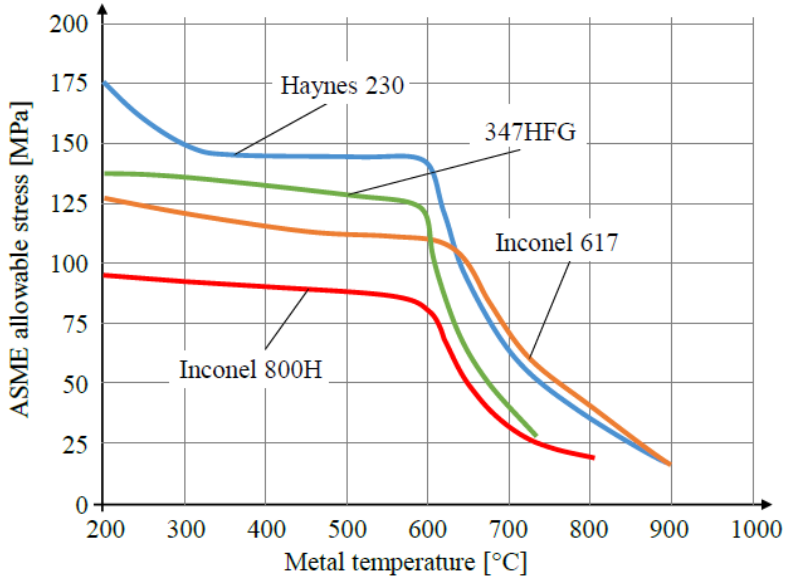

Figure 2.2: ASME Boiler and Pressure Vessel code allowable stresses as a function of operating temperature for three Nickel-based alloys (Inconel 800H, Inconel 617 and Haynes 230) and one stainless steel (347HFG) [31]

At operating temperatures below 650°C conventional stainless steels can generally be used, while above 650°C more expensive nickel-based alloys are required as they have better corrosion resistance, and they can ensure the required pressure without incurring in excessive material thickness.
Gas turbines bottoming cycle applications fall into the first category because they operate at lower temperatures and pressures than solar or nuclear powered sCO_2 cycles. As a result, cheaper materials can be used, reducing the overall capital cost of the power plant.

2.4.2. Turbomachinery

Turbomachines play a key role in sCO_2 cycles. They are required to handle high variations of mass flow rate since the main objective is to provide high flexibility. The thermodynamic and transport properties of sCO_2 lead either to advantages or challenges in the turbomachinery design.
One significant advantage, already mentioned in the sCO_2 thermodynamic properties paragraph, is related to the high CO_2 density near the critical point resulting in the possibility to design very compact turbomachines.

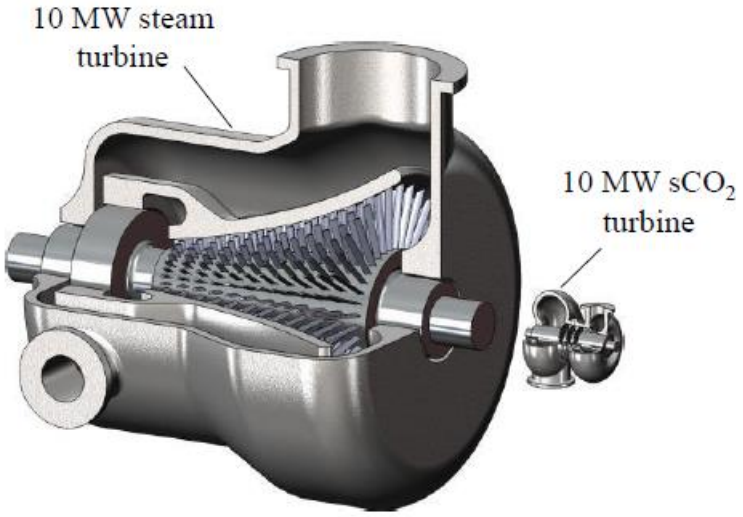

Figure 2.3: Size comparison between a 10 MW steam turbine and a sCO_2 turbine with the same power output [32]

Figure 2.3 shows a size comparison between a 10 MW turbine for steam (left) and sCO_2 (right). This compactness leads to less material required for the component's construction and consequently a reduction of manufacturing costs and footprint. On the other hand, these reduced dimensions bring high rotational speeds in order to guarantee high efficiencies. Therefore, such small mean diameters and such high rotational speeds lead to significant disk windage and leakage losses which can be mitigated only by advanced sealing systems.

2.4.2.1. Compressors

In the most studied sCO_2 cycle layouts up to two compressors can be employed. The first one, which has inlet condition near the critical point, is more difficult to design and control due to the high gradient of physical properties of sCO_2 with respect to pressure and temperature, as it was mentioned in the sCO_2 thermodynamic properties paragraph. Moreover, sCO_2 shows a substantial deviation from the ideal gas law with a compressibility factor Z ranging between 0.2 - 0.6 [18]. The cavitation phenomena may occur when the sCO_2 flow approaches the critical point under real gas conditions. It is therefore necessary to design a proper impeller to mitigate the effect of phase change and maintain the performance of the turbomachine [33].

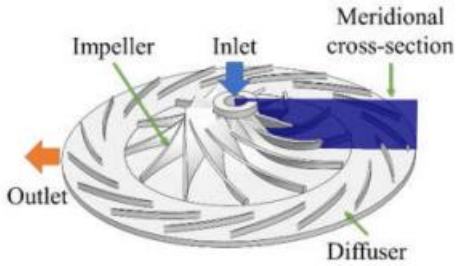

Figure 2.4: Geometric design of the compressor [33]

The second compressor is present only in few layouts. Having the input conditions far from the critical point it does not have the same problems as the main compressor, and it is generally easier to design.

In sCO_2 power cycles, it is generally preferred to employ centrifugal compressors regardless the cycle sizes, as this type is well suited to deal with the wide density fluctuations occurring near the critical point. In most studies, 85% is an accepted isentropic efficiency for either the main or recompression compressors [34]. Thus, this value is selected also as the nominal design efficiency of the compressors considered in this thesis work.

2.4.2.2. Turbines

Unlike compressors, turbines work at a significant distance from the critical point, hence the ideal fluid behavior of sCO_2 permits an easier design.
Considering off-design operations, adjustable guide vanes are not suitable in this case because it is impossible for them to reach the 30% load target. The solution to keep a good efficiency is hence operating in sliding pressure at partial load [24].
Special attention must be paid to the aerodynamic optimization of the inlet and exhaust as well as the blade path since the high density of sCO_2 is associated with high losses at high velocities [17].

Usually above 30 MW of net power output, it is preferable to use axial turbines. Regarding efficiency, several works on sCO_2 power applications suggest 90% as a standard and accepted isentropic efficiency assumption [34] for mid-to-large scale systems, as the expander design is not as complex as the compressor one thanks to the ideal gas behavior of CO_2 along the expansion and the larger volumetric flow rates. As in this work an sCO_2 power cycle of large scale is investigated (power output above 50 MW), an axial turbine is considered with a nominal isentropic efficiency value of 90%.

2.4.3. Primary heat exchanger (PHE)

The primary heat exchanger (PHE) has the task to transfer the thermal power from the heat source to the sCO_2 stream. The choice of the heat exchanger type to employ is not straightforward as it strongly depends on the considered application and the heat source.
The main classification can be made between direct or indirect primary heaters.
As in this work the flue gases exploited are fairly clean, a direct primary heater is selected and designed as a finned tube heat exchanger. The main assumptions selected for the PHE in this work are shown in Table 2.3.

Table 2.3: Main assumptions for the PHE design

PHE	
HX type	Finned tube HX
Tube internal diameter [mm]	20
Ratio of tube pitch to external diameter	1.25
Ratio of finned to plain external area	12
Tube material	Inconel 617
Heat transfer coefficient flue gas side	125 W/m^{2}K
Heat transfer correlation CO_2 side	Dittus-Boelter

2.4.4. Recuperators

The relatively small pressure ratio in sCO_2 power cycles, together with the high turbine outlet temperature, make mandatory the adoptions of recuperators to recover the great amount of CO_2 residual thermal power at the turbine outlet and enhance internal recovery efficiency.
As it was mentioned in the thermodynamic properties, compared to water/steam layouts sCO_2 does not have phase change occurring in the heat exchangers. Thus, the lower temperature differences between the two fluxes improve heat transfer performance.
Recuperators must withstand high temperatures and pressures and at the same time guarantee safe operation considering the large pressure difference between hot and cold sides. Having high pressure on one side of the recuperator helps to improve the heat exchanged process and to reduce pressure drops, but induces greater material thicknesses for piping, raising the costs.
Dealing with high temperatures is the other aspect to be analyzed. The use of expensive high content nickel alloys should be avoided because it would increase costs exponentially, as heat exchangers represent a large part of components expenditure. Hence, the temperature range should be compatible with the use of stainless steels, even if they should be in accordance with corrosion constraints.
The best solution for the recuperator's design is a compact heat exchanger structure featuring high thermal efficiency and thermomechanical strain tolerance. Other advantages are the reduction of the overall footprint and the limitation of the fluid inventory.

There are two main candidates architectures for this component:

i. Printed circuit heat exchangers (PCHEs)

Printed circuit heat exchangers (PCHEs) are well known and already employed in sCO_2 cycles. This type of recuperator is very compact (up to 1300 m^2/m^3 of surface area density [35]), robust, and features a high effectiveness. The CO_2 hot and cold streams generally flows through the heat exchanger in a counter-current or cross-flow (see Figure 2.5) arrangement, inside straight channels with a semi-circular cross-section. Even if straight channels are the most widely adopted and studied, other geometries can be realized, such as that one with zigzag channels or channels formed by S-shaped fines or by airfoil fins. The selection of a different kind of geometry allows to match the required exchanged thermal power and pressure-drop constraints.

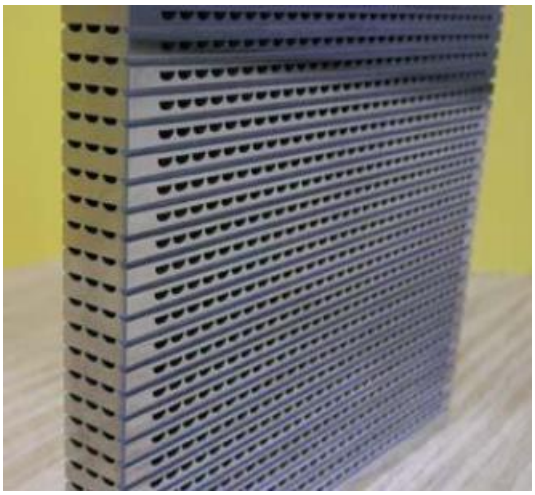

Figure 2.5: Section of a cross-flow PCHE with straight channels manufactured by HEATRIC [35]

ii. Plate and fins heat exchangers (PFHEs)

Plate and fins heat exchangers (PFHEs) are considered as a possible cost-effective alternative to PCHEs for sCO_2 recuperators. The structure is composed by corrugated metals fins arranged between flat plates and joined together by brazing. The fins geometry enhances the heat exchanger performance by remarkably increasing the available heat transfer surface. In addition, the PFHE technology allows for a compact and versatile design, it presents low weight per unit surface and a consequent small thermal inertia which could lead to fast transient operation.

Figure 2.6: Core assembly of a cross-flow plate and fin heat exchanger [36]

The main issue of this component is related to its mechanical resistance, which is significantly lower than PCHE technology [37]. However, some promising materials have been studied and tested as the 316Ti prototypes [38]. This solution allows the use of PFHE up to 500°C and for pressures up to 210 bar, conditions which are sufficient for their use in bottoming cycle application.

Among the two options, it is decided to choose the first one (i.e. PCHEs) for the recuperators included in the configurations studied, including LTR and HTR, since the technology is already widely used in sCO_2 power cycle applications. The heat exchanger material selected is the SS 316 due to the relatively low temperatures range. The main assumptions are reported in Table 2.4.

Table 2.4: Main assumptions for the recuperator design

REC/LTR/HTR	
HX type	PCHE
Thickness of plate [mm]	1.5
Diameter of the semi-circular channel [mm]	2
Thickness of wall between channels [mm]	0.4
Heat exchanger material	SS 316
Heat transfer correlation hot side	Gnielinski
Heat transfer correlation cold side	Gnielinski

2.4.5. Heat rejection unit (HRU)

The heat rejection unit (HRU) has the aim to cool down the CO_2 to the desired compressor inlet temperature (CIT). For this reason, the design of the HRU is not trivial and may strongly affect the operation of a sCO_2 power plant, especially because of the large volume of fluid contained in the component.

Depending on the availability, the cooling fluid could be either ambient air or water coming from a river or a sea. In this section, three possible HRU solutions are proposed:

i. Direct dry air-cooled

The technology uses ambient air drafted or pushed by fans to cool down the working fluid. The sCO_2 stream flows inside tube bundles generally arranged in V-shaped bays to reduce air-side pressure drops and component footprint.

Figure 2.7: LU-VE EHVD CO_2 gas coolers model designed for refrigeration industry [39]

Air-cooled HRUs permit to eliminate the power plant water consumption. Another positive characteristic is related to the numerous similarities with the CO_2 gas coolers and condensers adopted in the refrigeration industry (Figure 2.7). In particular, for both applications the CO_2 inlet temperature and pressure vary in the range 80-120°C and 60-100 bar respectively, and the CO_2 goes through a similar transformation with a final temperature close to the critical point [40]. This feature should allow a technological transfer from refrigeration industry to the power production sector with a consequent reduced manufacturing costs and economies of scale.

ii. Indirect dry air-cooled

An intermediate closed water circuit is used for indirect dry air-cooled HRU to transfer the heat from the supercritical fluid to the ambient air. The main advantage of water-to-CO_2 heat exchangers compared to air-to-CO_2 heat ones is a more compact design, resulting in easier control and lower pressure losses on the CO_2 side.
On the other hand, additional heat exchanger and intermediate circuit increase the investment cost of the system, while additional pump consumption and higher heat transfer temperature differences due to the intermediate water circuit reduce overall efficiency.

iii. Water-cooled

Water-cooled CO_2 coolers are usually designed as printed circuit or shell and tube heat exchangers. Using water requires more compact and efficient components, but also more maintenance due to corrosion and erosion issues.
S&T heat exchangers can be designed with the cooling stream flowing either in the shell side or in the tube side. The second arrangement facilitates cleaning of the tubes and allows them to be inspected individually for maintenance. Water velocities below 1 m/s and temperatures above 50°C should be avoided to prevent excessive deposition of sediments, which can lead to scaling and localized corrosion, while the maximum water speed is generally set at 2.5 m/s to prevent erosion [41].

In the following analyses it is decided to adopt the water-cooled system in the nominal study, while regarding the part-load and off-design analysis air cooling will also be investigated, in that case therefore a direct dry-air cooled system will be employed.
The main assumption for both water-cooled and direct dry-air cooled HRU are listed respectively in Table 2.5 and in Table 2.6.

Table 2.5: Main assumptions for the water cooled HRU design

HRU	
HX type	Shell&Tube
Tube internal diameter [mm]	20
Ratio of tube pitch to external diameter	1.25
Heat exchanger material	Copper/Aluminum
Heat transfer coefficient water side	7500 W/m^{2}K
Heat transfer correlation CO_2 side	Gnielinski

Table 2.6: Main assumptions for the direct dry-air cooled HRU design

HRU	
HX type	Direct dry-air cooled
Tube internal diameter [mm]	7.5
Ratio of tube pitch to external diameter	1.3
Ratio of finned to plain external area	12
Heat exchanger material	Copper/Aluminum
Nominal air heat transfer coefficient	75.8 W/m^{2}K
Heat transfer correlation CO_2 side	Gnielinski

2.5. Design assumptions

After having discussed the sCO_2 cycle's components and selected their typologies and the various assumptions. This section contains additional hypothesis made during the following sections.

Table 2.7: sCO_2 cycle's assumptions [34]

Minimum cycle temperature [°C]	33
Minimum PHE pinch point, $\Delta T_{pp,PHE}$ [°C]	25
Minimum recuperators/LTR/HTR pinch point, $\Delta T_{pp,rec}$ [°C]	10
Cooling water inlet temperature [°C]	20
Cooling water temperature rise [°C]	7
Cooling water Δp [bar]	1.5
PHE sCO_2 Δp $\left(\Delta p / p_{in}\right)$	4%
HRU sCO_2 $\left(\Delta p / p_{in}\right)$	2%
Recuperator sCO_2 hot side $\left(\Delta p / p_{in}\right)$	2%
Recuperator sCO_2 cold side $\left(\Delta p / p_{in}\right)$	0.4%
Turbine isentropic efficiency, $\eta_{iso,turb}$	90%
Compressor isentropic efficiency, $\eta_{iso,comp}$	85%
Water pump efficiency, $\eta_{water,pump}$	75%
Mechanical efficiency, η_{mec}	99%
Generator electrical efficiency	98.5%
Motor electrical efficiency	96.5%
Fan efficiency, $\eta_{air,fan}$ *	75%

* this assumption is used only in the part load analysis

To avoid operations in the two-phase fluid conditions, the minimum cycle temperature is set at 33°C, in order to exploit the high CO_2 density along compression due to real gas effects and to achieve low compression work and high cycle efficiency. All the pinch points of the recuperators, including HTR and LTR, are constant and equal to 10°C in order to fix the heat exchanger's area. While the PHE's one is 25°C [42].
The cooling water pump hydraulic efficiency is assumed equal to 75%, with an inlet HRU's temperature of 20°C, a maximum rise of 7°C and a pressure drop of 1.5 bar.

These last assumptions are taken from the literature, and they respect the usual range deployed in power generation applications [34].
Pressure losses through the PHE are relative and set to a value of 4%, while for the HRU and the hot side of the recuperator this value is equal to 2% [34].
Regarding the cold side of the recuperator, having the same number of channels of the hot side, and the same CO_2 mass flow rate (apart from the configurations including a bypass), its pressure drop is strictly linked to the one of the hot side. So, a value equal to 0.4% has been chosen by analyzing the density ratios between the hot and cold side CO_2 streams.
These and other hypothesis for the sCO_2 cycle are summarized in Table 2.7.

2.6. Cycle configurations

Seven configurations are studied and optimized, considering a heat source with variable temperature, typical of WHR applications.
Of the considered cycle configurations, five are already implemented in the numerical code: (i) the simple recuperative cycle (SRC), (ii) the recompressed recuperative cycle (RRC), (iii) the simple recuperative cycle with recuperator bypass (SRCB), (iv) the recompressed recuperative cycle with high temperature recuperator bypass (RRCB) and (v) the turbine split flow cycle (TSF) [42].
For what concern the other two, they are fully developed and implemented by the thesis author: (vi) the single heated cascade cycle (SHC) and (vii) the dual heated cascade cycle (BHC). They are particularly novel architectures tailored for WHR application as resulted from the literature review and a preliminary analysis.

2.6.1. Simple recuperative cycle (SRC)

The first configuration considered is the simple recuperative cycle (SRC). Apart from the non-recuperative simple cycle, this is the easiest possible design. The temperature at the outlet of the compressor (point 2) is increased up to the inlet of the PHE (point 3) by a recuperator that recovers heat from the outlet of the turbine (point 5).

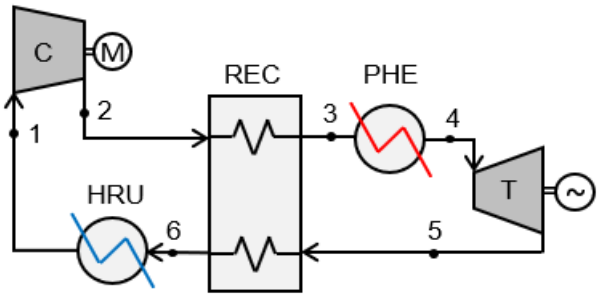

Figure 2.8: Simple recuperative cycle (SRC) layout

In WHR applications, the nominal design of the recuperator should be optimized to guarantee an optimal trade-off between the heat exchanged in the recuperative heat

exchanger and the heat exploited by the available heat source. Large recuperator surfaces can be detrimental for the recovery efficiency of the cycle.
As previously stated, sCO_2 cycle must operate with a minimum temperature and pressure sufficiently close to the critical point to decrease the compression work. On the other hand, real gas effects lead to a limitation of the efficacy of the recuperator. The difference in specific heat capacity of sCO_2 between the cold and the hot streams causes a significant temperature difference that increases going towards the hot end (Figure 2.9), raising the irreversibility due to the heat exchanged.

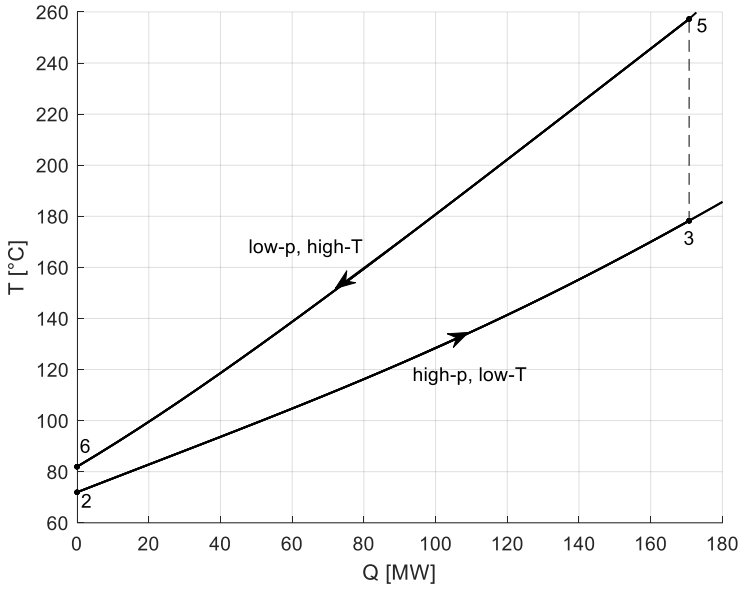

Figure 2.9: T-Q diagram of the recuperator in the SRC

In order to mitigate this penalization, the heat capacity of the two streams should be matched by regulating the cold side mass flow rate. A possible way is to place a flow split just before entering the recuperator, as it can be seen in the following cycle.

2.6.2. Recompressed recuperative cycle (RRC)

The second configuration investigated is the recompressed recuperative cycle (RRC). The splitter is placed at the hot side of the LTR outlet (point 8). The first fraction (8_a) is cooled down by the HRU and compressed in the main compressor, then it enters the LTR (point 2) where at the outlet is gathered with the other fraction. The second part is directed to the second compressor (point 8_b) which increases its pressure up to the one of the stream coming from the LTR cold side just before the mixing of the two flows.

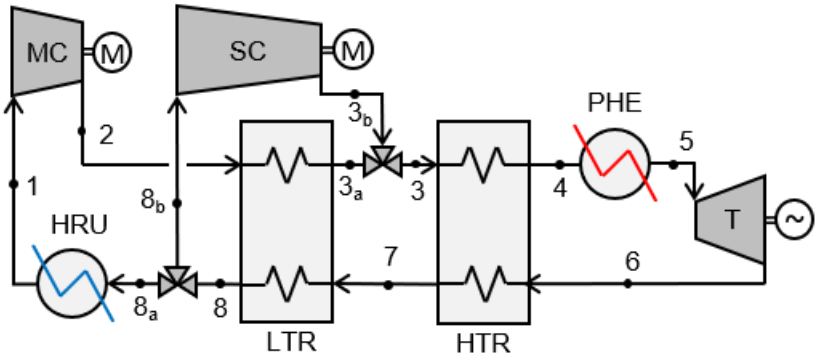

Figure 2.10: Recompressed recuperative cycle (RRC) layout

The advantage of this split is represented by the increase of thermodynamic efficiency of the cycle due to the balancing of the heat capacities between streams in the LTR, limiting the temperature differences in the heat exchanger and the irreversibility related to the heat transfer process.

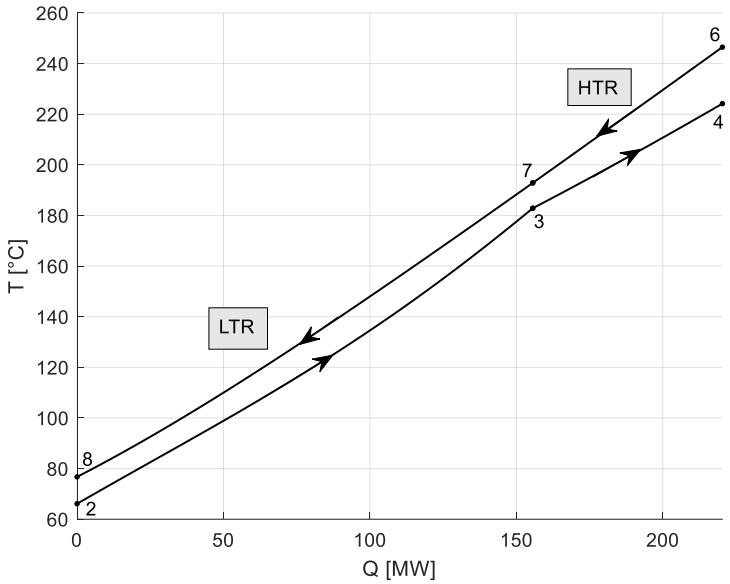

Figure 2.11: T-Q diagram of LTR and HTR in the RRC

However, the high effectiveness of the internal recuperative process may limit the exploitation of the variable temperature heat sources, especially if characterized by a high cooling rate, leading to a lower recover efficiency and a consequent reduction of the power output. For this reason, this configuration is widely proposed in literature for applications with a high average temperature of the heat source, such as CSP and nuclear power plants.

Both simple recuperative cycle and recompressed recuperative cycle have the possibility to introduce a recuperator bypass where a part of the sCO_2 is split and heated up by the flue gases in a secondary heater. This allows to reduce the

temperature difference in the recuperator and to increase the heat source exploitation by further cooling of the exhaust gases.

2.6.3. Simple recuperative cycle with recuperator bypass (SRCB)

In the simple recuperative cycle with recuperator bypass (SRCB) the recuperator split is at the inlet of the cold side of the recuperator (point 2). The first stream (point 2_a) goes as before through the recuperative heat exchanger, but the second one (point 2_b) is directed to the bypass heat exchangers. At the outlet the two fluxes are gathered, and the rest of the cycle does not change following the scheme of the SRC.
This configuration is particularly interesting as it features good heat recovery and conversion efficiencies while maintaining a simple plant layout.

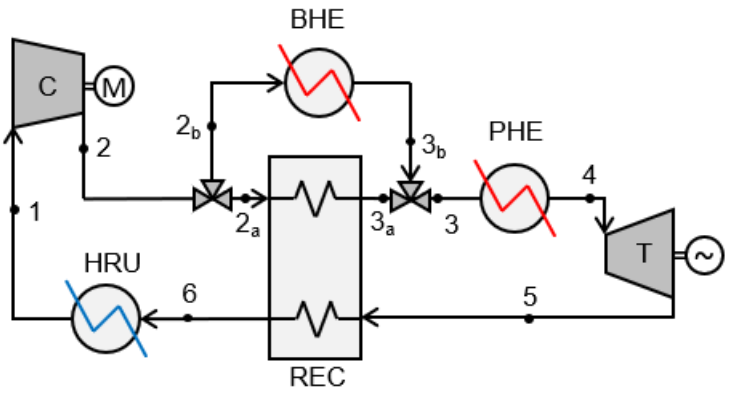

Figure 2.12: Simple recuperative cycle with recuperator bypass (SRCB) layout

2.6.4. Recompressed recuperative cycle with high temperature recuperator bypass (RRCB)

In the recompressed recuperative cycle with high temperature recuperator bypass (RRCB) the split fraction is at the inlet of the cold side of the HTR (point 3). The first part goes as before through the HTR cold side, while the second one is directed to the bypass heat exchanger. At the outlet the two streams are reunited, and the cycle goes on like the RRC.
This modification allows to mitigate the issues caused by the high sCO_2 temperature at the PHE inlet, which are typical of recompressed layouts, and it combines a higher heat recovery factor and a higher thermodynamic efficiency at the expense of an additional heater.

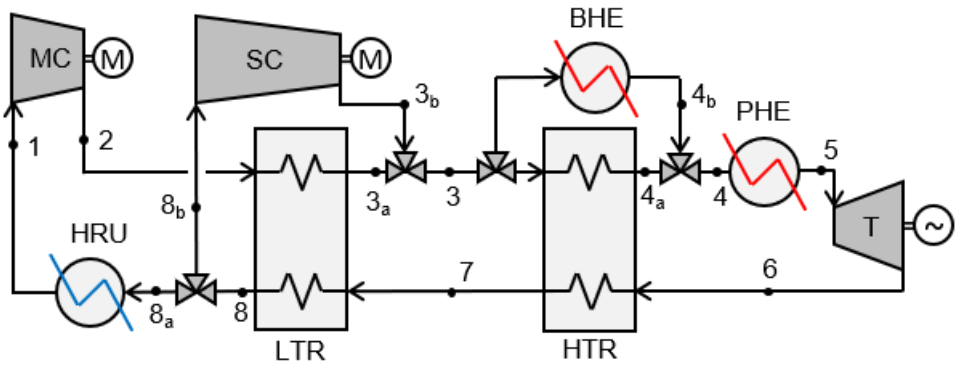

Figure 2.13: Recompressed recuperative cycle with high temperature recuperator bypass (RRCB) layout

2.6.5. Turbine split flow cycle (TSF)

The fifth configuration is the turbine split flow cycle (TSF). This layout has two turbines and one compressor, and it aims to minimize the temperature differences in the recuperators and to enhance the WHR efficiency.

The stream at the outlet of the compressor (point 2) is split and the first fraction reaches the inlet of the first turbine (point 4_a) after being heated up in the LTR and by the burned gases in the PHE. The residual heat available at the outlet of the turbine is used for the second stream fraction in the HTR, then it goes to the inlet of the second turbine (point 3_b). While the residual heat at the outlet of the second turbine is used in the LTR to heat up the first stream.

As a result, this cycle configuration enables a better exploitation of the heat source than the precedent cycles, but it has a more complex layout.

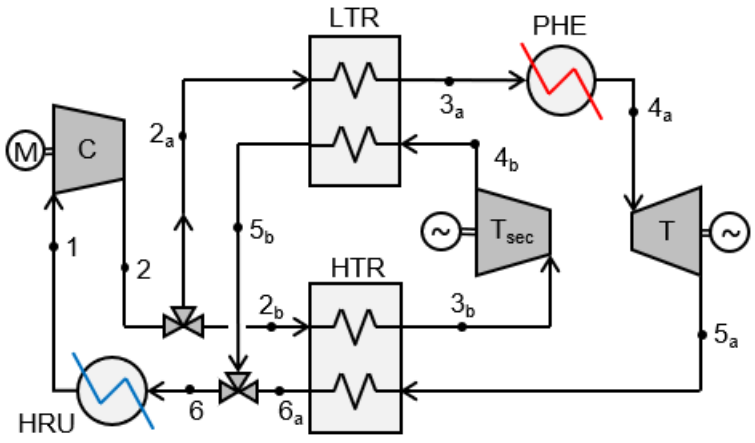

Figure 2.14: Turbine split flow (TSF) layout

Considering now the two new configurations implemented. Bibliographic research was carried out to find the optimal layouts.

2.6.6. Single heated cascade cycle (SHC)

The single heated cascade cycle (SHC) was immediately considered as one of the best candidates because it has the same number of components of the turbine split flow already implemented. The difference is the arrangement of the three heat exchangers. In this cycle the residual heat to reject can be minimized with two recuperation processes before the cooler, and the heat input can be enhanced due to the increased recovered heat, which is used for expansion process in a secondary turbine. Although there is only one heater, the final exhaust outlet temperature is quite low [43].
Considering the layout's structure: there is a split at the outlet of the compressor (point 2). The first stream goes directly to the PHE (point 2_a), it reaches the maximum temperature of the cycle, and it enters the first turbine (point 3_a). The residual heat at the outlet of the first turbine is exploited in the HTR where the other stream is heated up to the inlet of the second turbine (point 4_b). The outlet of this turbine is mixed with the hot flow of the HTR. To reduce the irreversibility due to the mix, the difference temperature between the two fluxes must be chosen as the closest possible to zero. Finally, the whole fluid is cooled down in the LTR where it gives heat to the second fraction.
Having the inlet of the PHE at the same condition of the outlet of the compressor gives the opportunity to decrease the outlet temperature of the exhaust gases therefore improving the utilization of the available sensible heat from the heat source.

2.6.6.1. Brief literature review of the SHC

Min Seok Kim et al. [43] made a comparison of nine sCO_2 bottoming power cycles, including the SHC layout, in conjunction with a topping cycle of landfill gas (LFG) fired 5 MWe gas turbine. A sensitivity study of the cycle design parameters for each of them is conducted and each thermodynamic performance is evaluated. It is found that a recompression cycle is not suitable for the bottoming system application, while the SHC has a relatively high net produced power, although the best configuration turns out to be the SRCB, which has a lower power output but a simpler layout with fewer components.
Brighenti et al. [44] presented a preliminary assessment of sCO_2 bottoming power plant's physical footprint with the aim of quantify trade-offs between cycle efficiency and plant complexity. They recommended the SHC for further investigation as it showed the best compromise between performance and physical footprint.
Steven A. Wright et al. [45] compared the SHC with the SRC, used as a reference power cycle. The improvements in power output are always featured considering different types of gas turbine topping cycle. However, even though the SHC system tends to produce more power and annual revenue than the reference case, the increased capital costs lower the rate of return, indicating that simpler sCO_2 bottoming cycles may offer the best economic benefit.

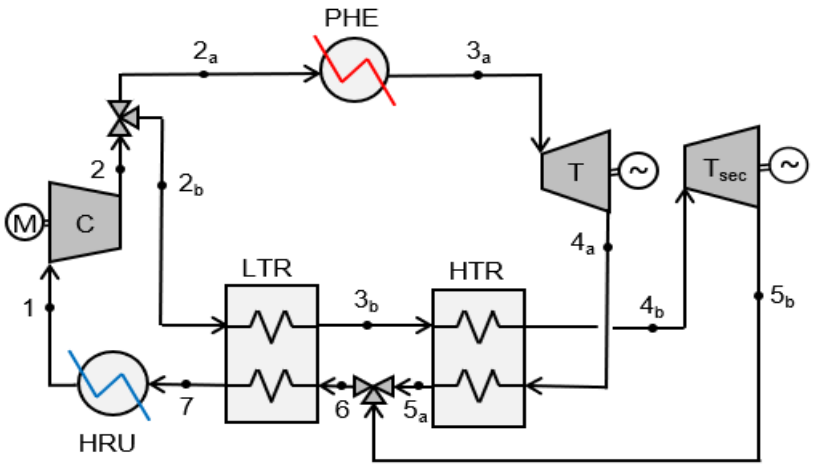

Figure 2.15: Single heated cascade (SHC) layout

2.6.7. Dual heated cascade cycle (BHC)

The final layout studied is the dual heated cascade cycle (BHC).
The dual heated cascade cycle's main difference from the single heated cascade cycle is an additional heater ahead of the first turbine. Since working fluid enters the cooler after two recuperation processes, the waste heat is minimized, and the recovered heat is used in the expansion process of a secondary turbine [43].
Having a look at the structure: as the SHC the split is at the outlet of the first compressor (point 2). The first stream is heated up in three heat exchangers (LTR, HTR, PHE) before entering the first turbine (point 5_a). While the second fraction goes though the secondary heat exchanger, and it enters the second turbine (point 3_b). Then at the outlet it mixes with the outlet hot side of the HTR (point 7_a), and the split is close.
It is studied because it shows high recovery efficiency, thanks to the double heat exchangers with the exhaust gases. It is also capable of increasing the cycle efficiency with respect to the SHC, thus it has a significant total efficiency.
On the other hand, the main drawback is the complexity and the number of components, which is the highest value among the layouts studied.

2.6.7.1. Brief literature review of the BHC

Gianluca Carraro at al. [46] suggest the high potential of the dual heated cascade cycle with always a power output greater than or equal to the one of SRCB, considered as the benchmark case in their report. As regards configurations with one splitter-junction couple, the dual heated cascade layout outperforms the SRCB for heat source temperatures of 500°C and 700°C, improving the power output respectively by 7.7% and 7.1%.

Min Seok Kim et al. [43], in addition to the SHC, also investigated the BHC, finding how it has the highest net power output among the nine configurations analyzed, however it has disadvantages of possessing a high number of components and complex operations which require more sophisticated process strategies.

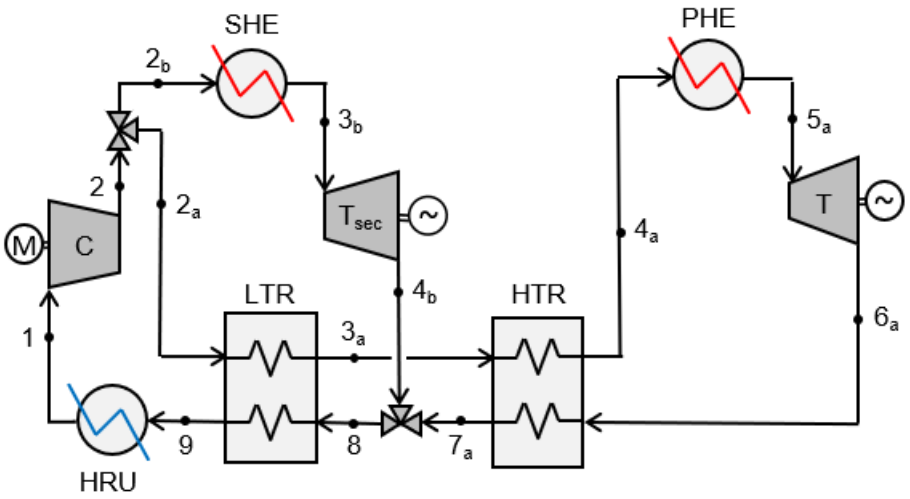

Figure 2.16: Dual heated cascade (BHC) layout

2.7. Energy analysis

The governing equations for steady state conditions are the mass and energy balances. For each component of the system (i.e. heat exchangers and turbomachinery) equations (1) - (2) respectively apply:

(1) $\dot{m}_{in} = \dot{m}_{out}$

(2) $\sum_{j=1}^{IN} \dot{m}_{in} h_{in} = \sum_{j=1}^{OUT} \dot{m}_{out} h_{out} + \dot{Q}_{out} + \dot{W}_{out}$

Isentropic efficiencies are applied for the turbomachines following the two equations below respectively for the compressors (3) and the turbines (4):

(3) $\eta_{iso,comp} = \frac{h_{out,iso} - h_{in}}{h_{out} - h_{in}}$

(4) $\eta_{iso,turb} = \frac{h_{in} - h_{out}}{h_{in} - h_{out,iso}}$

Electrical power produced by the turbines or required by the compressors is computed following the equations (5) and (6). The parameters η_{mec} (mechanical efficiency) and η_{el} (electrical efficiency) are reported in Table 2.7. In addition, there is the consumption of the HRU auxiliaries, pumps or fans according to the cooling fluid employed.
Then the net power output can be found with the equation (7):

(5) $\dot{W}_{comp} = \dot{m}_{comp}(h_{comp,out} - h_{comp,in})/(\eta_{mec}\eta_{el})$

(6) $\dot{W}_{turb} = \dot{m}_{turb}(h_{turb,in} - h_{turb,out})\eta_{mec}\eta_{el}$

(7) $\dot{W}_{net} = \sum_{j=1}^{n^\circ turb} \dot{W}_{turb,j} - \sum_{i=1}^{n^\circ comp} \dot{W}_{comp,i} - \dot{W}_{aux}$

Finally, by computing the maximum thermal power exploitable from the heat source (8) and the thermal power entering the cycle (9), four thermodynamic efficiencies are evaluated. The thermodynamic efficiency of the cycle (10), the thermal recovery efficiency (11), the total efficiency (12) and the power plant combined efficiency (13).

(8) $\dot{Q}_{max,hs} = \dot{m}_{hs}(h_{hs,max} - h_{hs,min})$

$h_{hs,min}$ is function of $T_{hs,min}$ that is the minimum temperature at which flue gases can be discharged into the environment.

(9) $\dot{Q}_{in,cycle} = \dot{m}_{hs}(h_{hs,max} - h_{hs,out})$

(10) $\eta_{cycle} = \frac{\dot{W}_{net}}{\dot{Q}_{in,cycle}}$

(11) $\eta_{rec} = \frac{\dot{Q}_{in,cycle}}{\dot{Q}_{max,hs}}$

(12) $\eta_{tot} = \eta_{cycle}\eta_{rec} = \frac{\dot{W}_{net}}{\dot{Q}_{max,hs}}$

(13) $\eta_{cc} = \frac{\dot{W}_{net} + \dot{W}_{net,gas\ turbine}}{\dot{Q}_{in,gas\ turbine}}$

2.8. Thermodynamic optimization

2.8.1. Methodology

The configurations are optimized by varying: (i) the compressor inlet pressure (CIP), (ii) the turbine inlet temperature (TIT) and (iii) the temperature differences between streams in the mixing processes.

The maximum cycle pressure and the minimum cycle temperature are set constant and equal respectively to 250 bar and 33°C. They are not optimized because the optimizer would push them respectively to the upper and to the lower bound of the interval.

A value equal to 10°C is chosen for all the pinch points of the recuperators, while the PHE's one is computed from the analysis considering a minimum value of 25°C. These values should be optimized from a technical-economic point of view, but in this first thermodynamic analysis, it is decided to keep them constant, as the optimizer would push their value to the lower bound.

Cycle maximum temperature (TIT) must be optimized because an increase of this variable will be beneficial for the efficiency of the cycle, while it will be detrimental for the recovery efficiency, hence a trade-off is needed.

The parameters (i) and (ii) are optimized by a dedicated optimization algorithm in Matlab, while parameter (iii) is varied by means of a sensitivity analysis and in all the cases the best option resulted to be a temperature difference of the mixing equal to zero (isothermal mixing).
The optimization algorithm selected to maximize the total efficiency of the cycle (equation 12 of the previous paragraph) is the *patternsearch* algorithm available in the Matlab optimization toolbox [25]. This algorithm is preferred to simple *fmincon* and complex *genetic* or *particle swarm* algorithms because it shows a good compromise between computational time and accuracy of the solution [18].
The optimization variables chosen for each cycle are reported in Table 2.8 with the range in which they are computed by the optimization algorithm.

Table 2.8: Optimization variables chosen for each cycle

	range	SRC	RRC	SRCB	RRCB	TSF	SHC	BHC
p_{min} [bar]	[50, 100]	X	X	X	X	X	X	X
T_{max} [°C]	[350, 550]	X	X	X	X	X	X	X
$dT_{mix,bypass,recup}$ [°C]	[-50, 50]			X				
$dT_{mix,bypass,HTR}$ [°C]	[-50, 50]				X			

All the other variables are fixed because either the optimization algorithm would push them to the upper-lower bounds, or their optimization is not relevant.
They are summarized in Table 2.9.

Table 2.9: Fixed variables chosen for each cycle

	Value	SRC	RRC	SRCB	RRCB	TSF	SHC	BHC
p_{max} [bar]	250	X	X	X	X	X	X	X
T_{min} [°C]	33	X	X	X	X	X	X	X
$dT_{mix,LTR}$ [°C]	0		X		X			
$dT_{hot,end,HTR}$ [°C]	10					X		
$dT_{mix,cascade}$ [°C]	0						X	X

2.8.2. Optimization variable analysis

For the SRC configuration, to understand the effect of each optimization variable on plant performance, a sensitivity analysis is carried out optimizing though a parametric approach both minimum pressure and maximum cycle temperature (at fixed optimal value of the other optimization variable).

2.8.2.1. CIP parametric analysis

Minimum cycle pressure is an optimization variable that needs to be studied. Increasing it decreases the specific volume of sCO_2, so the compression work reduces.

However, keeping fixed the maximum pressure of the cycle also the pressure ratio decreases, thus leading to a reduction in the expansion work. Hence, a trade-off between these two different effects is necessary to figure out what is the optimal minimum pressure value.
Furthermore, reducing the minimum pressure from the optimal value results in a sharper decrease in total efficiency than increasing it.
From Figure 2.18 it can be confirmed how the optimal value is in the range of 79 bar, more precisely 78.91 bar.

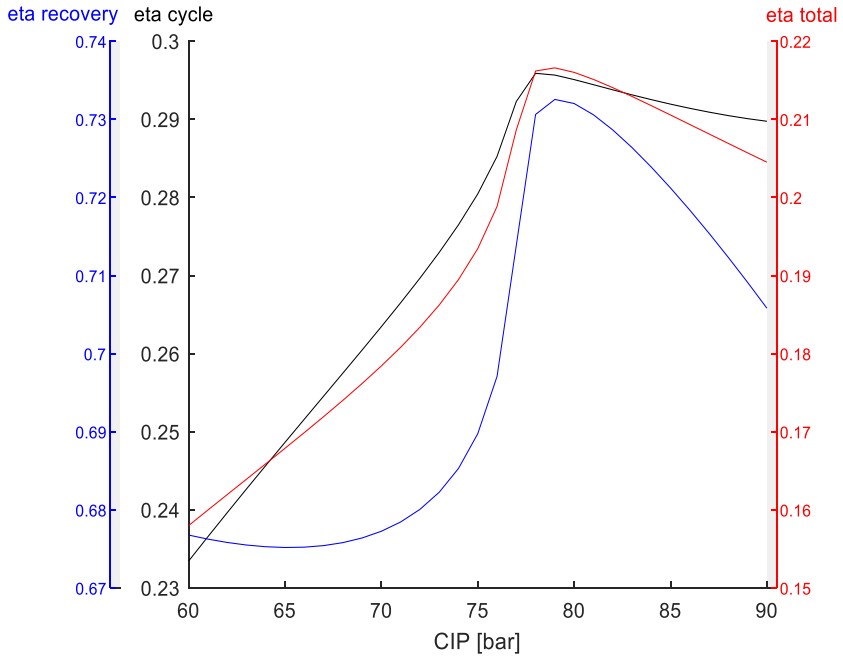

Figure 2.17: Cycle, recovery and total efficiencies of the SRC as a function of the CIP

2.8.2.2. TIT parametric analysis

Figure 2.19 (a) shows the trend of total thermodynamic efficiency as turbine inlet temperature changes. The optimum point is around 380°C, more precisely 379.55°C, as obtained from the optimization results.

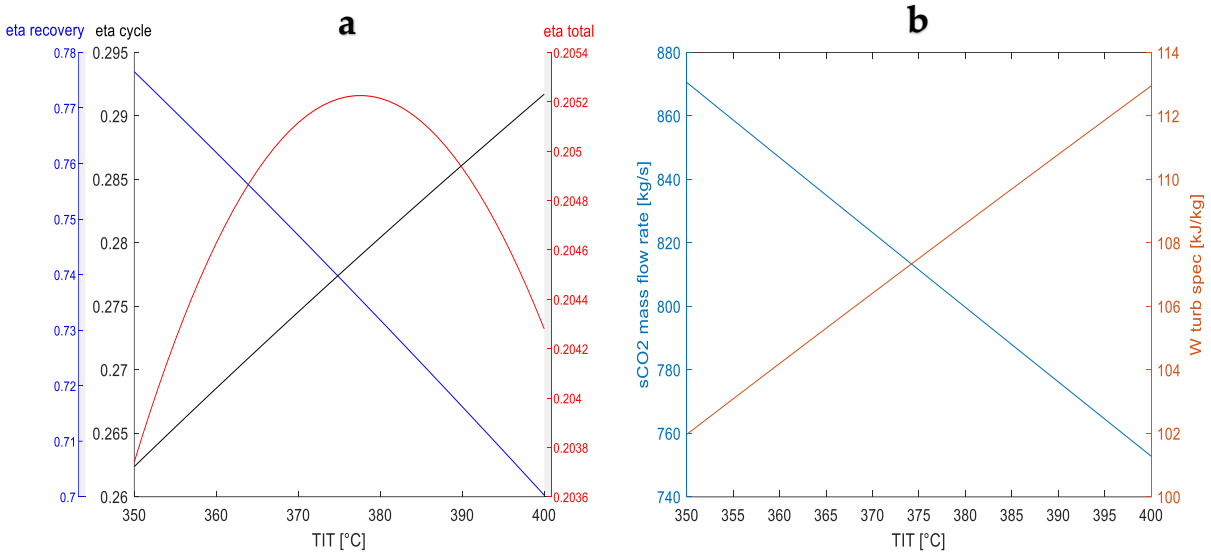

Figure 2.18: (a) Cycle, recovery and total efficiencies of the SRC as a function of the TIT (b) sCO_2 mass flow rate and specific turbine energy of the SRC as a function of the TIT

Moving from the optimal point towards higher TITs the cycle efficiency rises because the turbine's specific work increases (Figure 2.19 (b)). However, the heat source is exploited worse and the production of CO_2 is reduced (Figure 2.19(b)), leading the recovery efficiency to decrease.
On the other hand, decreasing TIT has the opposite effects, so specific work decreases along with cycle efficiency, while CO_2 production is enhanced due to the better exploitation of the heat source.
The combination of these impacts leads to the shape of the total efficiency curve.

2.8.3. Results

In this section, the main results are proposed reporting for each configuration the net power output, the cycle efficiency, the thermal recovery efficiency, the total efficiency and the combined cycle efficiency for the optimized operating parameters.

The best cycle efficiency is the one of the TSF (30.58%). However, it does not have a recovery efficiency of 100% as for other configurations, so it turns out that the cycle with the best total efficiency is the dual cascade (27.63%).

A recovery efficiency of 100% indicates that the cycle considered can cool down the exhaust gases to the minimum temperature indicated (i.e. 90°C in this case).
It is evident how the dual heat cascade cycle is the best performing layout, as it shows not only the highest power output but also a greatest recovery efficiency achieving a

remarkable combined cycle's efficiency of 52.56%. However, its main issues are the large number of components and the complexity in operation due to the double heater. The other new configuration implemented has quite comparable performance and cost to the TSF. The number of components is the same, but the heat exchangers are rearranged differently, leading the SHC to have lower cycle efficiency but better heat recovery from the exhaust gases.

Table 2.10: (a) Net powers and efficiencies results for each cycle

	SRC	RRC	SRCB	RRCB	TSF	SHC	BHC
W net [MW]	55.42	49.44	71.83	53.85	71.03	70.13	77.72
η cycle [%]	27.07	28.60	25.66	27.90	30.58	25.30	27.94
η rec [%]	72.81	61.46	99.54	68.64	82.59	98.56	98.91
η tot [%]	19.71	17.58	25.54	19.15	25.25	24.94	27.63
η cc [%]	48.31	47.17	51.44	48.01	51.29	51.11	52.56

Table 2.10: (b) Optimal results of the variable analyzed for each cycle

	SRC	RRC	SRCB	RRCB	TSF	SHC	BHC
p_{min} [bar]	78.91	81.91	80.93	91.13	79.01	78.88	79.44
T_{max} [°C]	379.6	366.0	357.0	361.4	496.3	496.3	455.0
$dT_{mix,bypass,recup}$ [°C]			≈0				
$dT_{mix,bypass,HTR}$ [°C]				≈0			

2.9. Techno economic analysis

A thermodynamic analysis alone is not sufficient to fully understand the commercial feasibility of the solution. For this reason, it is decided to study the configurations from an economic perspective as well.

2.9.1. Cost correlations

An evaluation of the capital investment cost for the seven cycle configurations is then carried out, where each component has a cost correlation from a NETL publication found in the literature [34]. Unfortunately NETL component cost correlations do not

include a specific one for sCO2/exhaust heat exchangers (BHE and PHE), so a different one is retrieved from a work by [9], [45].

All the cost correlations are function of a specific scaling parameter as in the following equation:

$$i_c = c_c(1) * s_p^{c_c(2)} * f(T)$$

Where:

- $i_c = investment\ cost$
- $c_c = cost\ coefficient$ is an array containing all the cost correlation values for each component
- $s_p = scaling\ parameter$
- $f(T) = Temperature\ correction\ factor$

The scaling parameter depends on the cycle component considered.
For turbines and compressors, it is the shaft power while for all the recuperators (LTR, HTR, HRU) and the PHE is the total heat transfer coefficient (UA_{tot}).

2.9.2. Results

After optimizing all the seven configurations from a thermodynamic point of view, the total investment cost and the specific cost are calculated through the functions already implemented in MATLAB. The specific cost is defined as the ratio between the total cost and the net power produced by the cycle.
Total investment and specific costs are here summarized for each cycle in Table 2.13.

Considering only the total investment cost, the simple recuperative cycle shows the lowest value among all layouts. This is due to the simplicity of the configuration and the fact that there are only five components operating.
The consideration does not change looking at the specific cost, hence the increase in complexity and thus a higher power output is not repaid in the others layout.
However, it is also observed the distribution of costs among the various components of the cycle. Therefore, a list of total investment costs for each component and for each cycle configuration is given below.

It is important to note that the sum of investment costs for each component is not pare to the total investment cost due to two additional costs:

- Engineering cost, due to all engineering decisions such as project development, risk analysis and budgeting.
- Contingency cost, which takes into account additional costs that may arise during the project phase or later.

These two values have been retrieved from NREL databases employed in system advisor modelling (SAM) software.

All costs have been converted from Dollars to Euros considering a currency exchange rate of 1.1 $/€.

Table 2.11: Cost composition for each configuration

	SRC	RRC	SRCB	RRCB	TSF	SHC	BHC
PHE	12.89	10.68	10.21	9.75	29.99	26.88	13.4
BHE	-	-	14.8	3.45	-	-	18.02
Turb1	2.41	2.63	2.75	7.14	2.1	1.98	2.36
Turb2	-	-	-	-	1.65	1.81	1.59
Generator/s	1.09	1.20	1.26	1.22	1.22	1.22	1.3
Main comp	5.35	4.75	6.11	4.84	5.55	5.72	6.08
Sec comp	-	5.65	-	5,45	-	-	-
Recup/LTR	5.29	10.37	12.38	11.59	2.5	4.88	10.37
HTR	-	4.92	-	9.46	7.39	3.79	5.18
HRU	7.26	6.11	9.25	6.03	7.69	10.99	12.18
Contingency	2.4	3.24	3.97	3.81	4.06	4.01	4.93
Engineering	3.77	5.09	6.25	5.99	6.39	6.3	7.75
TOT [M€]	**40.49**	**54.63**	**66.97**	**64.25**	**68.54**	**67.59**	**83.15**
SC[€/kW]	**0.73**	**1.11**	**0.94**	**1.19**	**0.96**	**0.96**	**1.07**

2.10. Simple recuperative cycle (SRC) results

From the results in the previous paragraphs, it can be concluded how SRC is a basic configuration with modest thermodynamic performance but with a great advantage in terms of investment costs. It is precisely these good results in the economic analysis that lead this layout to be chosen for the off-design analysis.
From thermodynamic optimization the variables to be optimized are obtained with the following values: $CIP = 78.91\ bar$ and $TIT = 379.55\ °C$.
All the other thermodynamic points are listed hereafter along with the Ts and TQ diagrams of the cycle.

Table 2.12: Thermodynamic points of the SRC configuration

Tdn point	m [kg/s]	T [°C]	p [bar]	h [kJ/kg]	s [kJ/kgK]	Density [kg/m³]
1	794.25	33	78.91	310.52	1.359	588.20
2	794.25	71.36	250	340.15	1.372	730.04
3	794.25	186.21	249.27	562.45	1.935	344.90
4	794.25	379.55	239.30	820.29	2.414	193.09
5	794.25	267.60	82.16	715.53	2.436	83.35
6	794.25	81.36	80.52	493.23	1.931	160.18

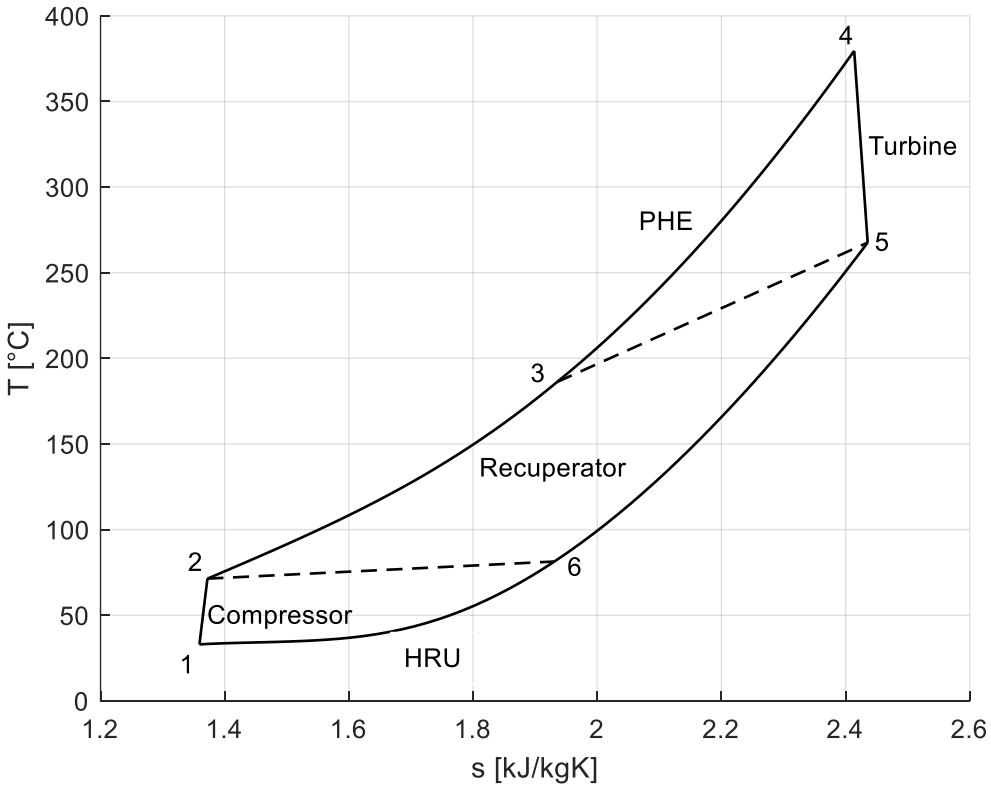

Figure 2.19: Ts diagram of the SRC configuration

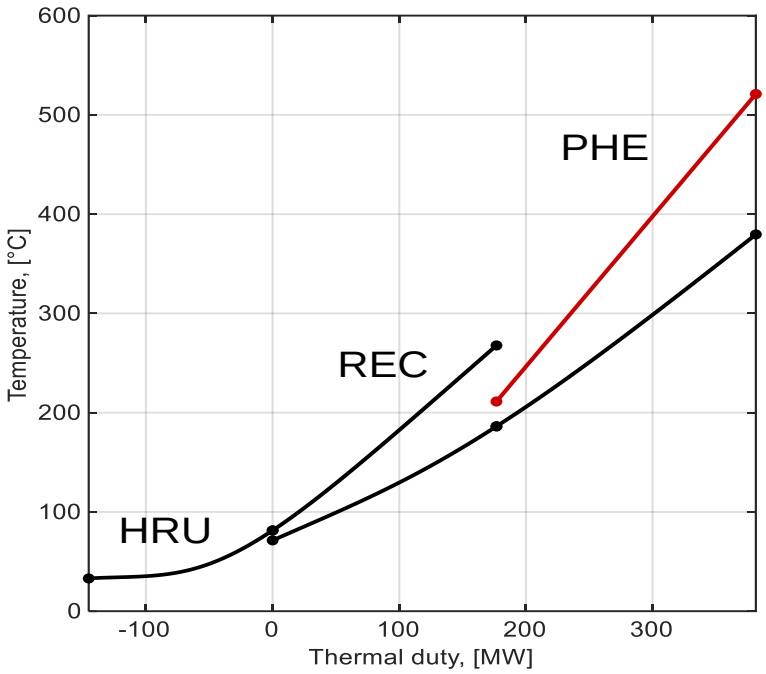

Figure 2.20: TQ diagram of the SRC configuration

3 Part load analysis

As mentioned in the introduction, in the future energy scenarios the role of conventional power plants must change. Facilities of this type must evolve from baseload operation to provide fluctuating back-up power as they must meet the unpredictable short-term load variations caused by renewable energy sources that will dominate the energy market. The CO2OLHEAT project aims to design a new generation of power plants capable of ensuring flexibility and high performance at partial loads [17].

The numerical part load and off-design analyses are here carried out in order to understand how the sCO_2 power cycle behaves after a variation of the heat source mass flow rate and inlet thermodynamic conditions.
The study is highly dependent on the cycle configuration chosen. In order to reduce the number of investigated cases, the partial load assessment is performed only for the simple recuperative cycle (SRC).
The main reasons for this choice are:

- The application studied must be very flexible, so the simplest and the most compact configuration is preferred even if it performs with lower efficiencies.
- The cycle chosen for the DEMO plant of the CO2OLHEAT project (Cement plant sector) is precisely a simple recuperative cycle, therefore, it may make sense for replicability to analyze the same plant layout.
- Being a first-of-a-kind plant is particularly important to have it simple so that its operation and the performance of its components can be monitored as best as possible.
- Finally, since it is a peaker plant, which therefore works a few hours per year, it would not be convenient to study a plant with higher investment cost, and a more compact design would allow to follow the load variation more easily.

3.1. Boundary conditions

First of all, it is important to define the new boundary conditions of the bottoming cycle, so to compute the following quantities:

- Heat source mass flow rate m_{hs} [kg/s]
- Heat source inlet temperature T_{hs} [°C]
- Heat source molar compositions xCO_2, xH_2O, xO_2, xN_2, xAr

The values of the ambient temperatures are selected considering the site envisaged for the replication of CO2OLHEAT system is in the Paris region, precisely in Montereau Fault Yonne [17].

It is located at the confluence of the Yonne river and the Seine river, therefore the abundance of water is an important factor to take into consideration for the power plant cooling system.
Year-round hourly ambient temperature data are obtained through *Renewables.ninja* site [47]. Due to data availability, 2019 is selected as the reference year and in Figure 3.1 it is noticeable how the temperatures stay within a range between -5°C and 45°C. The equivalent hours for the temperatures below 5°C and above 35°C are relatively low. Therefore, the following simulations are performed considering only ambient temperature in the relevant interval 5-35°C with a step of 10°C. In the other points, data interpolation is used.

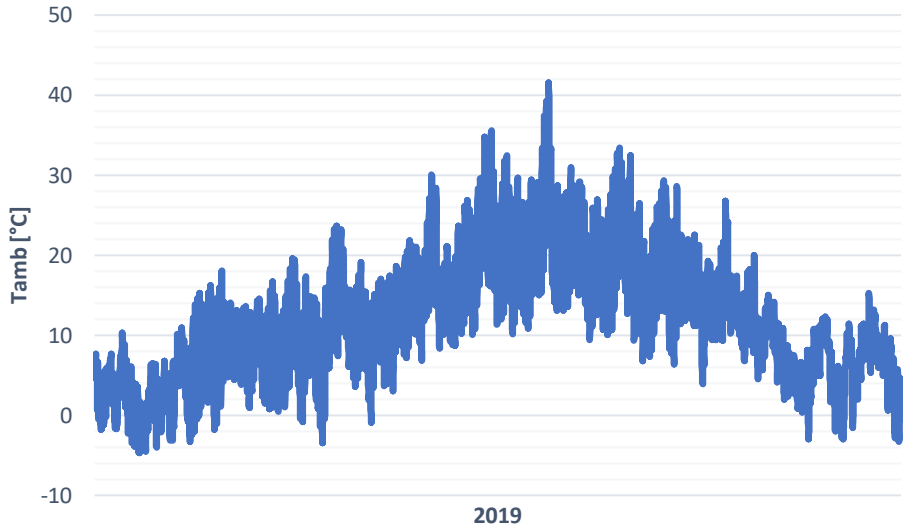

Figure 3.1: Ambient temperature variation over the year 2019 in Montereau Fault Yonne (France)

As mentioned earlier, the gas turbine (GT13E2) is highly flexible and can operate down to partial loads of 30 percent [30]. Therefore, the range considered is from 100% (on-design condition) to 30%, with a step of 10% to reduce the number of the following computations.
Having then chosen ambient temperature and load range of the gas turbine, using Thermoflex software [28], the flue gases stack conditions are computed, and the heat source is defined (i.e. temperatures, flow rates and compositions of the exhaust gases). In Figure 3.2 is showed respectively the flue gases mass flow rate, temperature, and heat power inlet variation as a function of the gas turbine load and the ambient temperature.
An increase in ambient temperature causes a decrease in air density consequently the gas flow rate at the outlet decreases as well. However, the greatest effect on the mass flow rate variation comes from the change of turbine's load.
For what concerns flue gases temperature, the effect of ambient temperature is trivial while a decrease of turbine's load provokes a rise of flue gases temperature, until a

limit value of 564.9°C is reached, then the turbine cooling system is acted on to keep outlet temperature constant.
The heat power inlet plot is a consequence of the previous two diagrams and follows the formula:

$$\dot{Q}_{in,cycle} = \dot{m}_{hs}\left(h_{hs,in} - h_{hs,min,out}\right)$$

Where $h_{hs,in}$ is function of the temperature and the composition of the flue gases entering the PHE while $h_{hs,min,out}$ is function of 90°C (the minimum outlet temperature of the burned gases) and the composition.

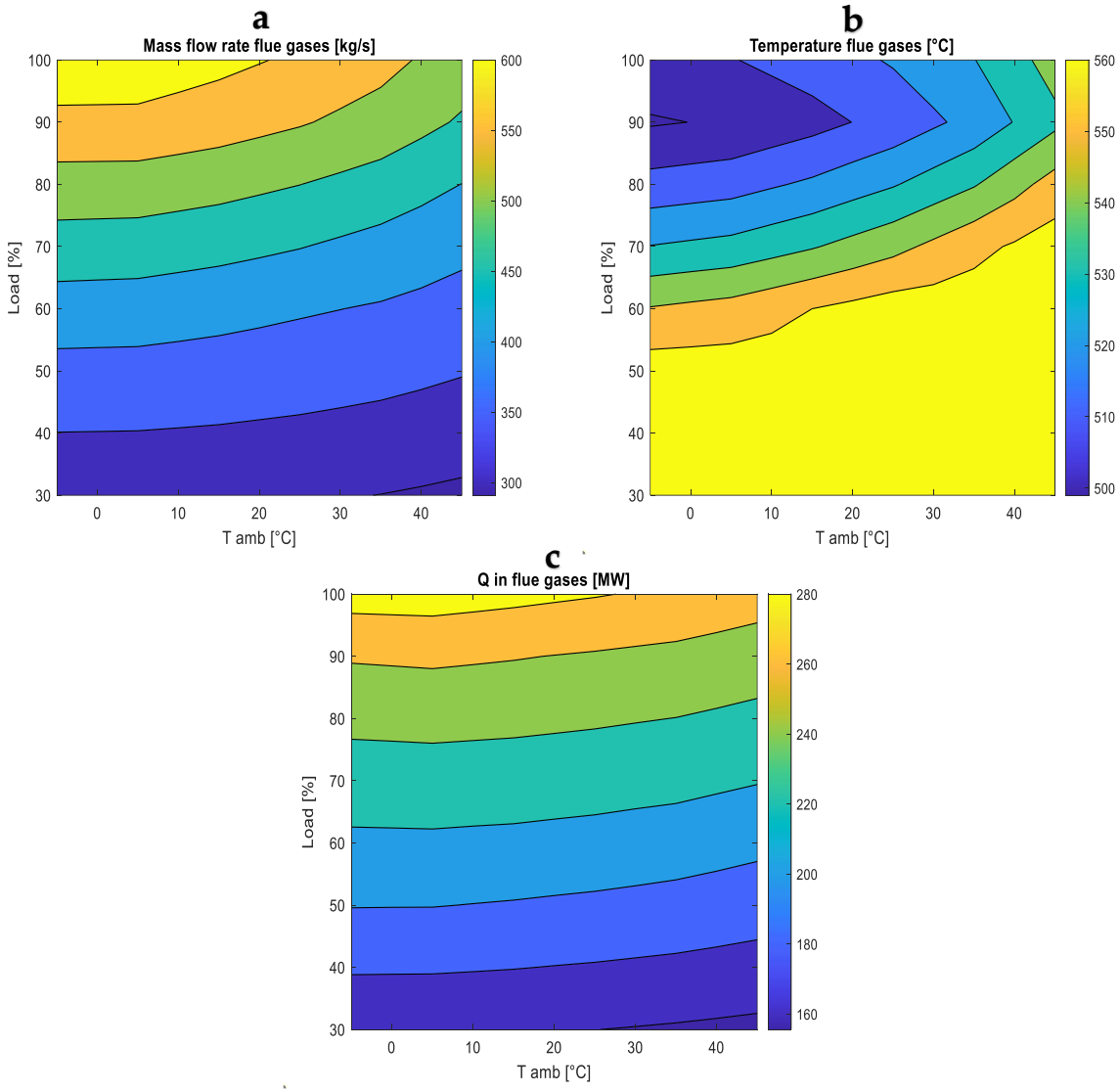

Figure 3.2: Flue gases mass flow rate (a), temperature (b) and heat power inlet variation (c) as a function of the gas turbine load and the ambient temperature

3.2. Methodology

After calculating the boundary conditions of the bottoming cycle, it is decided to perform a parametric analysis to find the optimum points at different gas turbine loads and ambient temperatures.
The starting point is the result of the SRC optimization performed in the thermodynamic analysis. The main results are summarized here in the following tables distinguishing the two cases with different cooling fluids, water and air.

Table 3.1: Main results of the water cooled SRC thermodynamic optimization

TIT [°C]	CIP [bar]	Net power [MW]	η cycle	η rec	η tot
379.55	78.91	55.48	27.09%	72.82%	19.73%

Table 3.2: Main results of the air cooled SRC thermodynamic optimization

TIT [°C]	CIP [bar]	Net power [MW]	η cycle	η rec	η tot
375.66	78.71	55.21	26.75%	73.40%	19.63%

As it was mentioned before the plant is located at the confluence of two rivers, hence it was initially decided to set the HRU as water cooling based since water availability should not be an issue. The assumptions of the cooling fluid are inlet temperature of 20°C and temperature rise of 7°C. Nevertheless, following the EU's directives on water safeguards, the air case is also taken into account with the aim of minimizing water consumption. In this scenario, the assumption of the cooling air nominal temperature rise across the heat exchanger is 20°C.
From Table 3.1 and 3.2 it is noticeable how the water cooled systems perform better than the air cooled one, even if the differences are tiny. Hence, fan consumption impacts the plant more than pump consumption.
In the next sections the CO_2 inventory within the cycle is studied with the possibility of varying it or keeping it constant. Therefore, various assumptions are set to design the plant and calculate the amount of CO_2 inside the system.
The length of the pipes connecting the PHE and the HRU is set at 15 m, while the others linked are long 2 m. The pipe's diameter is selected in order to avoid any erosion inside [42].
These and other assumptions are summarized in Table 3.3.

Table 3.3: Main assumptions of the piping structure inside the bottoming cycle

Pipes	v [m/s]	D int [m]	Length [m]	V [m³]	m fluid [kg]	Thickness [m]
1	5.06	0.59	15	4.09	2383	0.017
2	4.53	0.56	2	0.49	355	0.056
3	6.53	0.67	15	5.29	1845	0.068
4	8.75	0.78	15	7.08	1378	0.093
5	13.32	0.96	2	1.44	121	0.033
6	9.68	0.82	15	7.84	1245	0.025

From now on two methodologies, each related to the cooling fluid, are described.

3.2.1. Water cooled

Initially, it is necessary to define the control variables (i.e. those variables selected for cycle optimization). Each of them will generate a specific plant operation that will be subsequently analyzed. Furthermore, it is also important to settle the range and the step of operation of these variables in order to get reasonable results.
The control variables selected are: the CIP, that is changed from the design pressure (i.e. 78.91 bar) to 100 bar with a number of 25 pressure values equidistant, and the TIT, which is varied from -20°C to +20°C with a step of 2°C from the optimal temperature of the preceding load iteration. Pressures values below the nominal one are not studied because they would mostly be outside the compressor operating map and it is preferred to avoid entering the two-phase fluid conditions.
CIT is not investigated because, even trying to optimize it, the variable remains fixed at nominal condition in order to maximize fluid density.
Summing up, there are two control variables studied within the parametric optimization. For clearness they are summarized in Table 3.4 with their associated ranges and steps.

Table 3.4: Control variables with associated ranges and steps for the parametric optimization in the water cooled case

Control variables	Interval	Step or number of values
TIT	[TIT opt - 20 , TIT opt + 20]°C	2°C
CIP	[p des , 100] bar	25 values

The optimization is initialed by fixing the ambient temperature and varying only the gas turbine load.
Starting at 100% load, the cycle is solved using the off-design solver function by varying TIT or CIP in the selected range at each iteration. The off-design solver computes iteratively the solution of the system (i.e., the sCO_2 bottoming cycle

operating conditions) solving a set of nonlinear equations which represent the off-design behavior of each system component.

Table 3.5: Numerical constraints and closing variables for the system of non-linear equations representing the off design numerical problem for the SRC configuration. Closing variables directly handled by the solving numerical algorithm are labelled with *.

System constraint	Closing variable
$A_{HRU}^{off\ des} = A_{HRU}^{des}$	$\Delta T_{cooling\ fluid}^{off\ des-(*)}$
$A_{REC}^{off\ des} = A_{REC}^{des}$	$\Delta T_{REC,cold\ end}^{off\ des-(*)}$
$\Delta p_{REC,cold}^{off\ des-(*)} = \Delta p_{REC,cold}^{off\ des-calc}$	$\Delta p_{REC,cold}^{off\ des-(*)}$
$\Delta p_{REC,hot}^{off\ des-(*)} = \Delta p_{REC,hot}^{off\ des-calc}$	$\Delta p_{REC,hot}^{off\ des-(*)}$
$\Delta p_{PHE,cold}^{off\ des-(*)} = \Delta p_{PHE,cold}^{off\ des-calc}$	$\Delta p_{PHE,cold}^{off\ des-(*)}$
$\Delta p_{HRU,hot}^{off\ des-(*)} = \Delta p_{HRU,hot}^{off\ des-calc}$	$\Delta p_{HRU,hot}^{off\ des-(*)}$
$\eta_{comp}^{off\ des-(*)} = \eta_{comp}^{off\ des-calc}$	$\eta_{comp}^{off\ des-(*)}$
$\eta_{turb}^{off\ des-(*)} = \eta_{turb}^{off\ des-calc}$	$\eta_{turb}^{off\ des-(*)}$

Table 3.5 reports the closing variables of the off-design problem, namely those variables which are unknown a priori and are thus changed iteratively by the solving algorithm to satisfy the system constraints. Once the correct solution is found, the electrical power output is computed and the CO_2 inventory variation within the system is calculated from the internal volume of each component, the connecting piping volume and the new thermodynamic conditions of the sCO_2 power cycle.

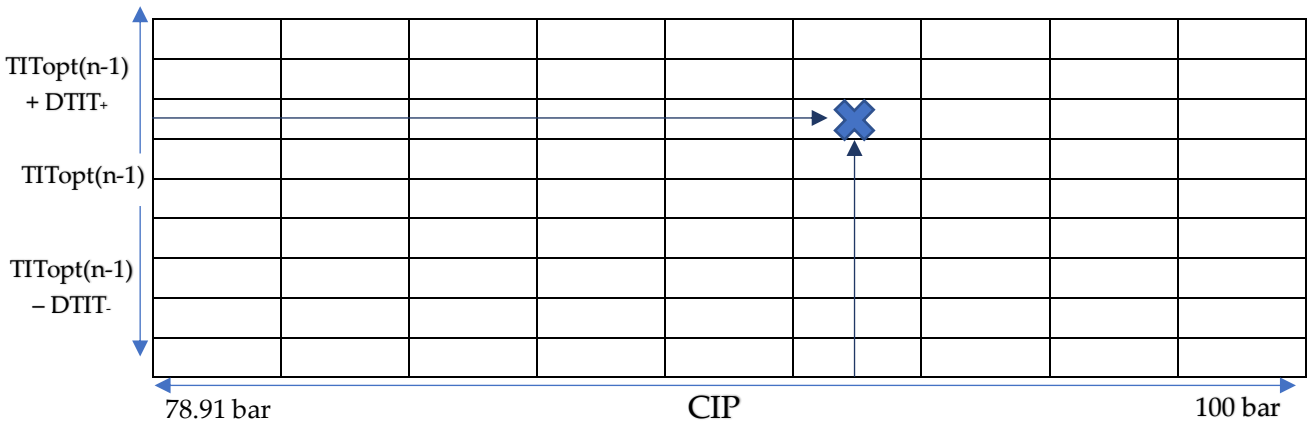

Figure 3.3: Graphical representation of TIT and CIP variation in the parametric optimization where n is the load index

Figure 3.3 depicts the graphical representation of the optimization procedure. For each load, CIP and TIT are changed withing their corresponding intervals, finding a possible solution of the cycle at each iteration. This procedure is executed for all the chosen loads.

Afterwards, the optimization is performed for the other selected ambient temperatures with the same method.

3.2.2. Air cooled

In the air-cooled case the control variables are increased to three. The CIP is kept with the same interval and step. While at TIT the range is changed, from -40°C to +20°C with a step of 1°C from the design temperature of 375.66°C. In this scenario the CIT must be optimized as it is strictly dependent on the ambient temperature value. It is varied from the nominal compressor inlet temperature of 33°C to 40°C with a step of 0.5°C.
All these variables with their corresponding intervals and steps are listed in Table 3.6.

Table 3.6: Control variables with associated ranges and steps for the parametric optimization in the air cooled case

Control variables	Interval	Step or number of values
CIT	[33 , 40]°C	0.5°C
CIP	[p des , 100] bar	25 values
TIT	[TIT des - 40 , TIT des + 20]°C	1°C

As before the optimization is initialed by fixing the ambient temperature and varying only the gas turbine load. The procedure with the off-design solver is equal and the closing variables are the same as Table 3.4, but instead of TIT is varied CIT.
In this case the minimum load achieved is 40% due to operability limits of the code.

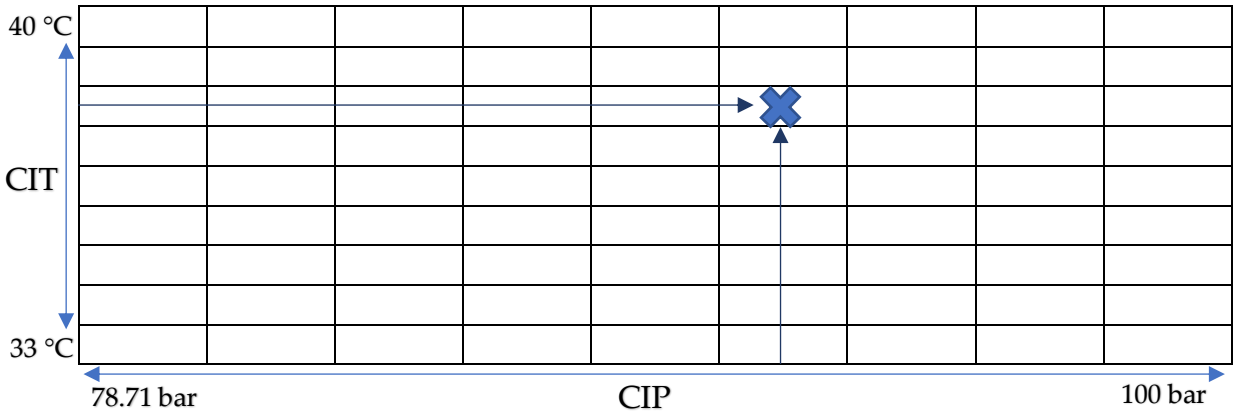

Figure 3.4: Graphical representation of CIT and CIP variation in the parametric optimization

Figure 3.4 shows the graphical representation of the optimization operation. For each load, CIP and CIT are changed withing their corresponding intervals, finding a possible solution of the cycle at each iteration.

As before, the optimization is continued by varying the ambient temperature in the chosen values.
Finally, the TIT is parametrically optimized by first setting the ambient temperature and varying the load, and then changing the other temperatures as well.

3.3. Part load operations of the components

In this section the assessment of each component's behavior in off-design conditions is addressed. In Chapter 1 the analysis was described for the nominal operations, while in this paragraph the off-design assumptions and modelling for the performance estimations are briefly summarized.

3.3.1. Recuperator off-design modelling

In off-design conditions, the recuperator is modelled adopting the same heat transfer coefficient and pressure drops of the design analysis. The thermodynamic properties of the streams are defined for each part load simulations where they need to satisfy the cycle operation and component's constraints. In particular the mass and the energy balance of the recuperator needs to be verified as well as the characteristic equation of the heat exchanger:

$$Q_{HX} = U\, A_{HX}\, \Delta T_{ml}$$

Where Q_{HX}[W] is the thermal power exchanged in the recuperator, U[W/m²K] is the global heat transfer coefficient referred to A_{HX}[m²], the heat exchanger area, and ΔT_{ml}[K] is the logarithmic mean temperature across the component.

3.3.2. Compressor off-design modelling

It is decided to employ a multistage centrifugal compressor connected to a variable-speed motor, as it was designed withing the sCO2-flex project for similar sizes.
Compressor off-design optimal operation is evaluated thanks to the non-dimensional performance map shown in Figure 3.5. The working points are computed as function of the volumetric flow rate ratio $\frac{\dot{V}_{in,comp}}{\dot{V}_{in,comp\ nom}}$ and the enthalpy rise ratio $\frac{\Delta h_{comp}}{\Delta h_{comp\ nom}}$. The map is dimensionless and the efficiencies are reported here only qualitatively for NDA reasons.
Looking at the map it is clear that it is convenient to work near the compressor's surge line where polytropic efficiencies are higher. Hence, it is useful to vary the shaft rotational speed adopting IGV control only at low or high volumetric flow rates, thus only in startup or shutdown operations or when the load is significantly low.

However, in order to preserve compressor operability and lifetime it is important to avoid the surge phenomenon. Thanks to an anti-surge loop installed in the system, when the flow rate circulating in a compressor is lower than the safety limit defined as 1.1 times its corresponding surge limit value, the anti-surge valves are opened ensuring stable compressor operation. The drawback of this equipment is a higher compressor consumption and thus a lower overall plant efficiency.

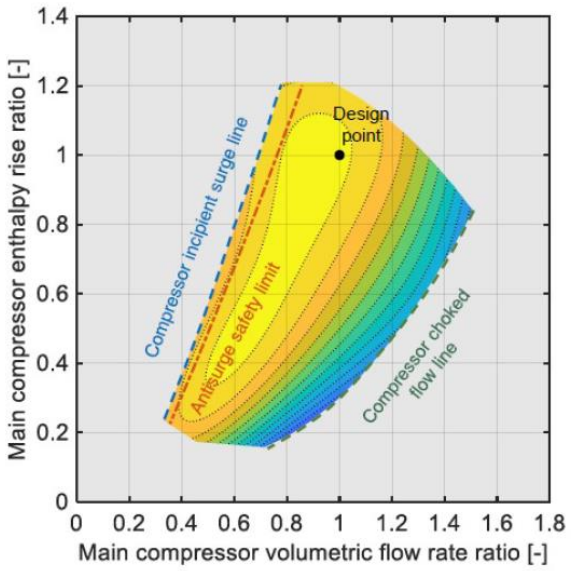

Figure 3.5: Compressor's dimensionless operational map

The other aspect that needs to be considered concerns the choke phenomenon. The compressor choked flow line shows the maximum volumetric flow rate that the turbomachinery is able to process with the maximum value of RPM and IGV regulation. In contrast to the surge operation, the choke phenomenon is not easily solved and if neglected could lead to the plant forced shutdown.

3.3.3. Turbine off-design modelling

In off-design conditions, turbine is controlled in sliding pressure following the flow coefficient Φ formula:

$$\Phi = \frac{\dot{m}_4\sqrt{T_4}}{p_4 A_{in,turb}}$$

Where $\dot{m}_4$[kg/s] stands for the sCO_2 mass flow rate entering the turbine, T_4[K] is the turbine inlet temperature, p_4[bar] is the turbine inlet pressure [bar] and $A_{in,turb}$[m²] is the area of the turbine's inlet.

3.3.4. HRU off-design modelling

HRU's off design condition is dependent on the choice of the cooling fluid. In the water case, it is made the assumptions of water widely available at a temperature of 20°C

always lower than the minimum cycle one (i.e. 33°C). While in the air case, ambient air conditions are linked to the off-design case studied. For high ambient temperatures some thermodynamic cycles might not be feasible because the air's inlet temperature in the HRU will be greater than the minimum cycle one. This aspect is studied more in detail in the following paragraph.

3.4. Cycle operational limits

3.4.1. Compressor

With the described methodology, it is found how, set a multiple load of 10 from 100% to 40%, there is a cycle solution for each CIT and CIP in the air cooled case.
However, it is important to consider that the developed code is not able to solve every working points due to compressor operational limits.
In Figure 3.6 is possible to notice in a qualitative way the area (high CITs and low CIPs) within which all the cycle solutions are not feasible, hence they must be removed.
It is also noted how this area is a function of the load percentage, the surface will indeed decrease in the direction shown in the figure along with the load decrease, due to the reduction of the CO_2 mass flow rate.

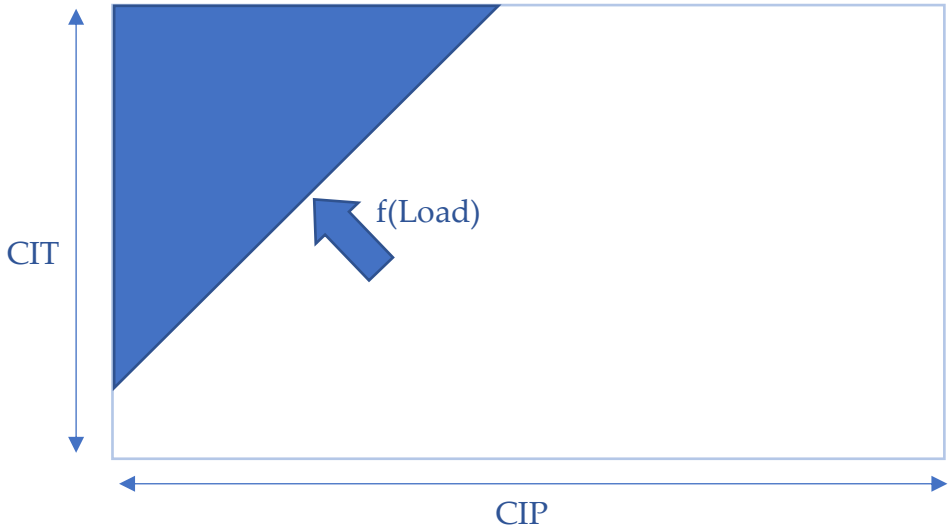

Figure 3.6: Compressor operational limits

3.4.2. HRU

Afterwards it is important to consider also the HRU operation and the ambient temperature. In the simulations this component is computed after having solved the cycle, therefore, its boundaries must be checked. The HRU presents a limit in its operation set as +25% of the commutated fans rotational speed. By increasing the ambient temperature, the cycle might not be able anymore to respect this threshold, hence some points will be considered unfeasible.

In Figure 3.7 the points excluded by the constraint are qualitatively shown (low CITs and CIPs). The exclusion area is clearly function of the ambient temperature and it will decrease in the direction marked in the figure along with an ambient temperature reduction.
Furthermore, in the air cooled case, all the cycle temperatures below the ambient one must be cancelled out to avoid unfeasible HRU operations.

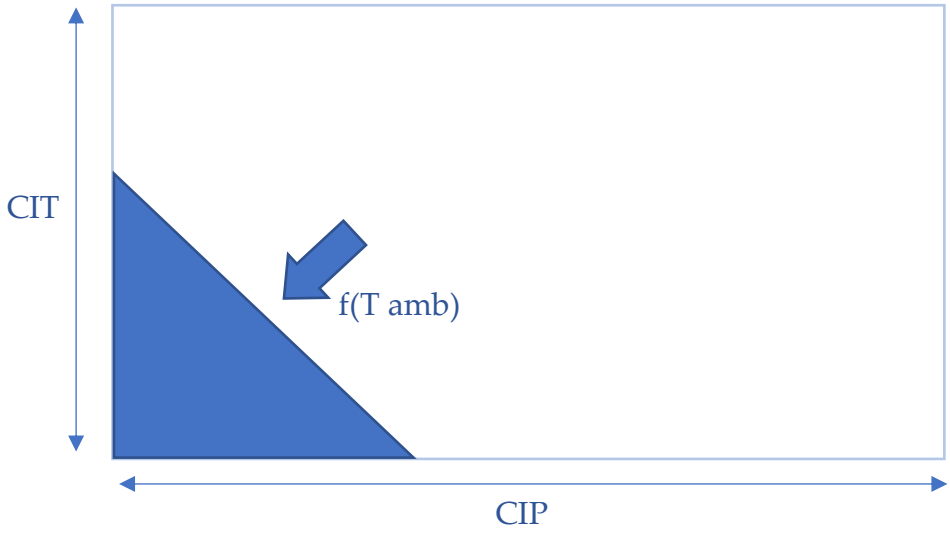

Figure 3.7: HRU operational limits

3.5. Operating strategies

In power plants, the part load and off-design operation strategy are strongly linked to system dynamic and control. As boundary conditions change, the system undergoes controlled transitions to ensure proper functioning of various components and maximize performance under the new steady-state operating conditions.
For simplicity, the MATLAB steady-state code is developed assuming that the operations listed below to control the sCO_2 power cycle can be performed by a well-designed control system.
It is important to note that this list of actions should not be viewed as a sequence of steps, as all operations must be performed concurrently:

- The mass flow rate of the cooling medium is varied to control the CO_2 inlet temperature or density at the compressor through variable speed cooling water pump, when the cooling medium is water, or fan, in the case of cooling air.
- The desired turbine inlet temperature is obtained by the variation of compressor volumetric mass flow rate.
- As it was mentioned earlier, turbine is generally not controlled with rotational speed, NGV or partial arc admission, instead this component is operated by following its sliding pressure operational curve, which determines the cycle maximum pressure as a function of turbine inlet temperature and mass flow rate.

- Compressor operating point is adjusted based on IGV opening and/or rotational speed to compress the desired CO_2 mass flow at the required outlet pressure while maximizing component efficiency.
- Cycle minimum pressure is controlled thanks to fluid inventory variation. Since the turbine works in sliding pressure, cycle maximum pressure decreases when CO_2 mass flow rate is reduced and, without an active control on fluid inventory, the minimum cycle pressure would increase to compensate the density reduction of CO_2 in the high pressure part of the cycle. Having a pressurized CO_2 storage vessel permits to change the mass flow rate in the system, freely varying the minimum pressure.

By implementing one or more of these measures, many different part-load and off-design control strategies can be applied. The choice of the optimal strategy depends largely on the cycle configuration and application under study.
For the SRC under investigation, two main regulation strategies are identified.

Strategy S1

Strategy S1 aims at optimizing cycle power output by varying all the control variables. For the water cooled case, the best option is to keep CIT at the nominal point. Increasing it, (i.e. reducing the mass flow rate of cooling water) is generally detrimental from a thermodynamic perspective since it involves an increase of main compressor specific work due to the CO_2 density reduction. On the other hand, a lower CIT may improve the cycle efficiency, but it could involve issues related to cavitation in the compressor due to vapor bubbles formation during acceleration in the stator. On the other hand, when the cooling fluid is ambient air, CIT has to be optimized since it is strictly linked to the ambient temperature.
Regarding TIT, it needs to be optimized in either case because, unlike steam cycles where it is convenient to rise it as high as possible, in recovery bottoming cycles a lower TIT causes a decrease in cycle efficiency, but an increase in recovery efficiency, hence a tradeoff is necessary.

Strategy S2

Strategy S2 aims to optimize control variables while maintaining constant cycle inventory.
The inventory variation inevitably leads to a more complex and expensive power plant because it involves the adoption of a CO_2 storage system and an accurate control system. The regulation aspect represents a non-trivial challenge because of the transient related to charging and discharging operation of the carbon dioxide vessels. For this reason, the possibility to design a totally sealed system that does not required inventory variation during part load operations looks particularly attractive.
As mentioned before, since the turbine works in sliding pressure and without the possibility to vary fluid inventory, CIP cannot be optimized and it is function of CO_2 density variation.

Table 3.7: Off-design operating strategy for the water cooled SRC configuration

Strategy	Strategy control variables		Strategy constraints
	TIT	CIP	Constant inventory
S1	Optimized	Optimized	Not active
S2	Optimized	Calculated	Active

Table 3.8: Off-design operating strategy for the air cooled SRC configuration

Strategy	Strategy control variables			Strategy constraints
	TIT	CIT	CIP	Constant inventory
S1	Optimized	Optimized	Optimized	Not active
S2	Optimized	Optimized	Calculated	Active

3.6. Results

In this final section all the results obtained from the off-design analysis are proposed and commented. Since two different methodologies are used, it is decided to divide the results exposition into two parts according to the cooling method employed.

3.6.1. Boundary conditions

Initially, to understand the results of the part load analysis, it is important to comprehend the evolution of the cycle's boundary conditions as the ambient temperature and the gas turbine load change.

In Figure 3.8 the flue gases heat power inlet, mass flow rate and temperature as a function of the ambient temperature are depicted, keeping the gas turbine load fixed to the nominal condition (i.e. 100%).
In this way, it is simple to observe how increasing the ambient temperature, the heat power entering the sCO_2 bottoming cycle decreases.

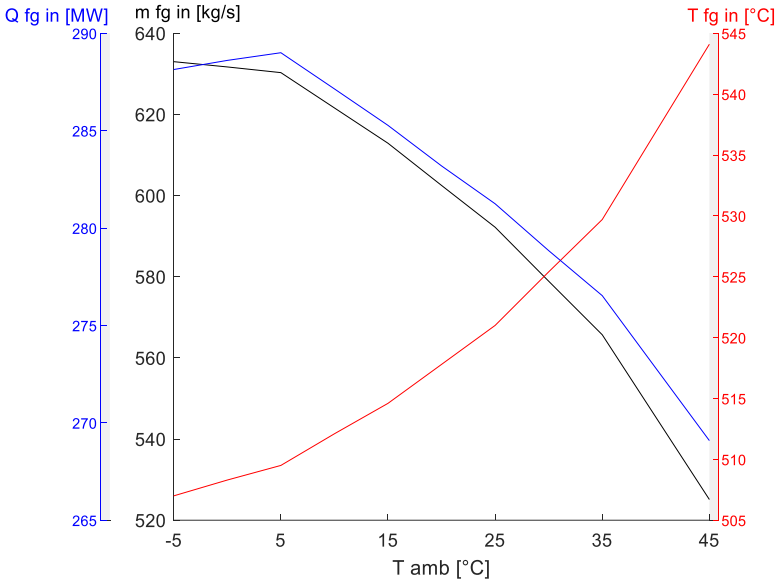

Figure 3.8: Flue gases heat power inlet, mass flow rate and temperature variation as a function of the ambient temperature with a gas turbine load of 100%

On the other hand, the effect is reversed when the ambient temperature is kept fix and the load is rised, as it can be seen in Figure 3.9 where the flue gases heat power inlet, mass flow rate and temperature as a function of the load are shown, maintaining the ambient temperature equal to the nominal condition one (i.e. 25°C).

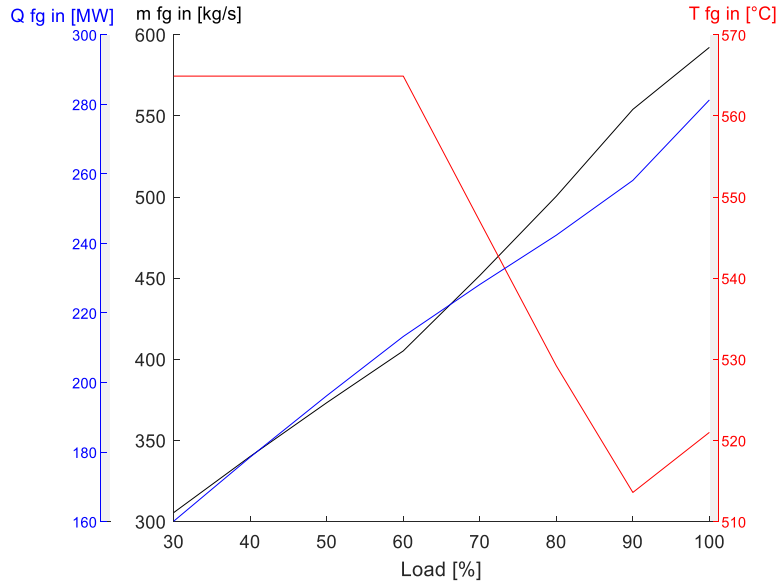

Figure 3.9: Flue gases heat power inlet, mass flow rate and temperature variation as a function of the gas turbine load with an ambient temperature of 25°C

3.6.2. HRU with water as cooling medium

In the following paragraphs the performance of the water cooled SRC in off design conditions will be studied. In particular, turbine inlet temperature (TIT) and compressor inlet pressure (CIP) will be analyzed specifically. Finally, an assessment will also be given on cycle inventory, discussing the two selected operating strategies.

3.6.2.1. Influence of TIT

As mentioned earlier, it may be meaningful to see how the net electrical power of the cycle changes as a function of the TIT variation from nominal conditions. Initially, the study is carried out at constant gas turbine load and CIP equal to design conditions, varying ambient temperature (5, 15, 25 and 35°C).

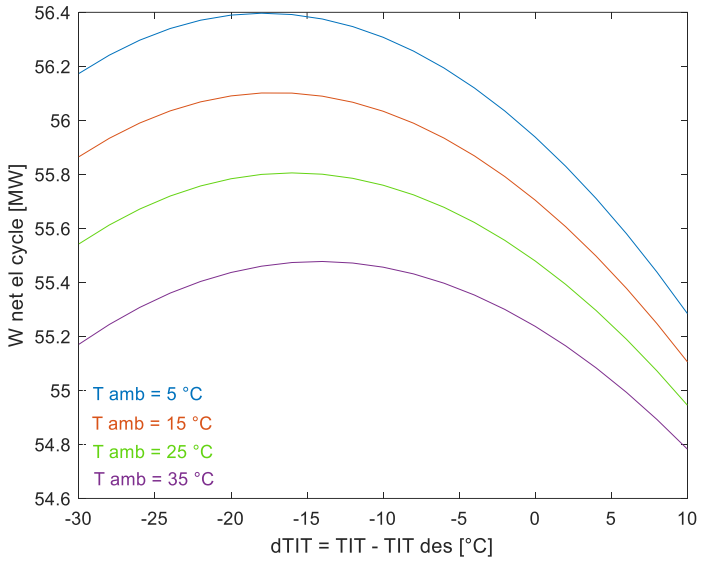

Figure 3.10: Trend of the net electrical power of the cycle against the variation of TIT and of the ambient temperature

It can be seen from Figure 3.10 how the net power optimum point shifts towards negative $Delta\,TIT$, where $Delta\,TIT = TIT_{studied} - TIT_{design}$, so TIT decreases compared to the nominal case.
It would expect to see the curve at ambient temperature 25°C (green line) with the optimum point at the design TIT, being the nominal case. However, in the off design optimization the PHE pinch point is variable and no longer constant as in the nominal case where it is fixed at 25°C. Hence, the optimal value from the Figure has a pinch point lower than 25°C, leading to a higher recovery efficiency, while the cycle efficiency is reduced due to the lower TIT. As a result there is a total cycle efficiency that is slightly higher when TIT is decrease by roughly 15°C from the nominal one.
Considering the change in ambient temperature, its increase causes a reduction of the net power and a shift of the maximum value towards the design TIT.

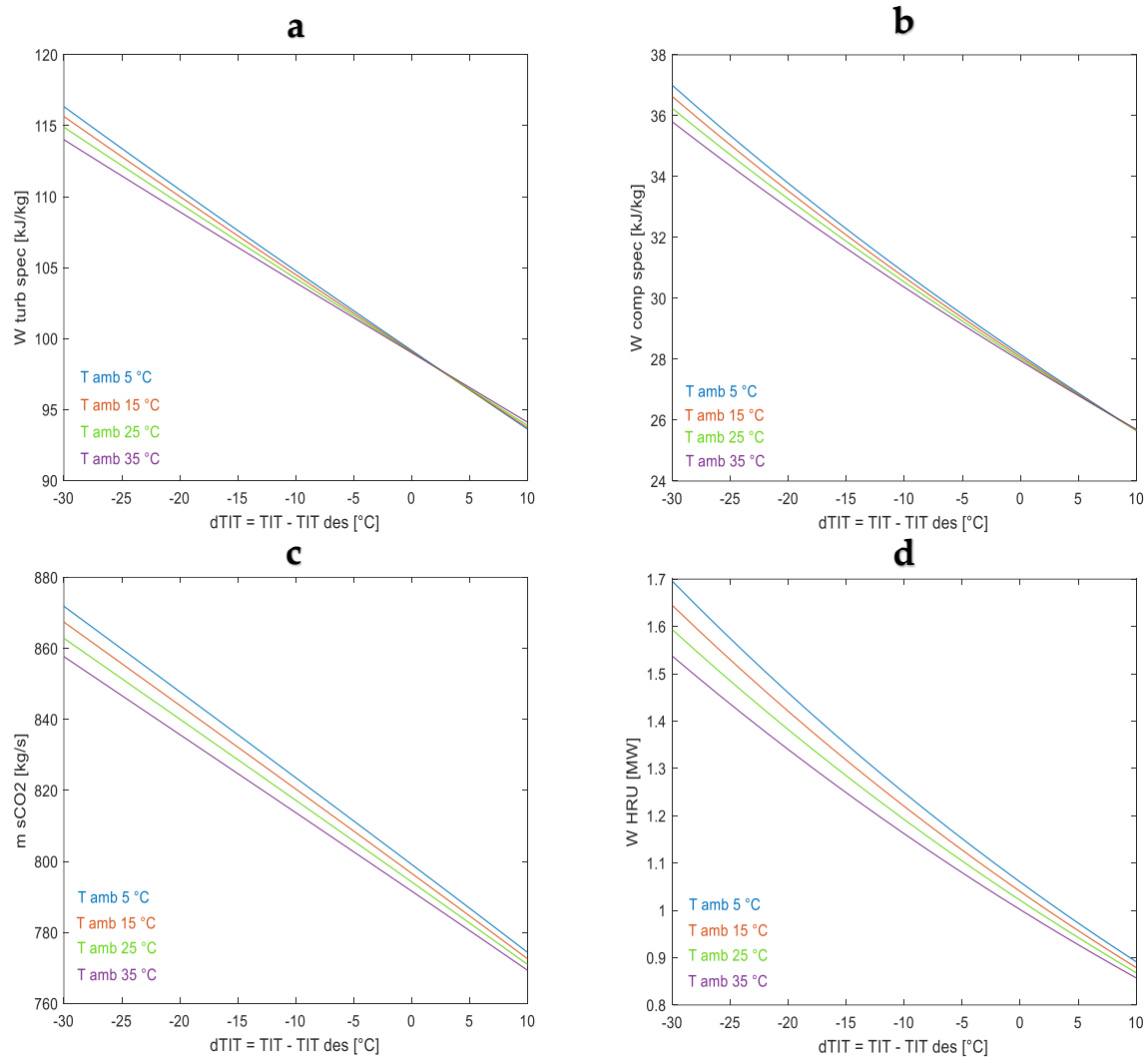

Figure 3.11: Trend of a) the specific turbine work, (b) the specific compressor work, (c) the sCO₂ mass flow rate and (d) the HRU power against the variation of TIT and of the ambient temperature

To understand the trend of the net electrical power of the cycle Figure 3.11 depicts the evolution of the specific turbine and compressor work, the sCO₂ mass flow rate and the HRU power as a function of the TIT and the ambient temperature variation. All these amounts rise when TIT is decreased from nominal conditions. Thus, looking at the formula above, two of them (m_{CO_2} and $W_{turb\ spec}$) have a positive effect on the net power, while the other two ($W_{comp\ spec}$ and W_{HRU}) a negative one leading to the trend shown in Figure 3.10.

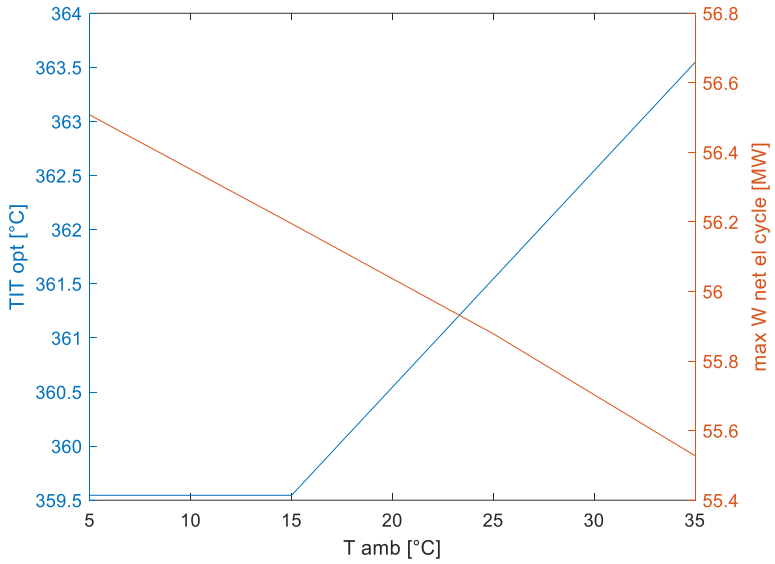

Figure 3.12: Trend of the optimal TIT and of the maximum net electrical power of the cycle against the variation of the ambient temperature

Finally, Figure 3.12 depicts the behavior of the optimal TIT and of the maximum net electrical power of the cycle, which respectively increase and decrease with a growth in ambient temperature.

Thereafter, the study continues by keeping the ambient temperature and the CIP equal to nominal conditions and varying the gas turbine load. For simplicity in Figure 3.13 only four loads are represented.
Since the scale of power output ranges from 35 MW to above 55 MW, the effect of the TIT variation is almost flat if compared to the load.

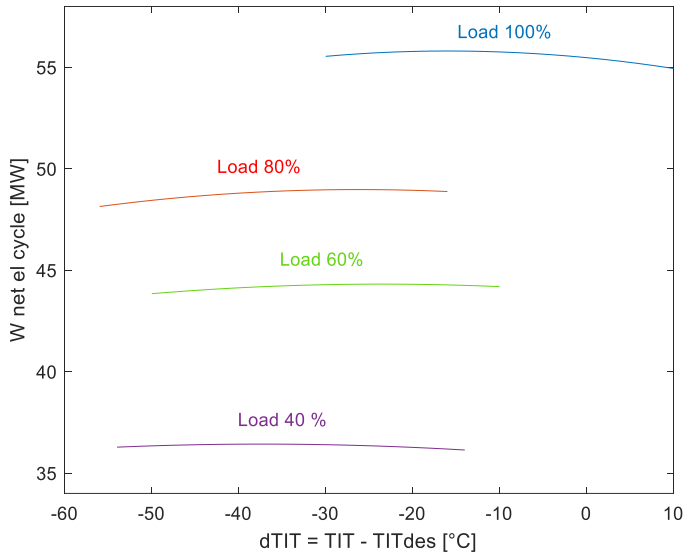

Figure 3.13: Trend of the net electrical power of the cycle against the variation of TIT and of the gas turbine load

While Figure 3.14 depicts how increasing the gas turbine load the maximum net power of the plant increases, but also the optimal TIT of the cycle rises as well. The increasing but irregular trend of the latter variable is related to the trend of combustion gases at partial loads as depicted in Figure 3.9. By decreasing the load initially, the exhaust temperature decreases to 90% and then increases towards the maximum limit value reaching 60% of load.

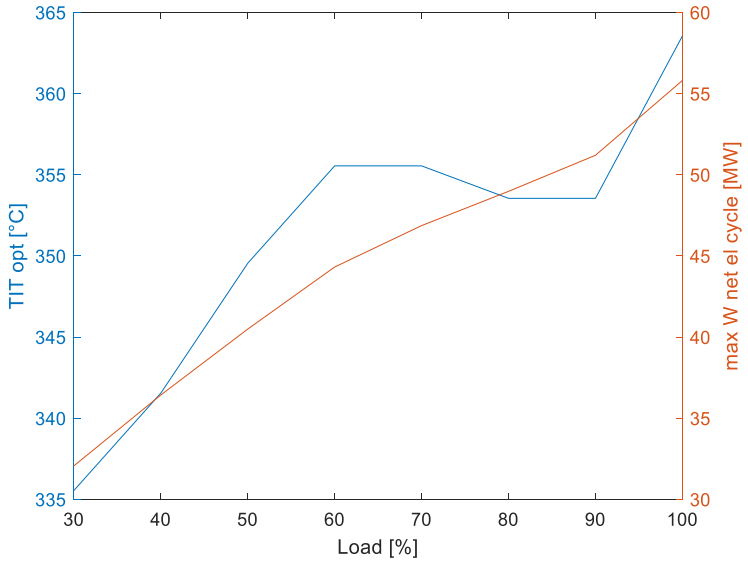

Figure 3.14: Trend of the optimal TIT and of the max net electrical power of the cycle against the variation of gas turbine load

3.6.2.2. Influence of CIP

As well as TIT, in a similar way, the influence of CIP on cycle performance is also taken into account. Nevertheless, Figure 3.15 shows how increasing the CIP does not bring advantages in terms of net power output and the optimal point stays around the nominal one.

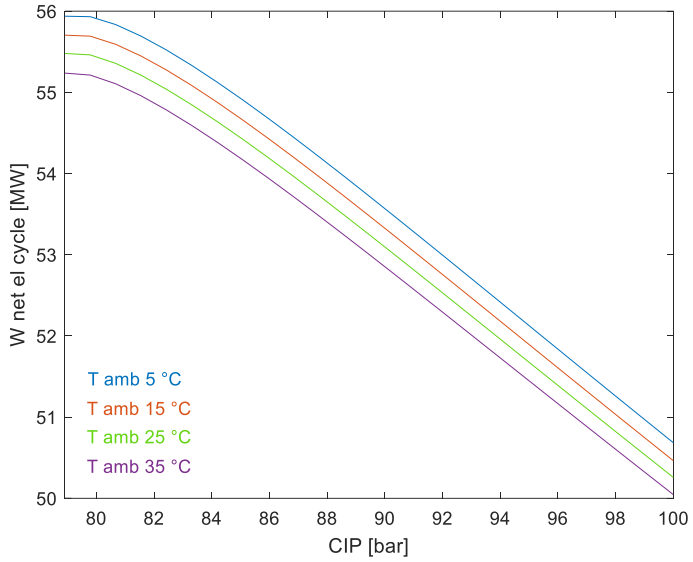

Figure 3.15: Trend of the net electrical power of the cycle against the variation of CIP and of the ambient temperature

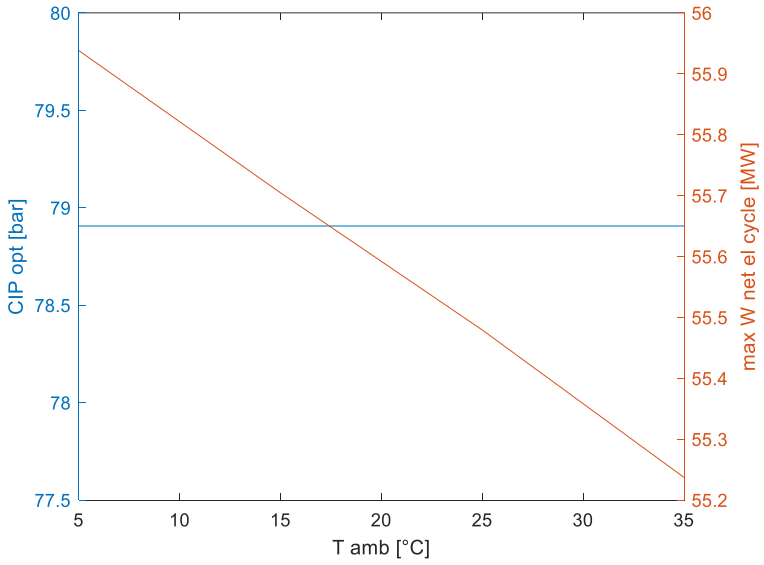

Figure 3.16: Trend of the optimal CIP and of the max net electrical power of the cycle against the variation of the ambient temperature

On the other hand, considering the influence of ambient temperature in Figure 3.16, it is visible how the optimal CIP remains constant, while as usual, the maximum net power point decreases by increasing the ambient temperature, although on the scale from 5 to 35°C the reduction is below 1 MW.

Instead, if the ambient temperature is fixed and the load is varied, the latter's influence is still more pronounced than the CIP variation, even if the optimal point remains in nominal conditions. These observations are represented in Figure 3.17 and Figure 3.18 where the optimal CIP is constant as the load increases, while the value of the maximum cycle power grows.

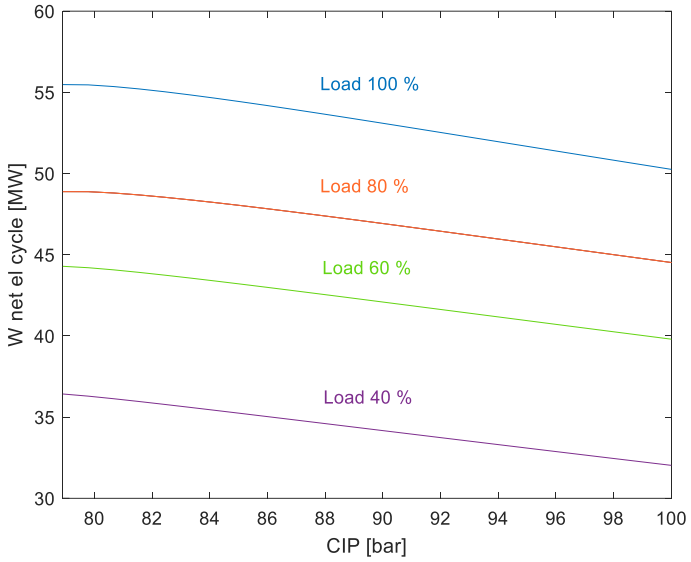

Figure 3.17: Trend of the net electrical power of the cycle against the variation of CIP and of the gas turbine load

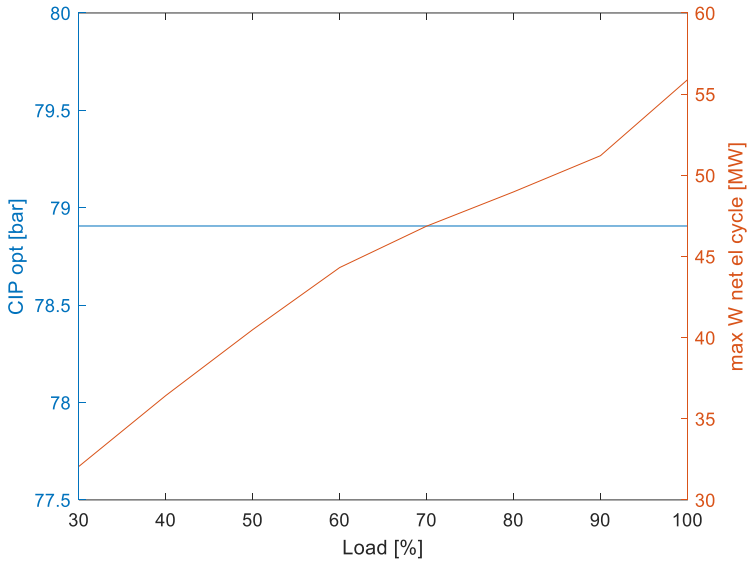

Figure 3.18: Trend of the optimal CIP and of the max net electrical power of the cycle against the variation of gas turbine load

3.6.2.3. Influence of inventory

In a past section, it was explained how having variable inventory brings about increased costs and problems from the control system point of view. Nevertheless, working at constant inventory reduces the range of operability resulting in a reduction in cycle performance. It is therefore investigated the case and understood when this solution might be beneficial.

Figure 3.19 represents four different ambient temperatures, where each of them has two optimal points, depending on the operating strategy applied.

It can be noticed how the optimal operation fir the strategy S1 is always at a TIT around 360°C–365°C and a CIP close to 80 bar. While the constant inventory line is at higher TITs, always greater than 380°C. Hence the optimal point for the strategy S2 is shifted. Working in this last operating point as opposed to the first one leads to a power loss on the order of 1 MW, where this difference is not particularly dependent on ambient temperature variation.

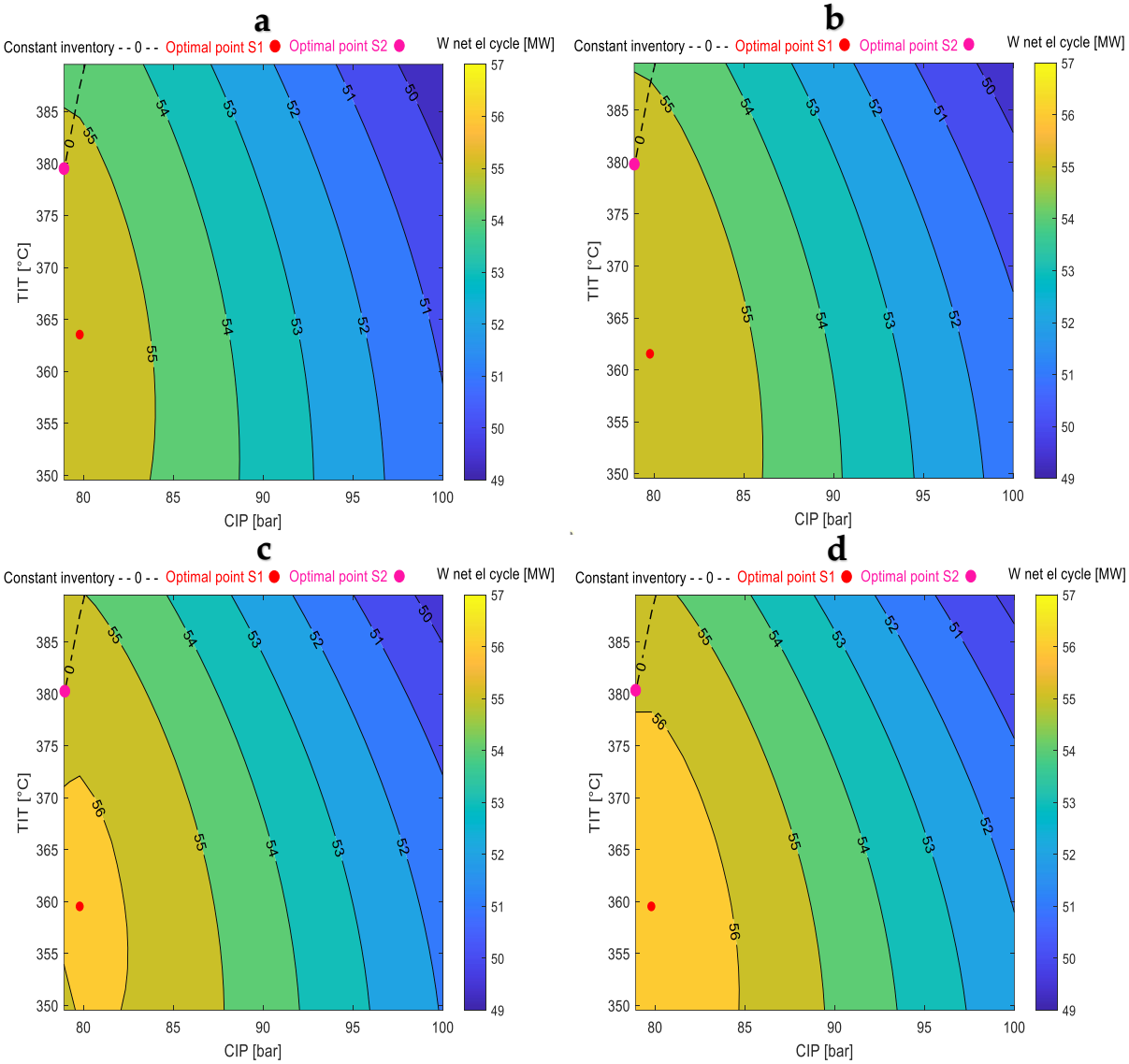

Figure 3.19: Trend of the net electrical power of the cycle against the variation of CIP and TIT with the optimal points for strategy S1 and S2, and the line at constant inventory with an ambient temperature of (a) 35°C, (b) 25°C, (c) 15°C and (d) 5°C

Trying instead to vary the load by keeping ambient temperature constant the results are shown in Figure 3.20. It is important to note how the ordinate values are not the same for each load, because the resolution method employed changes the simulation interval by centering it in the optimal TIT of the previous load iteration.

It is visible how, for both strategies, the optimal points shift towards lower TITs when the load is reduced and around the 60% they almost match. However, in all the other partial loads the strategy point S1 has a power output greater roughly than 1 MW with respect to the other strategy S2.

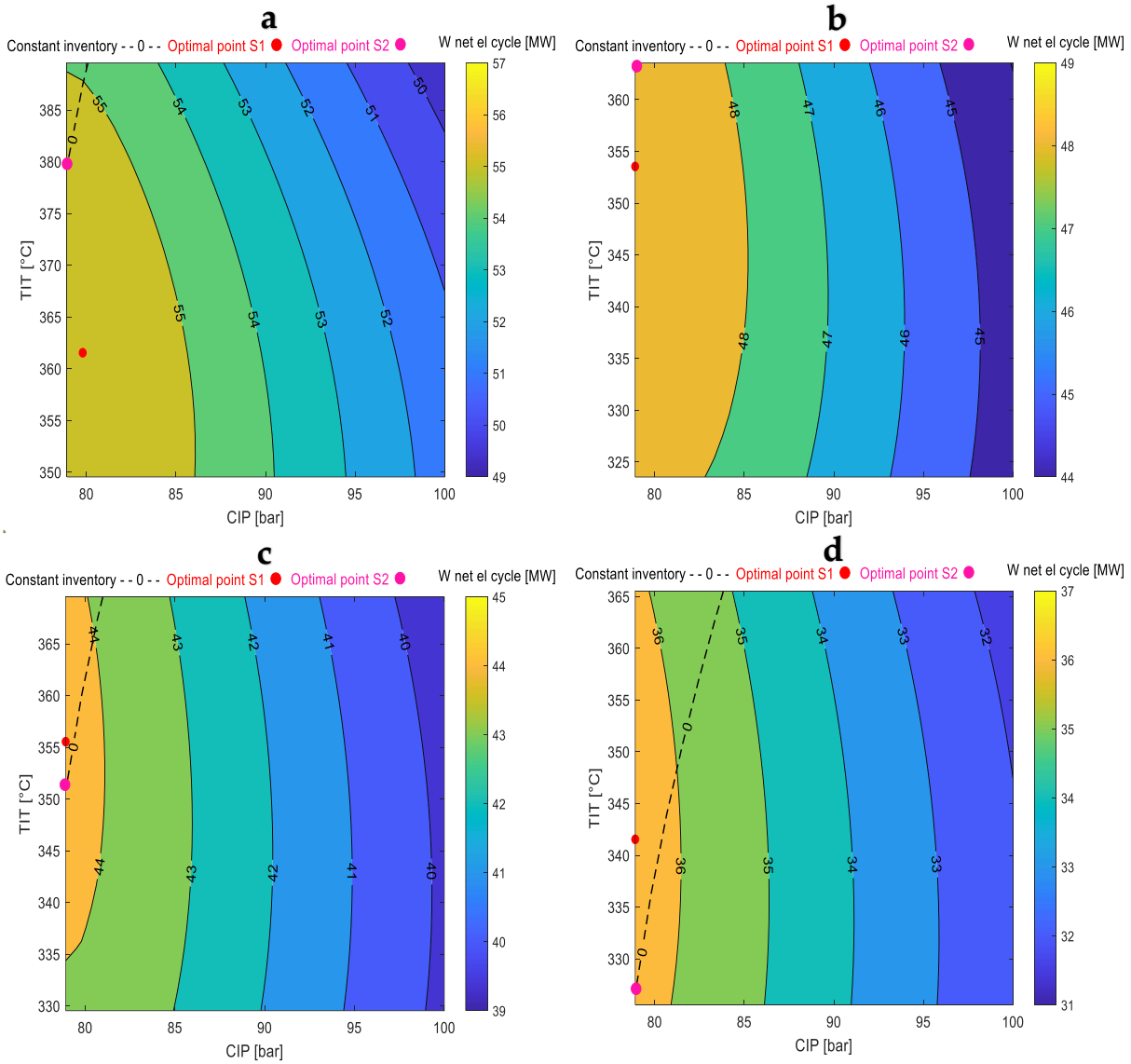

Figure 3.20: Trend of the net electrical power of the cycle against the variation of CIP and TIT with the optimal points for strategy S1 and S2, and the line at constant inventory with a gas turbine load of (a) 100%, (b) 80%, (c) 60% and (d) 40%

3.6.3. HRU with air as cooling medium

As done with the water cooled case, in the following paragraphs the performance of the air cooled SRC in off design conditions will be studied. In particular, turbine inlet temperature (TIT), compressor inlet pressure (CIP) and temperature (CIT) will be analyzed specifically. Furthermore, an assessment will be made on whether or not to vary the cycle inventory with the two possible control strategies.

3.6.3.1. Influence of TIT

As mentioned earlier, it may be meaningful to see how the net electrical power of the cycle changes as a function of the TIT variation from nominal conditions. The trend is presented in Figure 3.21, adding a second variable to the TIT: the ambient temperature, and keeping the 100% of load with CIP and CIT equal to their optimal values for each iteration. Three different plots are shown at three different ambient temperatures: 5°C, 15°C, and 25°C. It is clear how, moving from design condition (i.e. Delta TIT = 0 °C), the maximum power shifts toward negative values of Delta TIT, where $Delta\ TIT = TIT_{studied} - TIT_{nominal}$. Hence, the increase in recovery efficiency more than compensates for the decrease in cycle efficiency.
As expected, an increase in ambient temperature causes a decrease in power, but it is further noted that as the ambient temperature decreases, the maximum power shifts towards increasingly negative values of delta TIT. Furthermore, even if the three temperatures are equidistant by a ΔT of 10°C, the net power reduction is more pronounced going from 15°C to 25°C than from 5°C to 15°C. This is due to the boundary conditions and to the fact that the reduction of the inlet heat power is not linear with an ambient temperature increase.

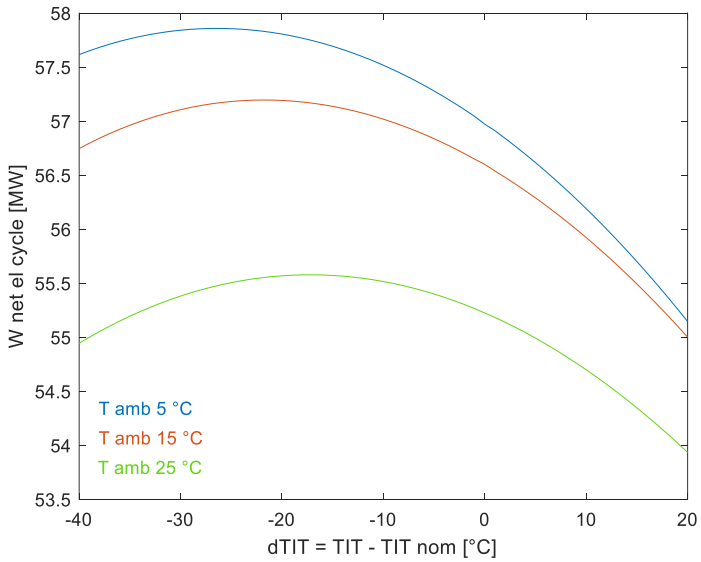

Figure 3.21: Trend of the net electrical power of the cycle against the variation of TIT and of the ambient temperature

Changing the ambient temperature with the gas turbine load, the same trend is displayed in Figure 3.22. In this case, the ambient temperature is equal to 25°C and, as before, CIP and CIT are fixed to their optimal values for each iteration.
It is important to highlight how the power range axis has widened compared with the previous case, because the effect of load on net power output is greater than that one of ambient temperature. As a result the Delta TIT variation's impact is quite flat.

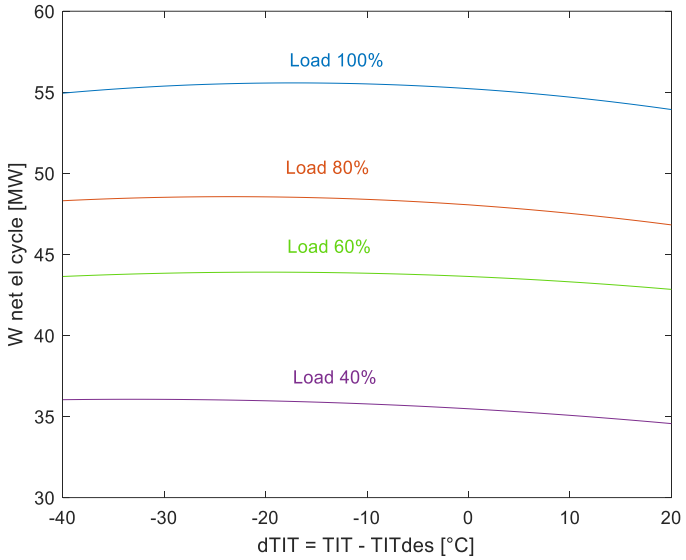

Figure 3.22: Trend of the net electric power of the cycle against the variation of TIT and of the gas turbine load

3.6.3.2. Influence of CIP

Having a look now at the influence of CIP on cycle performance and maintaining the load and the TIT with nominal values. In Figure 3.23 it is visible how trying to increase the pressure is not beneficial for a higher power output, since the optimal pressure remains close to the nominal one.

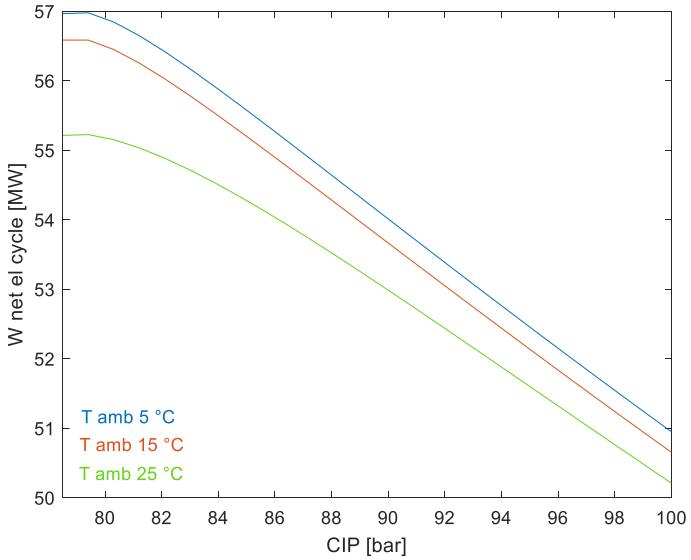

Figure 3.23: Trend of the net electrical power of the cycle against the variation of CIP and of the ambient temperature

As expected and confirmed by the trend in Figure 3.24, when the ambient temperature rises the maximum cycle's net electrical power decreases while the optimal CIP keeps constant.

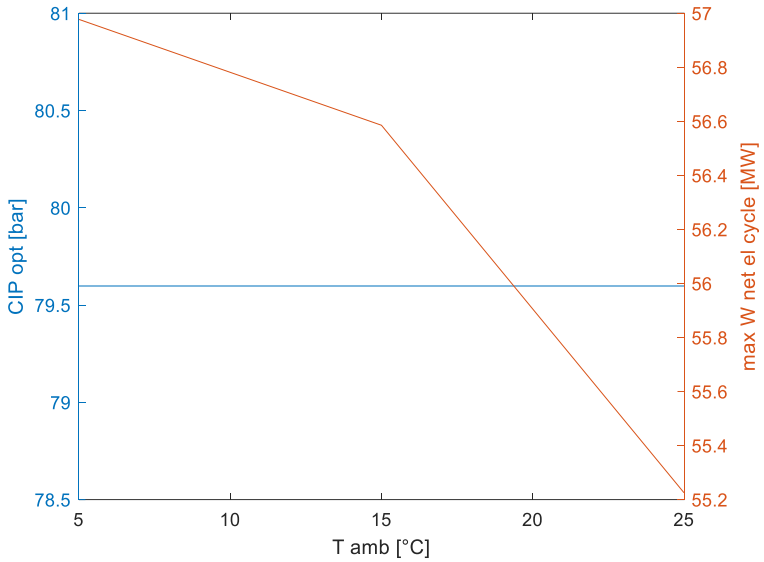

Figure 3.24: Trend of the optimal CIP and of the max net electrical power of the cycle against the variation of the ambient temperature

The same pattern can be seen by changing the gas turbine load and keeping the ambient temperature fixed at 25°C. As in the previous paragraph, it can be observed the marked effect of gas turbine load variation on the cycle's net power output.

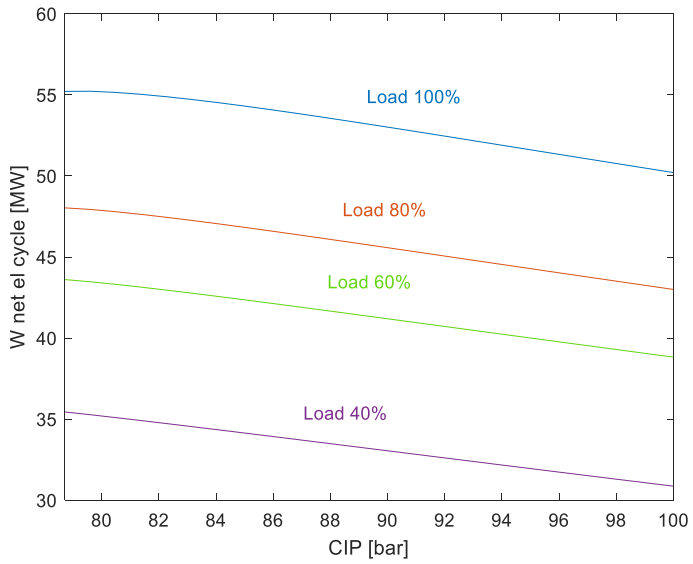

Figure 3.25: Trend of the net electrical power of the cycle against the variation of CIP and of the gas turbine load

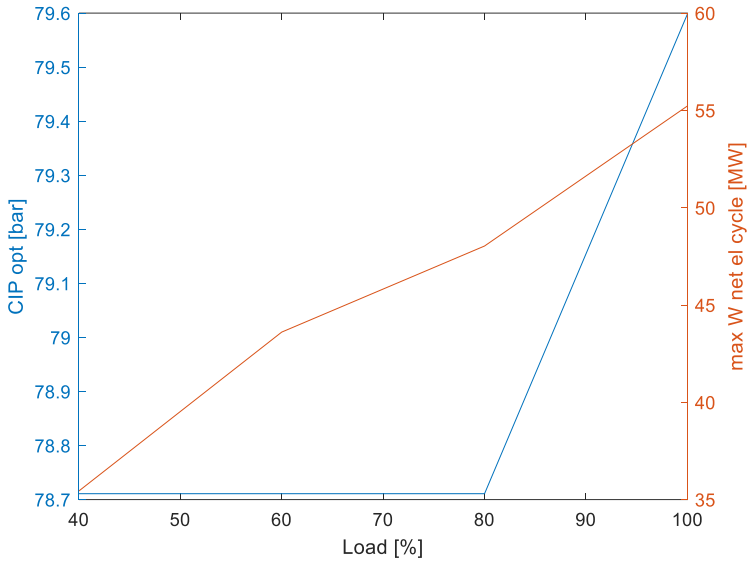

Figure 3.26: Trend of the optimal CIP and of the max net electrical power of the cycle against the variation of gas turbine load

3.6.3.3. Influence of CIT

In the previous sections, the ambient temperature of 5°C was not considered because many thermodynamic points are unfeasible due to the limits of the compressor map and fan speeds, as explained in the "Cycle operational limits" paragraph.

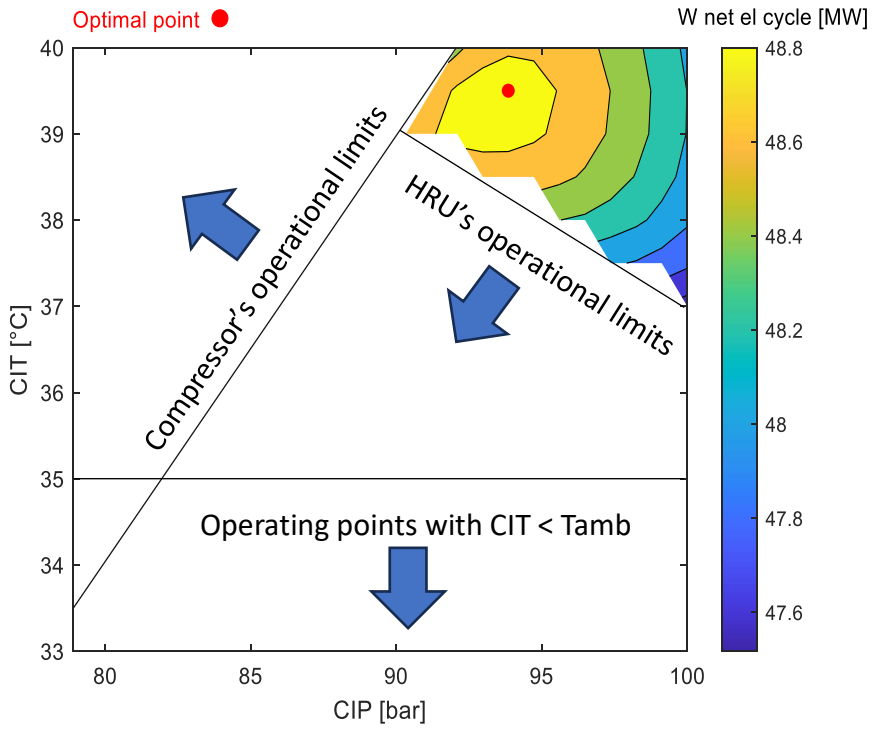

Figure 3.27: Trend of the net electrical power of the cycle at 35°C of ambient temperature and 100% of gas turbine load against the variation of CIP and CIT

In Figure 3.27 it can be noted how at an ambient temperature of 35°C and with the ranges of CIP and CIT considered, the operating points are only in the upper right extreme, at high CIPs and CITs. This is due to three exclusion areas:

- At high CITs and low CIPs the developed code is not able to solve every working points due to compressor operational problems.
- When the ambient temperature is increased until 35 °C, there are some points with the CIT below this value, leading to a flows' intersection in the HRU.
- The maximum fans rotational speed is set at 125% of the rated value to avoid excessive mechanical stress. However, there are thermodynamic points that need fan speeds above that threshold in order to cool down to the defined CIT. Therefore, these points are removed.

It might also be considered to expand the range of variables considered (i.e. CIT and CIP). However, as can be seen from the graph, the point of optimum is not at the extremes and the highest net power island is already contained within the chosen intervals.

3.6.3.4. Influence of inventory

As done in the water cooled case, it is studied how the inventory influences the cycle's performance.
Figure 3.28 depicts the trends of the cycle's net electrical power output and the optimal points for both strategies with 100% (a), 80% (b), 60% (c), and 40% (d) of gas turbine's load. This is all as a function of CIP and CIT with nominal ambient temperature and TIT.
It is appreciable how by reducing the gas turbine load, the constant inventory line shifts towards higher CIPs, while the optimal S1 point remains more or less within the range of nominal conditions. Thus, if at 100% of load the S1 point is roughly in the constant inventory area, by reducing the load the distance between them increases. Therefore at high loads, working at constant inventory does not cause such a marked drop in net power output, while at low loads the reduction can be on the order of 15-20%.

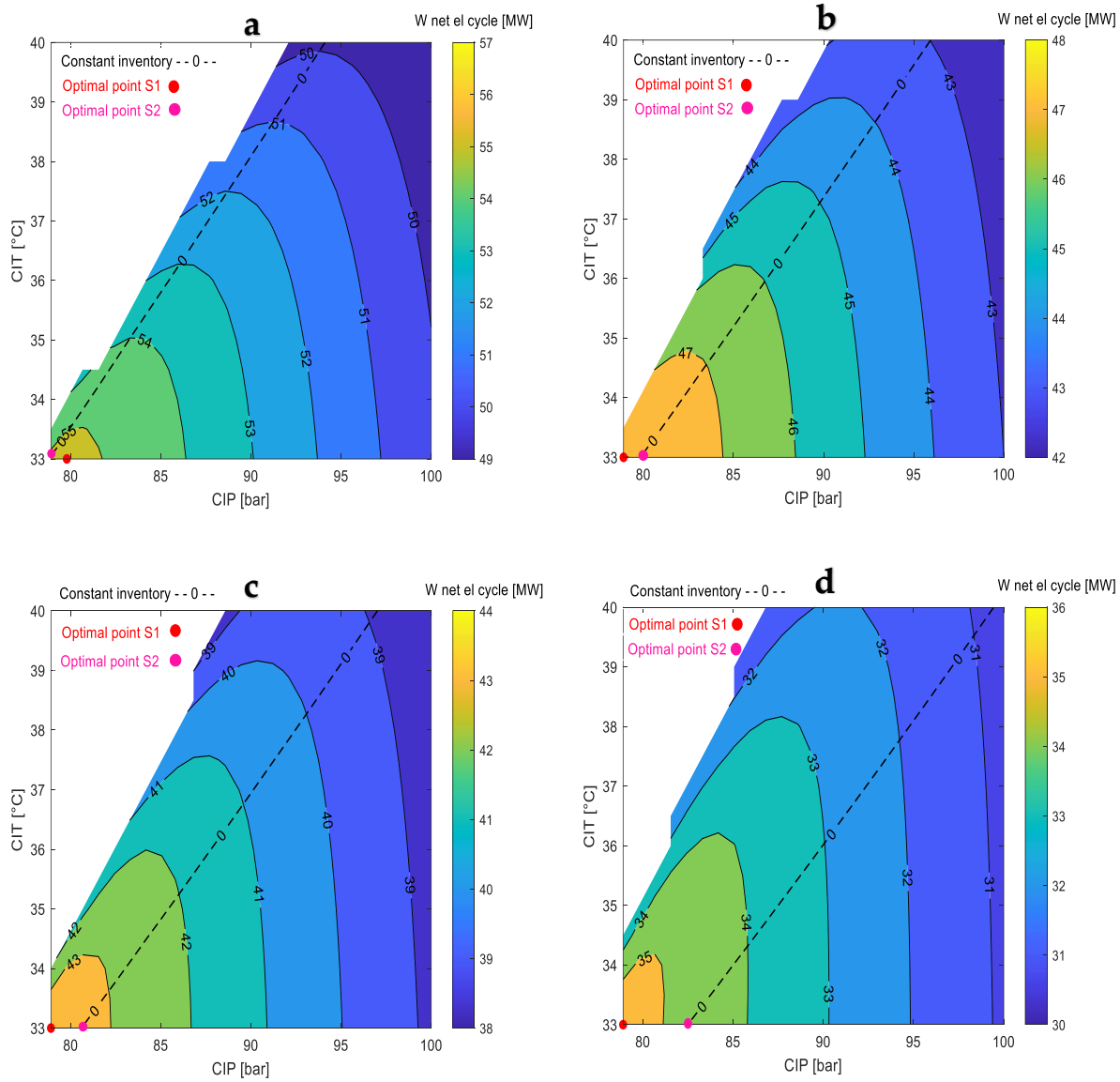

Figure 3.28: Trend of the net electrical power of the cycle at 25°C of ambient temperature against the variation of CIP and CIT with the optimal points for strategy S1 and S2, and the line at constant inventory with a gas turbine load of (a) 100%, (b) 80%, (c) 60% and (d) 40%

Switching the gas turbine load with the ambient temperature, the same pattern is displayed in Figure 3.29 with values of 5°C, 15°C, and 25°C. Load and TIT are in nominal conditions.

A similar consideration to the previous case can be made. In fact, by lowering the ambient temperature, the line of the constant inventory points shifts towards higher CIP values. Therefore, at nominal ambient temperature it is convenient to work with constant inventory, while in winter conditions, when temperatures are lower, there will be a loss in net power output on the order of 5-10%.

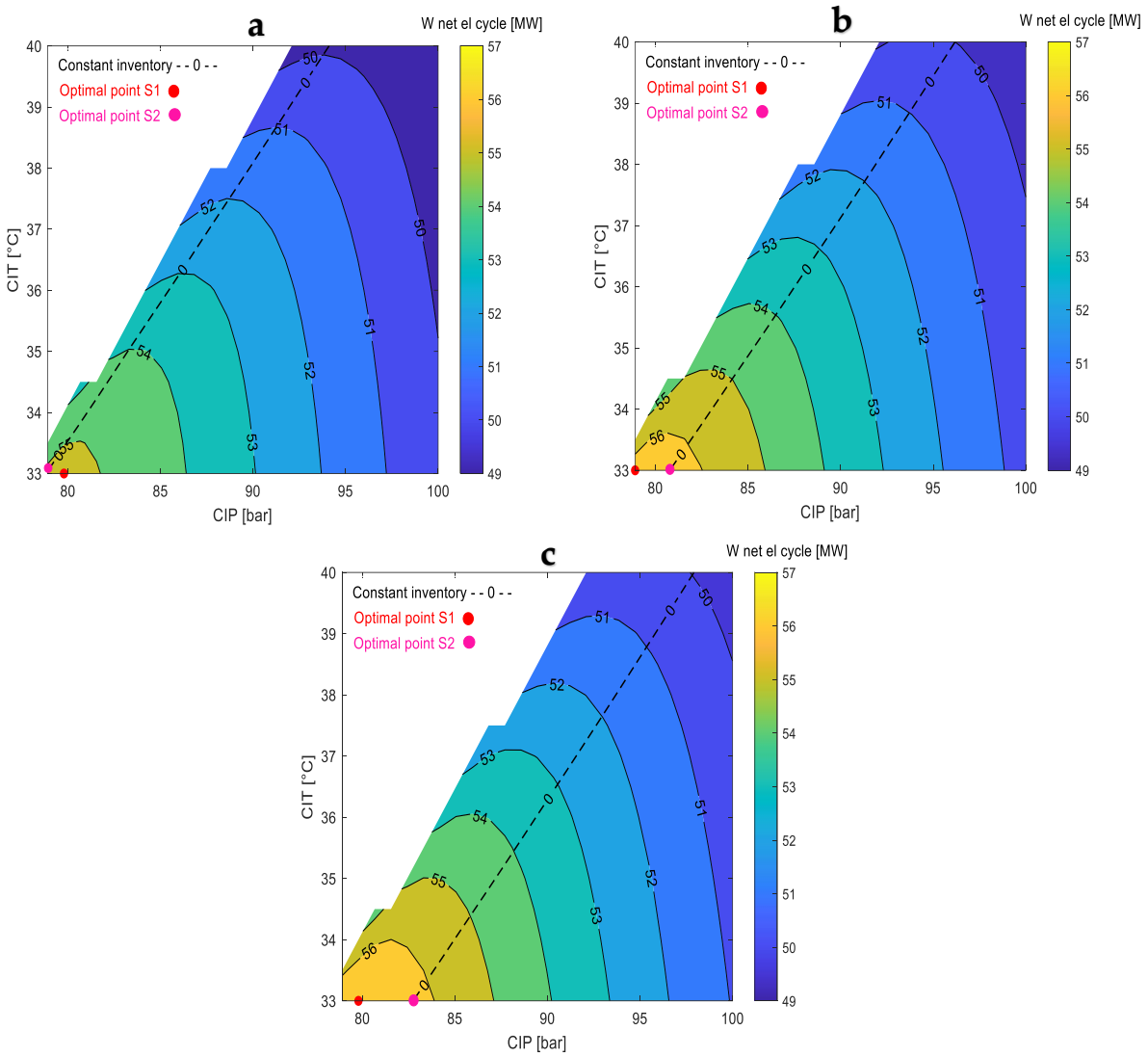

Figure 3.29: Trend of the net electrical power of the cycle at 100% of gas turbine load against the variation of CIP and CIT with the optimal points for strategy S1 and S2, and the line at constant inventory with an ambient temperature of (a) 25°C, (b) 15°C and (c) 5°C

3.6.4. Compressor operations

This section reports the compressor maps in off design conditions comparing the two different cases of water and air cooling.
Figure 3.30 shows the operating points of the compressor as the load decreases.
In both scenarios, with a reduction of the load, the thermal input power and consequently the CO_2 flow rate circulating within the cycle decreases, reducing the main compressor volumetric flow rate ratio.

The main compressor enthalpy rise ratio decreases as well, because the turbine operates in sliding pressure, so the turbine inlet pressure also decreases, while the minimum pressure remains almost constant, leading to a decrease in the compressor enthalpy difference.

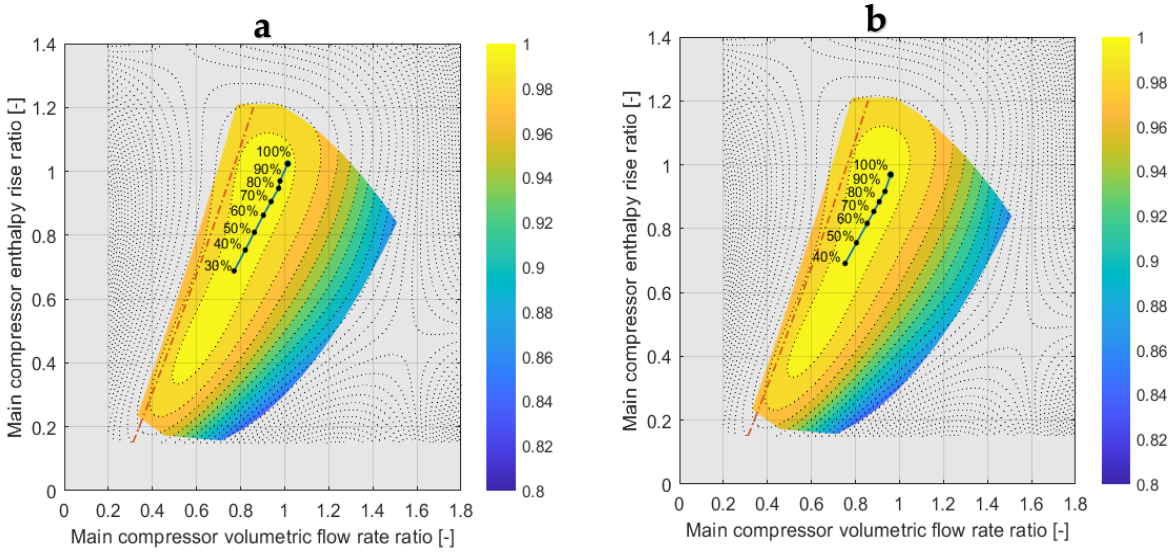

Figure 3.30: Compressor operating points as a function of load variations in the water (a) and (b) air cooled case

Looking instead at the change in ambient temperature, as shown in Figures 3.31, in the water case the variations are minimal because the CIT is fixed at the design value.
On the other hand, in the air case, it is varied from 33 to 40 °C with a step of 0.5 °C. The particular trend depicted is due to the high density variation near the critical point. At a fixed pressure of about 80 bar and given the temperature range above, there is more than a halving of the CO_2 density.

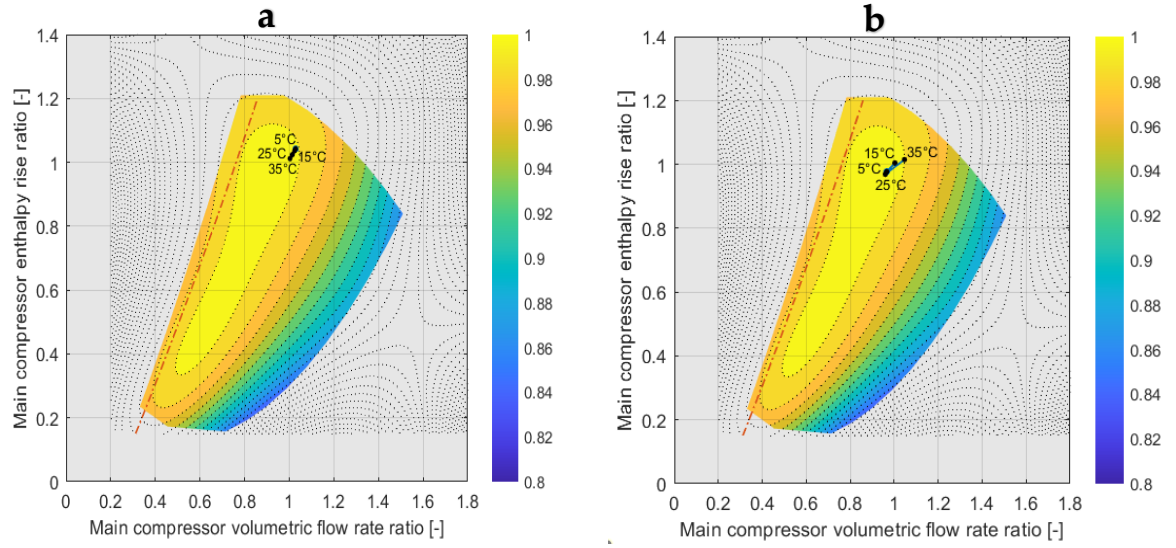

Figure 3.31: Compressor operating points as a function of ambient temperature variations in the water (a) and (b) air cooled case

3.6.5. Comparison between the cooling mediums

In this paragraph the results of the optimal cycle operational points are shown depending on the defined ambient temperature and gas turbine load conditions. Characteristics quantities such as the net power output, the thermodynamic efficiencies, the control variables or the inventory variation are here displayed, and a comparison is made between the two different cooling methods.

3.6.5.1. Inventory variation

The first variable shown is the inventory variation. Delta inventory is defined as the difference between the mass of fluid inside the cycle in off design conditions and the mass of fluid in nominal conditions.
There are significant variations in both cases. In the water scenario, the difference of inventory can reach more than 2000 kg of CO_2 from the minimum to the maximum value. While in the other case, the same overall variation can be over than 5000 kg.

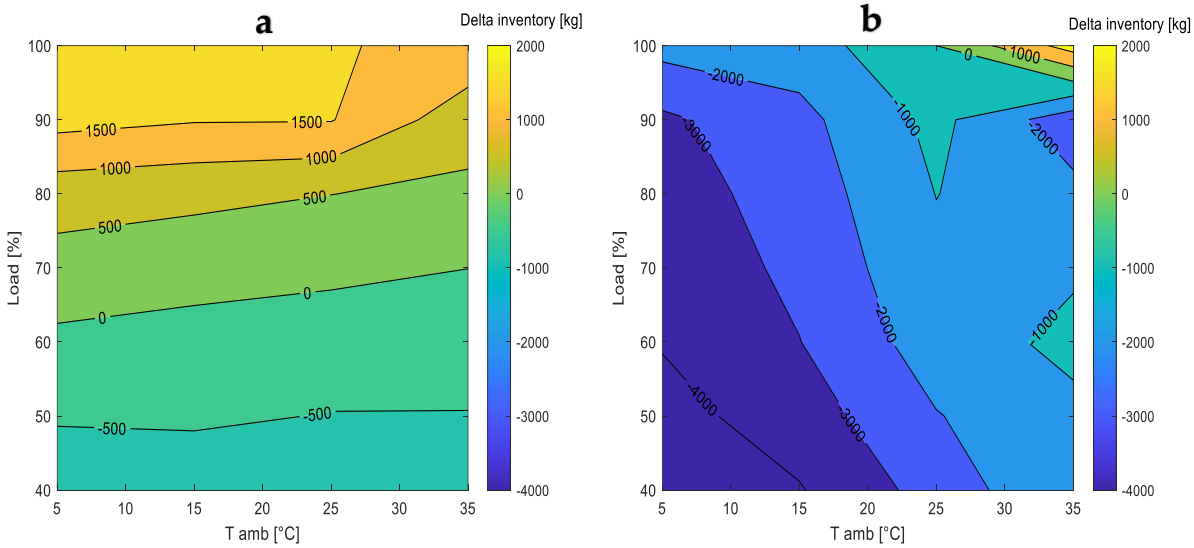

Figure 3.32: Trend of the inventory variation compared to nominal conditions against the variation of gas turbine load and ambient temperature in the (a) water and (b) air cooled case

A preliminary analysis is carried out in order to design the CO_2 storage in both cases. The vessel should be able to supply the cycle with the amount of fluid required for all off-design operations. Therefore, it is sized by considering the following equation:

$$total\ mass\ storage = \max(Delta\ inventory) - \min(Delta\ Inventory)$$

Considering nominal conditions, a vessel temperature equal to CIT is taken, while for what concern the pressure the average between the maximum and minimum pressure of the cycle is assumed, approximately 160 bar. With these quantities, it is then possible to derive the density of CO_2 inside the storage and thus also the vessel's volume.
The cost of the vessel is also calculated through a correlation found in the literature [48] with the following form:

$$total\ cost\ [€] = \ln(V) + a * V^2 + b * V + c$$

Where a, b and c are constant and V is the volume of the storage.
The results are listed in Table 3.9.

Table 3.9: Characteristic quantities of the CO_2 storage for both methodologies

	Air cooled	**Water cooled**
Mass [kg]	6500	2750
Volume [m³]	7.75	3.28
Total cost [M€]	0.013	0.009

The obtained costs of the storage are negligible if compared to the total investment cost of the bottoming power plant, which is more than 40 M€. It is fair to point out that control and compression costs have been neglected, but having obtained such a low value it can be concluded how the variable inventory solution is the best operating control strategy.

3.6.5.2. CIP

In the water case, the optimal CIP always remains near the design point with a variation in all load and ambient temperature ranges that is less than 1 bar.
On the other hand, in the air case, there is a sudden increase in optimal CIP by rising the temperature from nominal conditions, with values up to 92 bar.

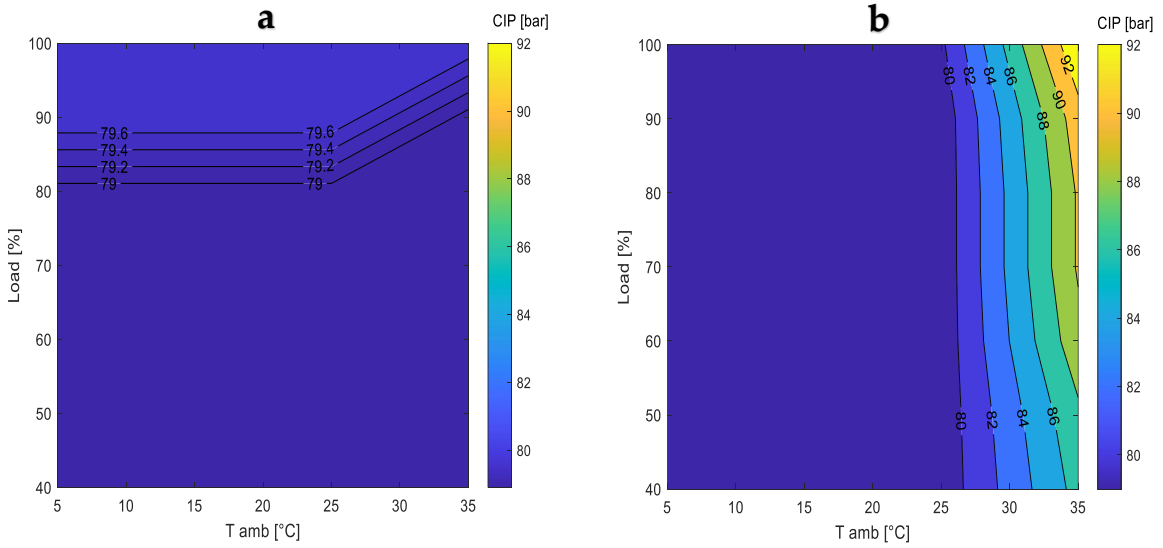

Figure 3.33: Trend of the cycle optimal's CIP against the variation of gas turbine load and ambient temperature in the (a) water and (b) air cooled case

3.6.5.3. Net power output of the cycle

The maximum optimum power of the bottoming cycle is just above 55 MW and can decrease depending on ambient temperature and load until values slightly below 35 MW in both cases.
The trend is depicted in Figure 3.34 and it is quite similar for temperatures below the design one (i.e. 25°C).
However in the air scenario, it is evident how at high ambient temperatures, there is a drop in performance. This is due to the HRU and compressor's limits already discussed in the previous sections.

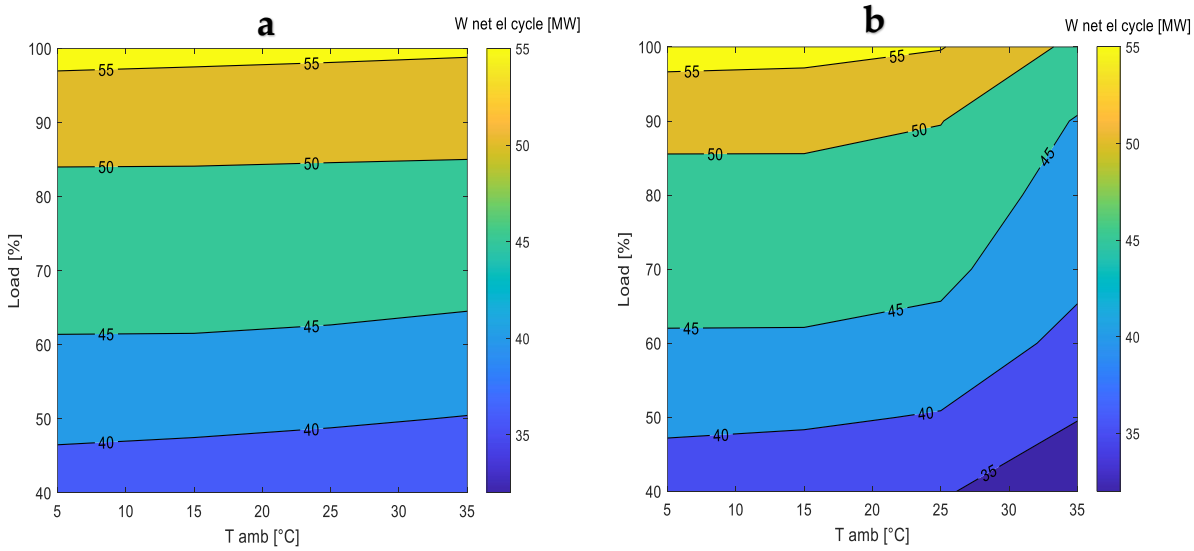

Figure 3.34: Trend of the cycle's net power output against the variation of gas turbine load and ambient temperature in the (a) water and (b) air cooled case

3.6.5.4. Flue gases outlet temperatures

It is interesting to find out how much the SRC layout can cool down the exhaust gases. Hence, how much heat the cycle can recovery from the gas turbine, increasing efficiency.
Figure 3.35 shows the profile of the flue gases outlet temperature from the PHE.
With water the maximum values are around 195°C and they decrease with a lowering of the load until roughly 174°C, while the ambient temperature has not a great impact except small variation.
On the opposite, with air as cooling medium, the ambient temperature has a significant effect on the outlet temperatures, increasing them until values of 224°C.
Considering both scenarios, since the minimum value is around 174°C, it would be useful to rise the minimum exhaust temperature of 90°C for the SRC design.

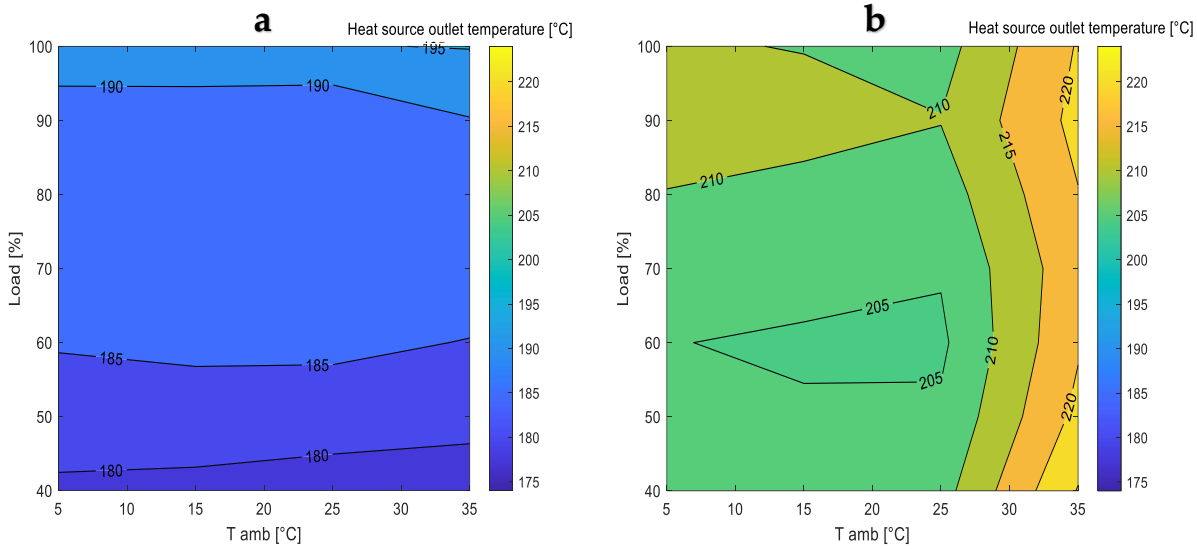

Figure 3.35: Trend of the heat source outlet temperature against the variation of gas turbine load and ambient temperature in the (a) water and (b) air cooled case

3.6.5.5. Recovery efficiency

The recovery efficiency pattern is closely related to the temperature of the gases leaving the PHE and the inlet temperature. Figure 3.36 showed how this last temperature increases with a reduction of load, while in the previous section it was discussed how the outlet temperature decreases. The combination of these two trends lead the recovery efficiency to increase at partial loads in both scenarios, although in the air cooled case there is always a decline in performance at temperatures higher than 25°C.

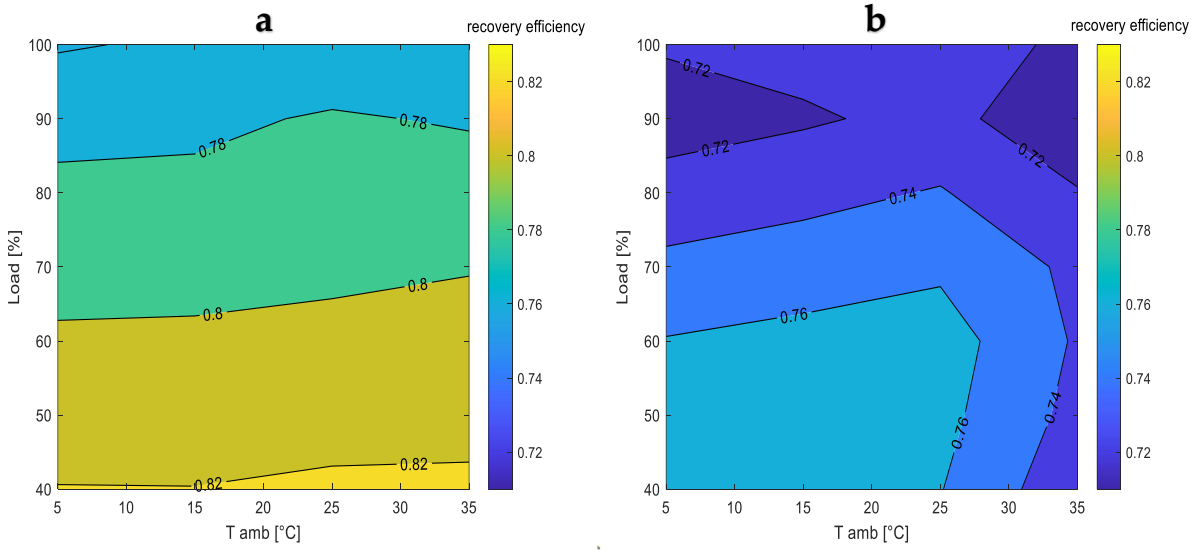

Figure 3.36: Trend of the cycle's recovery efficiency against the variation of gas turbine load and ambient temperature in the (a) water and (b) air cooled case

3.6.5.6. Cycle efficiency

In the air case, cycle efficiency is highly dependent on air temperature and decreases as air temperature increases. While in the water case there is no such dependence, but instead there is a slight decrease working at partial loads below 50%, even if the maximum variation is on the order of 1 percentage point.

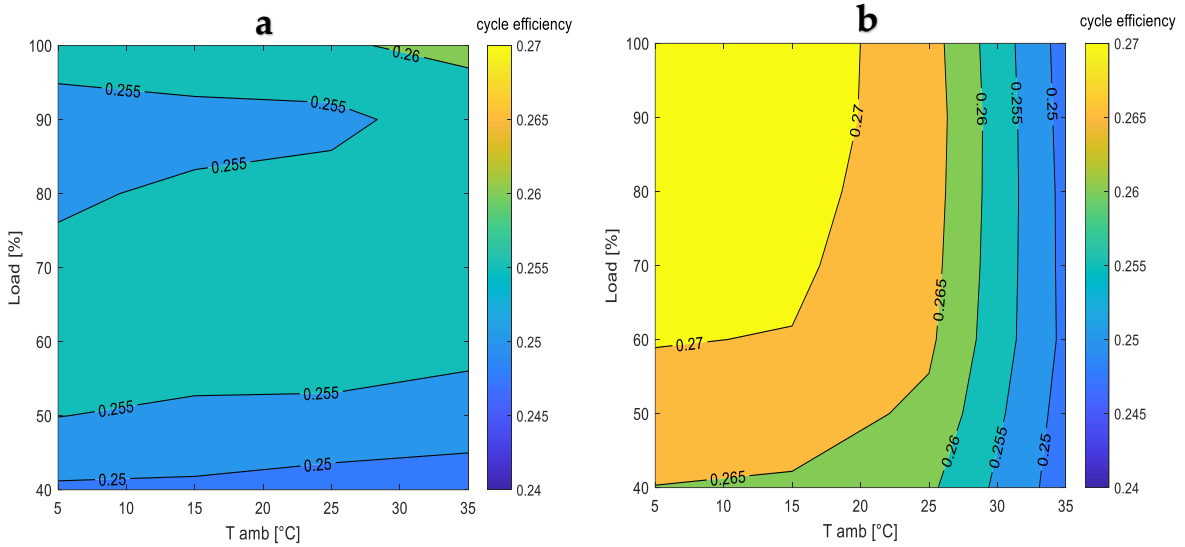

Figure 3.37: Trend of the cycle efficiency against the variation of gas turbine load and ambient temperature in the (a) water and (b) air cooled case

3.6.5.7. Total efficiency

The combination of cycle efficiency and recovery efficiency leads to the total efficiency's trend shown in Figure 3.38.

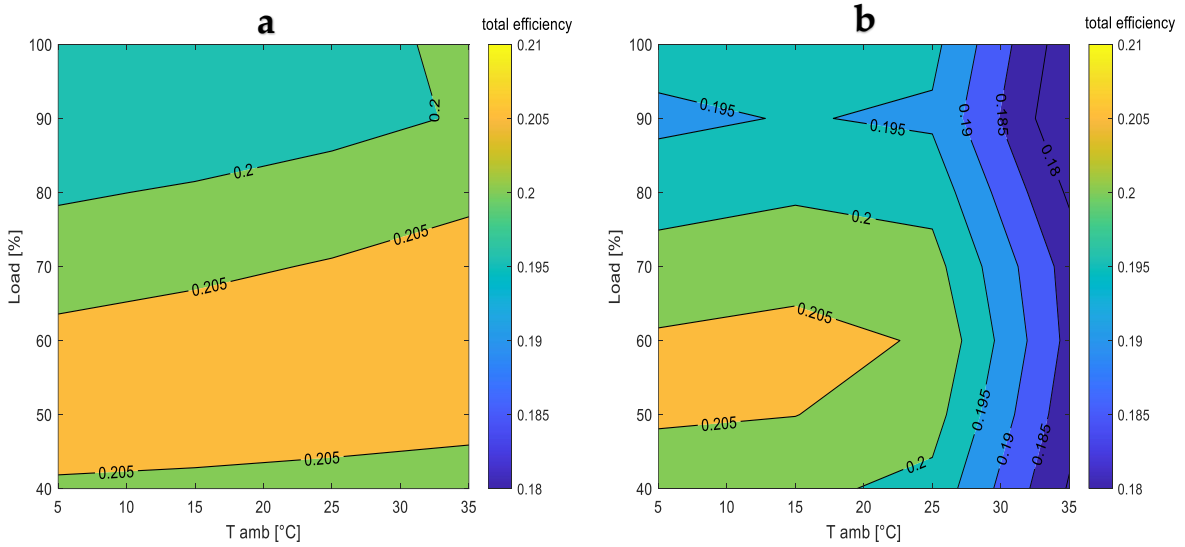

Figure 3.38: Trend of the total efficiency of the cycle against the variation of gas turbine load and ambient temperature in the (a) water and (b) air cooled case

For both, the highest total efficiency results within an area of partial loads of 50-60%, but in the air scenario, over 25°C of ambient temperature, there is a drop until a minimum value below 18% reaching 35°C.

3.6.5.8. Combined cycle efficiency

Finally, also the combined cycle efficiency is shown.
Since the gas turbine's power output in nominal conditions is on the order of 210 MW, while the SRC one is around 50 MW, the influence of the latter is low on the analyzed variable.
With both methodologies the maximum combined cycle efficiency is greater than 48%. However, at partial loads it decreases constantly until values of 40%, while it is not affected greatly by the change in ambient temperature, except in the air case where there is always a drop from temperatures higher than 25°C.

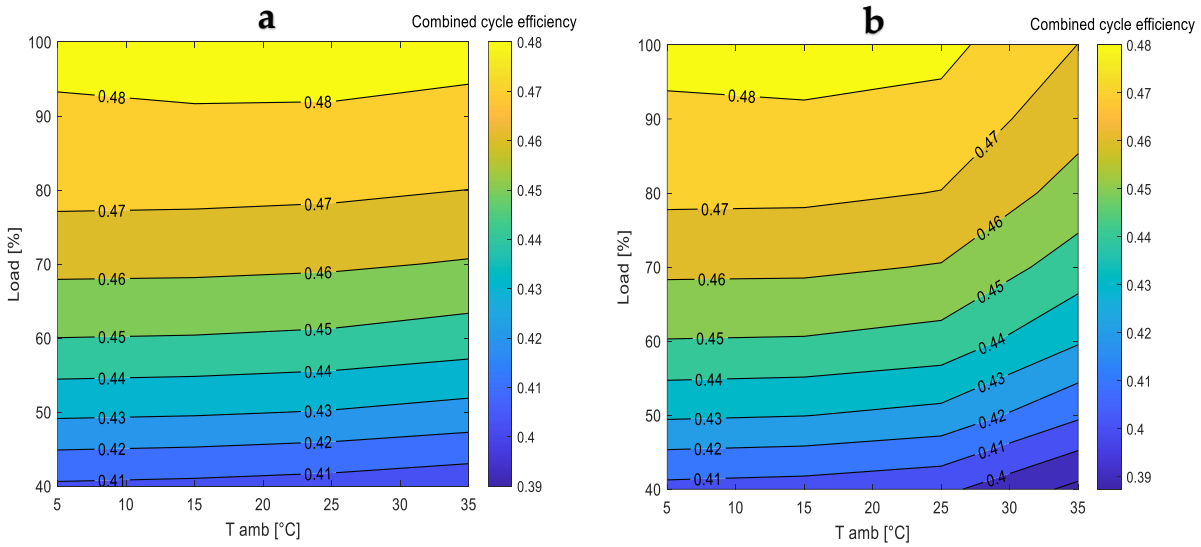

Figure 3.39: Trend of the combined cycle efficiency against the variation of gas turbine load and ambient temperature in the (a) water and (b) air cooled case

3.6.6. Preliminary annual economic analysis

In this final section, a preliminary study is conducted to compute the payback time of the sCO_2 bottoming system, considering the investment costs of the configuration analyzed in off design (i.e., SRC).
Three different real topping power plants are considered based on the loads distribution in France of the year 2019, taken as reference also for the ambient temperature.
The first one, located in Montereau, is the case study of the CO2OLHEAT project discussed in this thesis. It is a peaker-type plant and as can be seen from Figure 3.40 works only few hours per year.

The second load distribution does not belong to a single power plant, but it is the average of the peaker power plants located in France, hence its behavior is similar to the first one.
The third one is a conventional combined cycle power plant, located in Blenod, and it works more hours than the previous two, also working many hours at partial loads.

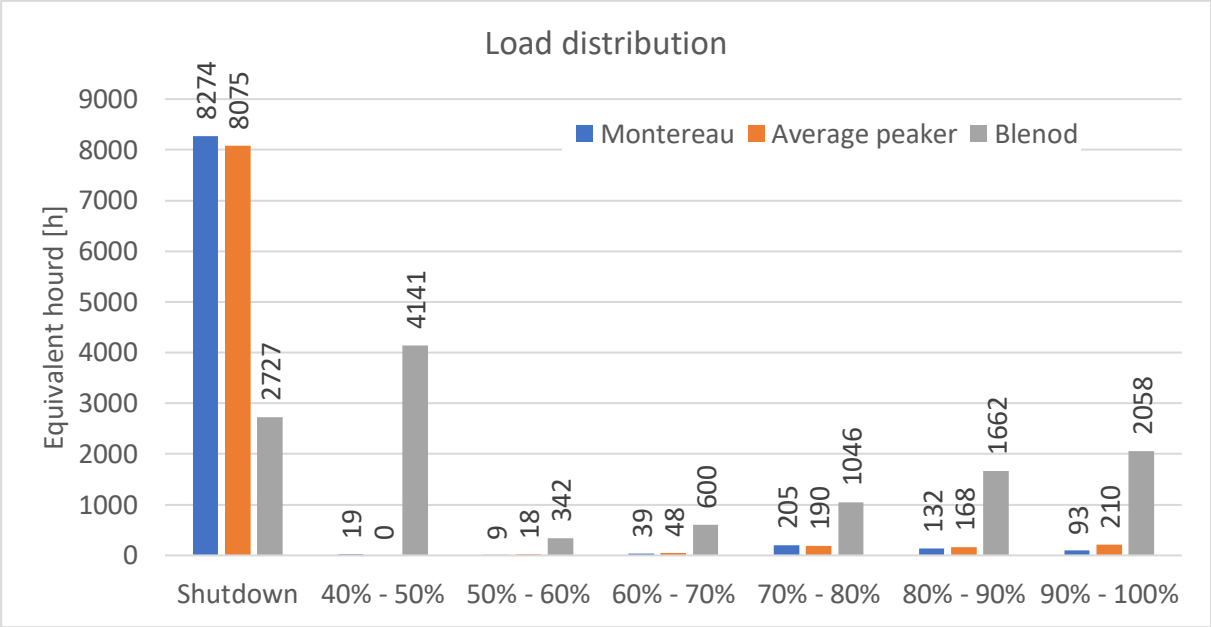

Figure 3.40: Load distribution of the three power plant selected

Thereafter, in Figure 3.41 is depicted the trend of the electricity price distribution for the year 2019 [49].

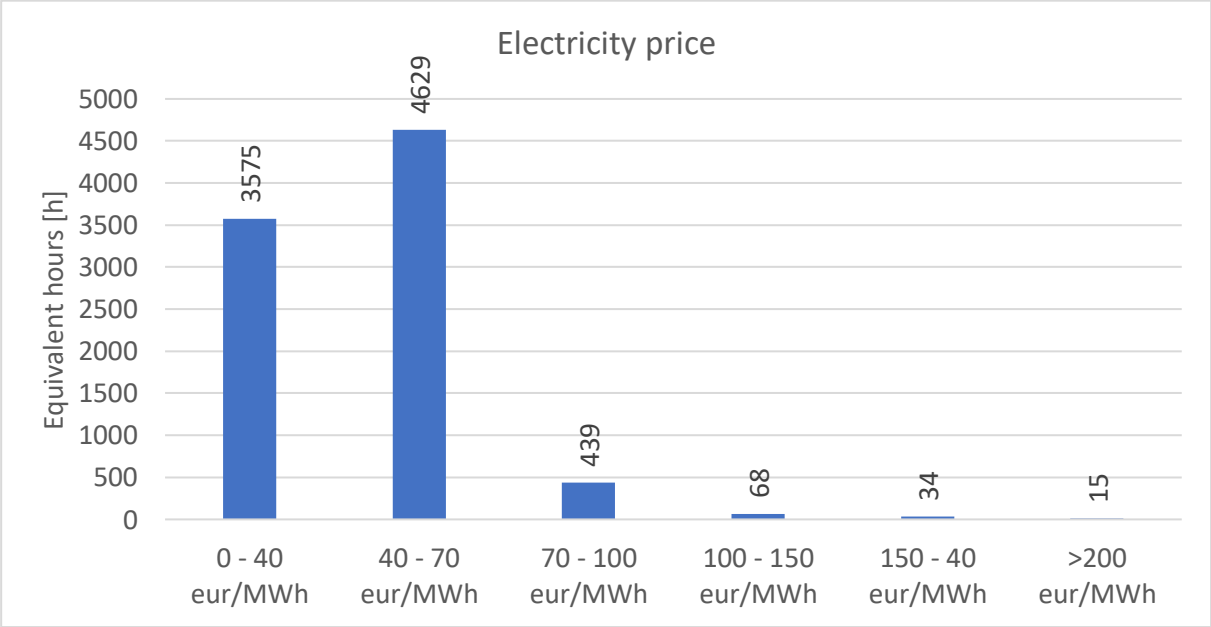

Figure 3.41: Electricity price distribution [49]

The majority of the values are under the threshold of 70 €/MWh. It must be noted that electricity prices skyrocketed after the Ukrainian crisis, and now they settled to almost

double the value of 2019. Thus, this assumptions on electricity price could be considered as conservative.

The ambient temperature trend is also shown in Figure 3.42.

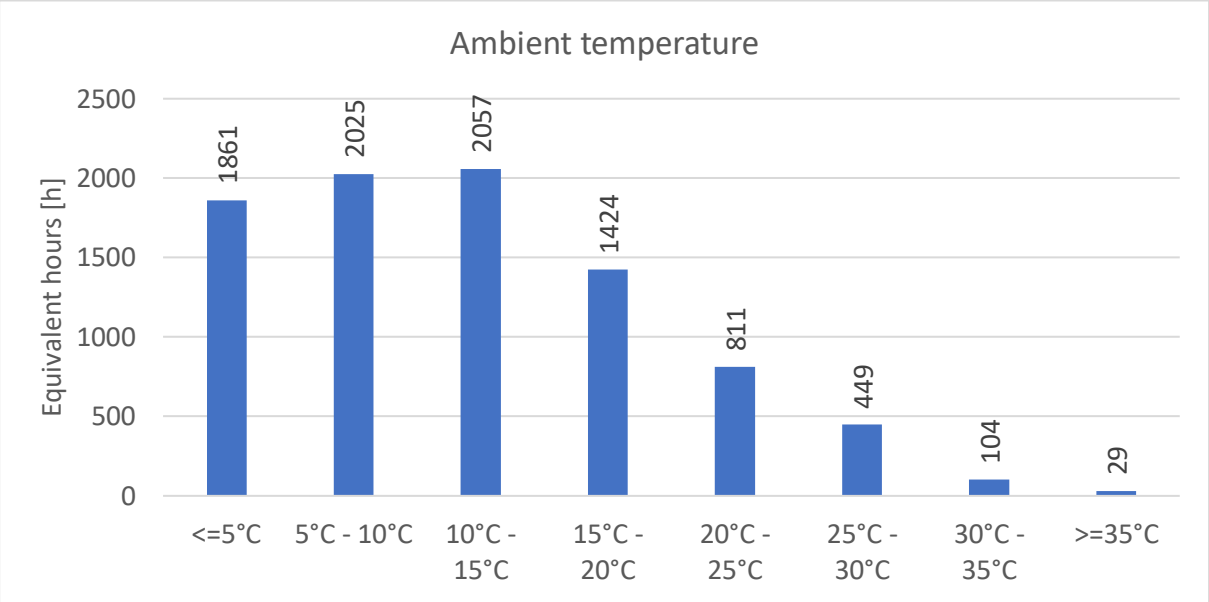

Figure 3.42: Ambient temperature distribution for the year 2019 in Montereau Fault Yonne

The final total revenues for the selected year 2019 are obtained by multiplying every hour per year the loads of each power plant and the electricity price. Following, the not discounted payback time is derived dividing the total investment cost of the SRC by total revenues.
The results are summarized in the Table 3.10 considering the scenario with water as cooling fluid.

Table 3.10: Total revenues and payback time for each power plant

	Total revenues [M€]	**PBT [years]**
Montereau	1.49	27.16
Average peaker	2.28	17.78
Blenod	19.47	2.08

It is evident how the payback period of the first two cases is not affordable. Since the operating hours of the plants are few, the return on investment occurs after several years. Only with the third scenario it seems convenient to enable the investment.
Nevertheless, in the near future power plants will have to work in between a peaker plant and a base load one, in the so called load-following mode, in order to adjust the power output as demand for electricity fluctuates throughout the year. Therefore, it is

reasonable to assume how in the previous case the solution stands in the middle and it is fair to expect a payback period lower than 10 years, especially considering the conservative assumptions on the electricity price.

4 Conclusion

This work was performed from the premises of the CO2OLHEAT project, which aspires to design next-generation power plants exploiting waste heat from several industrial processes by means of a power cycle employing CO_2 in supercritical conditions as working fluid.
It has been highlighted through a literature review that studies on the potential and opportunities of this application are growing steadily and will find more and more space in the upcoming future. This thesis project confirmed the initial considerations on the potential of this technology by studying one of the replication sites of the project, where EDF is proposing to convert a power plant located in the Paris region and consisting of two gas turbines into a combined cycle with a sCO_2-based-bottoming configuration.
The thesis work mainly focused on two consequent analyses: firstly the nominal design of the bottoming cycle and secondly its part-load and off design operation, also considering a brief economic evaluation and a preliminary yearly simulation.
Starting with the first one, the purpose was to find the optimal sCO2 bottoming cycle configuration to exploit the residual heat of the gas turbine exhaust gases. Thanks to a literature review on cycle architectures suitable for waste heat recovery applications, two novel configurations have been identified and integrated in the Politecnico di Milano numerical code designed in previous research projects (i.e. sCO2-flex project). The first configuration is the single heated cascade while the second is dual heated cascade layout, and both of them are between the most promising cycle configuration for WHR applications, as highlighted by the increasing number of studies on the topic.
After having implemented the new cycles, the optimization of all layouts under nominal conditions, maximizing the total efficiency, resulted in the following conclusions:

- The best performing configuration is the dual heated cascade, since it has the highest net power output (77.72 MW) and total efficiency (27.63%), although it suffers from significant investment costs (83.15 M€) due to the greatest number of components among the analyzed layouts and challenges in operations mainly due to the presence of two heaters.
- The other new configuration implemented (the single heated cascade) has quite comparable performance and cost to the Turbine Split Flow (TSF) configuration. The number of components is the same, but the heat exchangers are rearranged differently, leading the SHC to have lower cycle efficiency (25.30% vs. 30.58%) but significantly better recovery from flue gases (98.56% vs. 82.59%).
- Unlike other applications, such as nuclear power plants and CSP, the recompressed cycle is not suitable as a bottoming power system as it shows

poor recovery efficiencies and high investment costs due to the presence of an additional compressor and larger recuperators.

- Although the recuperative cycle (SRC) demonstrates modest thermodynamic performance, looking at the economics it lowers and, in some cases, even halves the investment cost compared to others. In addition, its low components number and the simplicity in operations, thanks to the absence of the flow split, make it an excellent case study for the partial load analysis.

This last configuration (SRC) was thus selected for the consecutive part-load analysis as it represents the optimal solution for the studied application: in fact, a peaker plant will have to work a limited amount of time per year, not justifying the increased investment cost of more complex configurations. Secondly, the bottoming cycle will have to follow the load curve in a fast and prompt way, thus a more compact cycle configuration make sense for this kind of application.

Considering then the study under off-design conditions, as explained before the analysis was divided into two cases, depending on the cooling fluid employed.
In the water-cooling scenario, where the availability of a cold cooling medium is assured for the whole year, it was observed how it may make sense to lower the turbine inlet temperature (TIT) in order to increase the cycle's net power output, while the compressor inlet pressure (CIP) remains close to nominal values for all the cases considered. This is due to the fact that it is always possible to cool down the working fluid to the nominal temperature value of 33°C, and thus the optimal value of the minimum pressure is not really affected.
Instead, considering air as cooling medium, the TIT has a similar behavior, while the ambient temperature has a great influence on both the CIPs and CIT (compressor inlet pressure). In fact, as the ambient temperature increase above 30°C the operation of the cycle becomes more and more constrained to higher CITs, limiting its efficiency mostly due to an increase of the fan auxiliaries consumption.
The influence of a change of cycle's inventory on the performances was another variable taken into consideration. It was found out how in both scenarios it seems profitable to provide a CO_2 storage in order to pressurize and depressurize the system at part load. By means of a brief investment cost analysis it has been highlighted that for a plant of this size the economic impact of adopting a vessel is really limited, thus it make sense to adopt it to increase the degrees of freedom of the plant operation during part load and off design operation.
By setting the boundaries (i.e. ambient temperature and gas turbine load) of the analysis, several operative and performances maps have been generated for both cooling options. These maps provides insights on how to operate the power cycle under optimal terms, knowing the optimized variables and inventory and obtaining the maximum power output under those conditions.
A final comparison on the optimal points of the two different cooling mediums shows how below the nominal temperature the two solutions are quite comparable, with

slightly higher performance of the water case due to the lower auxiliaries consumption. However, going to high temperatures the air-cooled system suffers greatly from the limitations imposed by the HRU and thus a drop in performance become more noticeable (around 7 MW of penalization at 100% of GT load and 35°C of ambient temperature.

Finally, the maps of the cycle optimal off-design operation have been employed for a preliminary yearly simulation and techno-economic analysis. Three different real topping power plants located in France were considered with their GT load distribution for the year 2019, two of them representative of peaker plants, the third one of a more traditional combined cycle. Using the trend of the ambient temperature of Montereau, France, and the French electricity price for the year 2019, the total revenues for the investigated cases are obtained by multiplying for every hour the electricity generated by the additional bottoming cycle and the electricity price. Finally, the not discounted payback time is derived dividing the total investment cost of the SRC by total revenues. It resulted evident how the payback period of the "peaker cases" is not sustainable: since the operating hours of the plants are few (less than 800 for both cases), the return on investment occurs only after several years (27 and 18 years). Only with the third scenario it seems convenient to enable the investment. However, it must be firstly noted that electricity prices in Europe rose drastically after the Ukrainian crisis, and secondly, that the number of operating hours of peaker plants will increase in the future, due to the higher share of non-dispatchable renewables, thus these results could be considered as quite conservative.
This final analysis confirms the techno-economic potential of the investigated solution in justify the growing interest in the adoption of this technology for waste heat recovery applications.

4.1. Future developments

This thesis research was a preliminary analysis of the potential of sCO_2 power cycles for gas turbine bottoming applications and even if it focused both on the design and part load operations of these systems, a number of improvements could enhance the quality of the work. During the literature review, other interesting layouts were discarded due to the complexity or the high number of components, since it was decided to favor the simplicity of the plant and its small size. In future studies it could be possible to also include them.
Nominal optimization was performed considering the pinch points of the heat exchangers as fixed parameters, although they should be optimized considering the cost as a function of the heat exchanger size.
In the economic analysis the operability and maintenance costs over the lifetime of the plant were neglected, due to the lack of information about them. Collaboration with industrial manufacturers could provide more insights about this topic, even if the author expects that the final results will not be affected too much.

Regarding the part load study, it was chosen the simplest cycle of the group for the reasons explained, nevertheless, it would be useful to derive the same maps of the SRC layout for other configurations like the SHC or the TSF, which shows significant efficiencies advantages.

Bibliography

[1] "Climate.gov," [Online]. Available: https://www.climate.gov/media/15021.

[2] E. Commission, "Climate change consequences," 2022. [Online]. Available: https://ec.europa.eu/clima/climate-change/climate-change-consequences_en.

[3] S. Re, "World economy set to lose up to 18% gdp from climate change if no action taken, reveals swiss re institute's stress-test analysis," 2021. [Online]. Available: https://www.swissre.com/media/press-release/nr-20210422-economics-of-climate-change-risks.html.

[4] "European Commission," [Online]. Available: https://commission.europa.eu/index_en.

[5] "Emissions by sector," Our World in Data, [Online]. Available: https://ourworldindata.org/emissions-by-sector#energy-electricity-heat-and-transport-73-2.

[6] I. (. R. E. Agency), "Battery Storage for Renewables : Market Status and Technology Outlook," 2015.

[7] I. (. R. E. Agency), "Innovation landscape brief: Flexibility in conventional power plants," 2019.

[8] "Global Energy & Climate Outlook 2050," [Online]. Available: https://eneroutlook.enerdata.net/forecast-world-energy-primary-consumption.html.

[9] M. Marchionni, Tassou, G. Bianchi and A. Savvas, "Techno-economic assessment of Joule-Brayton cycle architectures for heat to power conversion from high-grade heat sources using CO2 in the supercritical state," 2018.

[10] N. Galanis, E. Cayer, P. Roy, E. Denis and M. Désilets, "Electricity generation from low temperature sources," 2009.

[11] L. Liuchen, Y. Qiguo and C. Guomin, "Supercritical Carbon Dioxide (s-CO2) Power Cycle for Waste Heat Recovery: A Review from Thermodynamic Perspective," 2020.

[12] M. Marchionni, G. Bianchi, Tassou and A. Savvas, "Review of supercritical carbon dioxide (sCO2) technologies for high-grade waste heat to power conversion," 2020.

[13] C. Forman, I. Muritala, R. Pardemann and B. Meyer, "Estimating the global waste heat potential," 2016.

[14] L. Yaping, W. Ying and H. Diangui, "Supercritical CO2 Brayton cycle: A state-of-the-art review," 2019.

[15] M. Persichilli, A. Kacludis, E. Zdankiewicz and T. Held, "Supercritical CO2 Power Cycle Developments and Commercialization: Why sCO2 can Displace Steam," 2012.

[16] "https://pages.mtu.edu/~rluck/courses/spring2004/spring2004CH1110/lecture/Criticalco2.htm," [Online].

[17] "CO2OLHEAT," [Online]. Available: https://co2olheat-h2020.eu/.

[18] D. Alfani, "Supercritical CO2 cycles for flexible power generation: techno-economic optimization and part-load operational strategies," 2020.

[19] V. O. Combs, "An Investigation of the Supercritical CO2 Cycle (Feher Cycle) for Shipboard Application," 1977.

[20] M. Persichilli, T. Held, S. Hostler, E. Zdankiewicz and D. Klapp, "Transforming Waste Heat to Power through Development of a CO2-Based-Power Cycle, pp. 10-12," 2011.

[21] R. Allam, J. Fetvedt, B. Forrest and D. Freed, "The Oxy-Fuel, Supercritical CO2 Allam Cycle: New Cycle Developments to Produce Even Lower-Cost Electricity From Fossil Fuels Without Atmospheric Emissions," ASME Turbo Expo 2014: Turbine Technical Conference and Exposition, 2014.

[22] T. J. Held, "SUPERCRITICAL CO2 CYCLES FOR GAS TURBINE COMBINED CYCLE POWER PLANTS," 2010.

[23] P. Huck, S. Freund, M. Lehar and M. Peter, "Performance comparison of supercritical CO2 versus steam bottoming cycles for gas turbine combined cycle applications," 2016.

[24] T. b. sCO2flex, 2021. [Online]. Available: https://www.sco2-flex.eu/wp-content/uploads/2021/06/sCO2-brochure-doublepages-21-06-2021.pdf..

[25] T. F. Coleman, M. A. Branch and A. Grace, "Optimization toolbox : for use with MATLAB," 1999.

[26] "sCO2 flex project," [Online]. Available: https://www.sco2-flex.eu/.

[27] E. W. Lemmon, M. L. Huber and M. O. McLinden, "NIST Standard Reference Database 23: Reference Fluid Thermodynamic and Transport Properties (REFPROP), Version 9.0," Phys. Chem. Prop. …, 2010.

[28] "Thermoflow Inc.," 2020. [Online]. Available: https://www.thermoflow.com/.

[29] V. Gnielinski, "New equations for heat and mass transfer in the turbulent flow in pipes and channels," NASA STI/Recon Tech. Rep. A, vol. 41, no. 1, pp. 8–16, 1975.

[30] G. G. Power. [Online]. Available: https://www.ge.com/gas-power/products/gas-turbines/gt-13e2.

[31] ASME, "ASME International Boiler and Pressure Vessel Code," 2015.

[32] U. Gampe and al., "Concept and preliminary design of a 600°C+ sCO2 test facility," 2nd European sCO2 Conference, 2018.

[33] D. Shi and Y. Xie, "Aerodynamic Optimization Design of a 150 kW High Performance Supercritical Carbon Dioxide Centrifugal Compressor without a High Speed Requirement," 2020.

[34] N. Weiland and D. Thimsen, "A Practical Look at Assumptions and Constraints for Steady State Modeling of sCO2 Brayton Power Cycles," 2016.

[35] "Heatric Division of Meggitt (UK)," [Online]. Available: https://www.heatric.com.

[36] K. Brun, P. Friedman and R. Dennis, "Fundamentals and Applications of Supercritical Carbon Dioxide (SCO2) Based Power Cycles," 2017.

[37] D. Ranjan, "Fundamental study of key issues related to advanced sCO2 Brayton cycle: Prototypic HX development and cavitation. Report: Final report for NEUP project 14-6670.," USA, 2018.

[38] "Fives Group," [Online]. Available: https://www.fivesgroup.com/..

[39] "LU-VE S.p.A.," [Online]. Available: https://www.luvegroup.com/..

[40] S. Filippini and U. Merlo, "Air Cooled Heat Exchangers for CO2 Refrigeration Cycles," 2011.

[41] G. O. Musgrove, R. L. Pierres and J. Nash, "Heat Exchangers for Supercritical CO2 Power Cycle Applications," 2014.

[42] D. Alfani, M. Binotti, E. Macchi, M. Astolfi and P. Silva, "sCO2 power plants for waste heat recovery: design optimization and part-load operation strategies," 2021.

[43] K. M. Seok, A. Yoonhan, L. B. Kim and J. Ik, "Study on the supercritical CO2 power cycles for landfill gas firing gas turbine bottoming cycle," 2016.

[44] B. Giovanni, Z. Pavlos and A. Eduardo, "Parametric evaluation of S-CO2 Brayton cycles for bottoming applications," 2016.

[45] S. A. Wright, C. S. D. Scammell and O. William, "Thermo Economic Analysis of Four sCO2 Waste Heat Recovery Power Systems".

[46] G. Carraro, P. Danieli, A. Lazzaretto and T. Boatto, "A common thread in the evolution of the configurations of supercritical CO2 power systems for waste heat recovery," 2021.

[47] "Renewables.ninja," [Online]. Available: https://www.renewables.ninja/news/raw-weather-data.

[48] M. Shamoushaki, P. H. Niknam, L. Talluri, G. Manfrida and D. Fiaschi, "Development of Cost Correlations for the Economic Assessment of Power Plant Equipment," 2019.

[49] "RTE service portal," [Online]. Available: https://www.services-rte.com/en/home.html.

[50] D. Alfani, M. Astolfi, M. Binotti and P. Silva, "D6.1 - report consolidating the final results. Technical Report 6, sCO2flex," 2021.

A Appendix A

B Appendix B

List of Figures

Figure 1.1: Global average temperature increase difference year by year during the last century [1] 1

Figure 1.2: Total Primary Energy Consumption by Region from 2000 to 2050 [8] 3

Figure 1.3: Sectoral shares of worldwide waste heat distribution [11] 4

Figure 1.4: Thermodynamic cycles for waste heat recovery at various temperature levels and scales [11] 5

Figure 1.5: v-p diagram of CO_2 compression at different temperature levels [12] 7

Figure 1.6: Specific heat of CO_2 as a function of temperature and pressure [12] 7

Figure 1.7: T-Q diagrams of a HRSG (on the left) and a flue gases and sCO_2 PHE (on the right) [15]....8

Figure 1.8: Dual Rail's layout [22] 9

Figure 1.9: sCO2 power cycle schematic [23] 10

Figure 1.10: Schematic design of the sCO_2 power plant [24] 12

Figure 2.1: GT13E2 gas turbine's layout [28]....16

Figure 2.2: ASME Boiler and Pressure Vessel code allowable stresses as a function of operating temperature for three Nickel-based alloys (Inconel 800H, Inconel 617 and Haynes 230) and one stainless steel (347HFG) [31] 18

Figure 2.3: Size comparison between a 10 MW steam turbine and a sCO_2 turbine with the same power output [32]....19

Figure 2.4: Geometric design of the compressor [33] 19

Figure 2.5: Section of a cross-flow PCHE with straight channels manufactured by HEATRIC [35]....22

Figure 2.6: Core assembly of a cross-flow plate and fin heat exchanger [36]....23

Figure 2.7: LU-VE EHVD CO_2 gas coolers model designed for refrigeration industry [39] 24

Figure 2.8: Simple recuperative cycle (SRC) layout....27

Figure 2.9: T-Q diagram of the recuperator in the SRC....28

Figure 2.10: Recompressed recuperative cycle (RRC) layout 29

Figure 2.11: T-Q diagram of LTR and HTR in the RRC....29

Figure 2.12: Simple recuperative cycle with recuperator bypass (SRCB) layout 30

Figure 2.13: Recompressed recuperative cycle with high temperature recuperator bypass (RRCB) layout.....31

Figure 2.14: Turbine split flow (TSF) layout.....31

Figure 2.15: Single heated cascade (SHC) layout 33

Figure 2.16: Dual heated cascade (BHC) layout.....34

Figure 2.17: Cycle, recovery and total efficiencies of the SRC as a function of the CIP 37

Figure 2.18: (a) Cycle, recovery and total efficiencies of the SRC as a function of the TIT 38

Figure 2.19: Ts diagram of the SRC configuration.....42

Figure 2.20: TQ diagram of the SRC configuration.....43

Figure 3.1: Ambient temperature variation over the year 2019 in Montereau Fault Yonne (France) 45

Figure 3.2: Flue gases mass flow rate (a), temperature (b) and heat power inlet variation (c) as a function of the gas turbine load and the ambient temperature 46

Figure 3.3: Graphical representation of TIT and CIP variation in the parametric optimization where n is the load index 49

Figure 3.4: Graphical representation of CIT and CIP variation in the parametric optimization.....50

Figure 3.5: Compressor's dimensionless operational map 52

Figure 3.6: Compressor operational limits 53

Figure 3.7: HRU operational limits 54

Figure 3.8: Flue gases heat power inlet, mass flow rate and temperature variation as a function of the ambient temperature with a gas turbine load of 100%.....57

Figure 3.9: Flue gases heat power inlet, mass flow rate and temperature variation as a function of the gas turbine load with an ambient temperature of 25°C 57

Figure 3.10: Trend of the net electrical power of the cycle against the variation of TIT and of the ambient temperature.....58

Figure 3.11: Trend of a) the specific turbine work, (b) the specific compressor work, (c) the sCO_2 mass flow rate and (d) the HRU power against the variation of TIT and of the ambient temperature.....59

Figure 3.12: Trend of the optimal TIT and of the maximum net electrical power of the cycle against the variation of the ambient temperature.....60

Figure 3.13: Trend of the net electrical power of the cycle against the variation of TIT and of the gas turbine load 60

Figure 3.14: Trend of the optimal TIT and of the max net electrical power of the cycle against the variation of gas turbine load 61

Figure 3.15: Trend of the net electrical power of the cycle against the variation of CIP and of the ambient temperature 62

Figure 3.16: Trend of the optimal CIP and of the max net electrical power of the cycle against the variation of the ambient temperature.....62

Figure 3.17: Trend of the net electrical power of the cycle against the variation of CIP and of the gas turbine load 63

Figure 3.18: Trend of the optimal CIP and of the max net electrical power of the cycle against the variation of gas turbine load 63

Figure 3.19: Trend of the net electrical power of the cycle against the variation of CIP and TIT with the optimal points for strategy S1 and S2, and the line at constant inventory with an ambient temperature of (a) 35°C, (b) 25°C, (c) 15°C and (d) 5°C ...64

Figure 3.20: Trend of the net electrical power of the cycle against the variation of CIP and TIT with the optimal points for strategy S1 and S2, and the line at constant inventory with a gas turbine load of (a) 100%, (b) 80%, (c) 60% and (d) 40% 65

Figure 3.21: Trend of the net electrical power of the cycle against the variation of TIT and of the ambient temperature 66

Figure 3.22: Trend of the net electric power of the cycle against the variation of TIT and of the gas turbine load.....67

Figure 3.23: Trend of the net electrical power of the cycle against the variation of CIP and of the ambient temperature 67

Figure 3.24: Trend of the optimal CIP and of the max net electrical power of the cycle against the variation of the ambient temperature.....68

Figure 3.25: Trend of the net electrical power of the cycle against the variation of CIP and of the gas turbine load 68

Figure 3.26: Trend of the optimal CIP and of the max net electrical power of the cycle against the variation of gas turbine load 69

Figure 3.27: Trend of the net electrical power of the cycle at 35°C of ambient temperature and 100% of gas turbine load against the variation of CIP and CIT 69

Figure 3.28: Trend of the net electrical power of the cycle at 25°C of ambient temperature against the variation of CIP and CIT with the optimal points for strategy S1 and S2, and the line at constant inventory with a gas turbine load of (a) 100%, (b) 80%, (c) 60% and (d) 40% 71

Figure 3.29: Trend of the net electrical power of the cycle at 100% of gas turbine load against the variation of CIP and CIT with the optimal points for strategy S1 and S2, and the line at constant inventory with an ambient temperature of (a) 25°C, (b) 15°C and (c) 5°C 72

Figure 3.30: Compressor operating points as a function of load variations in the water (a) and (b) air cooled case 73

Figure 3.31: Compressor operating points as a function of ambient temperature variations in the water (a) and (b) air cooled case 73

Figure 3.32: Trend of the inventory variation compared to nominal conditions against the variation of gas turbine load and ambient temperature in the (a) water and (b) air cooled case 74

Figure 3.33: Trend of the cycle optimal's CIP against the variation of gas turbine load and ambient temperature in the (a) water and (b) air cooled case 75

Figure 3.34: Trend of the cycle's net power output against the variation of gas turbine load and ambient temperature in the (a) water and (b) air cooled case 76

Figure 3.35: Trend of the heat source outlet temperature against the variation of gas turbine load and ambient temperature in the (a) water and (b) air cooled case 77

Figure 3.36: Trend of the cycle's recovery efficiency against the variation of gas turbine load and ambient temperature in the (a) water and (b) air cooled case 77

Figure 3.37: Trend of the cycle efficiency against the variation of gas turbine load and ambient temperature in the (a) water and (b) air cooled case 78

Figure 3.38: Trend of the total efficiency of the cycle against the variation of gas turbine load and ambient temperature in the (a) water and (b) air cooled case 78

Figure 3.39: Trend of the combined cycle efficiency against the variation of gas turbine load and ambient temperature in the (a) water and (b) air cooled case 79

Figure 3.40: Load distribution of the three power plant selected 80

Figure 3.41: Electricity price distribution [49] 80

Figure 3.42: Ambient temperature distribution for the year 2019 in Montereau Fault Yonne 81

List of Tables

Table 1.1: Comparison of the main flexibility parameters (averages) for conventional types of power plants [7] 2

Table 2.1: Datasheet of a GT13E2 gas turbine [30] 16

Table 2.2: Exhaust gases composition at the outlet of the turbine 17

Table 2.3: Main assumptions for the PHE design 21

Table 2.4: Main assumptions for the recuperator design 23

Table 2.5: Main assumptions for the water cooled HRU design 25

Table 2.6: Main assumptions for the direct dry-air cooled HRU design 25

Table 2.7: sCO_2 cycle's assumptions [34] 26

Table 2.8: Optimization variables chosen for each cycle 36

Table 2.9: Fixed variables chosen for each cycle 36

Table 2.10: Net powers and efficiencies results for each cycle 39

Table 2.11: Cost composition for each configuration 41

Table 2.12: Thermodynamic points of the SRC configuration 42

Table 3.1: Main results of the water cooled SRC thermodynamic optimization 47

Table 3.2: Main results of the air cooled SRC thermodynamic optimization 47

Table 3.3: Main assumptions of the piping structure inside the bottoming cycle 48

Table 3.4: Control variables with associated ranges and steps for the parametric optimization in the water cooled case 48

Table 3.5: Numerical constraints and closing variables for the system of non-linear equations representing the off design numerical problem for the SRC configuration. Closing variables directly handled by the solving numerical algorithm are labelled with * 49

Table 3.6: Control variables with associated ranges and steps for the parametric optimization in the air cooled case 50

Table 3.7: Off-design operating strategy for the water cooled SRC configuration 56

Table 3.8: Off-design operating strategy for the air cooled SRC configuration 56

Table 3.9: Characteristic quantities of the CO_2 storage for both methodologies 75

Table 3.10: Total revenues and payback time for each power plant 81

List of symbols

Variable	Description	SI unit
GDP	Gross domestic product	€
WHR	Waste heat recovery	-
ORC	Organic Rankine cycle	-
CHP	Combined heat and power	-
LCOE	Levelized cost of electricity	€/MWh
CSP	Concentrating solar-thermal power	-
3PRH	Three-pressure reheat	-
LTR	Low temperature recuperator	-
HTR	High temperature recuperator	-
HRU	Heat recovery unit	-
PHE	Primary heat exchanger	-
HRSG	Heat recovery steam generator	-
SRC	Simple recuperative cycle	-
RRC	Recompressed recuperative cycle	-
SRCB	Simple recuperative cycle with recuperator bypass	-
RRCB	Recompressed recuperative cycle with high temperature recuperator bypass	-
TSF	Turbine split flow cycle	-
SHC	Single heated cascade cycle	-
BHC	Dual heated cascade cycle	-
Z	Compressibility factor	-
NGV	Nozzle Guide Vanes	-
IGV	Inlet Guide Vanes	-
CIT	Compressor inlet temperature	°C
CIP	Compressor inlet pressure	bar
TIT	Turbine inlet temperature	°C
S&T	Shell and tube	-
REIIs	Resource and energy intensive industries	-
WH2P	Waste heat to power	-
EDF	Électricité de France	-
PBT	Payback time	years